Durham E-Theses

Testing the standard model at future high energy colliders

Abu Leil-Cooper, Ghadir F.

TESTING THE STANDARD MODEL AT FUTURE HIGH ENERGY COLLIDERS

Ghadir F. Abu Leil–Cooper

Centre for Particle Theory

University of Durham

A thesis submitted to the University of Durham

for the Degree of Doctor of Philosophy

Spring 1995

Abstract

Throughout this thesis we test some aspects of the Standard Model (SM) at future high energy colliders. We start by examining the SU(2)$\times$ U(1) non–abelian nature of the SM. We consider the effect of anomalous couplings on the reaction $e^+e^- \to W^+W^-\gamma$, at $\sqrt{s} = 200$ GeV, where the photon is soft. We show that the dependence on the anomalous couplings is of the same order as, but different from, the dependence of the leading order $e^+e^- \to W^+W^-$ cross section. We therefore argue that the two processes are complementary in providing precision tests of the Standard Model electroweak vertices. We also study the same process, $e^+e^- \to W^+W^-\gamma$, at high-energy e^+e^- colliders to investigate the effect of genuine quartic $W^+W^-\gamma\gamma$ and $W^+W^-Z\gamma$ anomalous couplings on the cross section. Deviations from the Standard Model predictions are quantified. We show how bounds on the anomalous couplings can be improved by choosing specific initial state helicity combinations. The dependence of the anomalous contributions on the collider energy is studied. We then proceed to present a detailed analysis of soft photon radiation in $e^+e^- \to t\bar{t} \to bW^+\bar{b}W^-$. The radiation pattern is shown to depend sensitively on the top mass, width and energy, as well as the relative orientation of the initial and final state particles. Optimum conditions in which initial state radiation is minimised and the radiation pattern has the richest structure are discussed. Finally, the Higgs sector of the SM is visited, where the production of the SM Higgs ϕ with intermediate mass at the proposed CERN LEP$\otimes$LHC ep collider in $\gamma q(\bar{q}) \to W^{\pm}\phi q'(\bar{q}')$, $\gamma q(\bar{q}) \to Z^0\phi q(\bar{q})$ and $g\gamma \to q\bar{q}\phi$ events is studied. This is done for all possible (massive) flavours of the quarks $q(q')$ and using photons generated via Compton back–scattering of laser light. We study signatures in which the Higgs decays to $b\bar{b}$–pairs and the electroweak vector bosons $W^{\pm}$ and Z^0 decay either hadronically or leptonically. All possible backgrounds to these signals are also computed.

Acknowledgments

To Mum and Dad

Declaration

I declare that no material in this thesis has previously been submitted for a degree at this or any other university.

The research described in Chapters 4 and 5 has been carried out in collaboration with Prof. W.J. Stirling and Chapter 7 with Stefano Moretti. Parts of this thesis have been summarised in the following papers

1. Soft photon radiation in $e^+e^- \to t\bar{t} \to b\bar{b}W^+W^-$, G. Abu Leil, Mod. Phys. Lett. **A8**: 1191-1204, 1993.

2. Soft photon radiation and anomalous couplings in $e^+e^- \to W^+W^-$ at LEP-II, Ghadir Abu Leil and W.J. Stirling, Phys. Rev. **D49**: 3751-3754, 1994.

3. Anomalous quartic couplings in $W + W - \gamma$ production at e+ e- colliders, Ghadir Abu Leil and W.J. Stirling, J. Phys. G: Nucl. Part. Phys. **21**: 517-524, 1995.

4. The intermediate mass SM Higgs boson at LEP⊗LHC *ep* collider, Ghadir Abu Leil and Stefano Moretti, Durham University Center for Particle Physics preprint DTP-94-46.

The copyright of this thesis rests with the author.

Contents

Chapter 1

Introduction

Throughout the centuries man has striven to understand the world around him. In his quest for knowledge and in his effort to solve the ultimate puzzle, "Of what is matter made?", many theories have been proposed. Among the first was the ancient Greek theory by Anaximenes of Miletus [1] which states that the world is made of four fundamental elements: air, water, fire and earth; combinations of and interactions between these four elements are the cause of everything that exists. With the benefit of hindsight we can see that this theory contained the ideas of what we call chemistry. Anaximenes's theory was, in the Greek tradition, based on pure thought. Only with the advent of controlled experiments, many centuries later, were these theories developed into modern science. In particular, the work by Mendeleev in classifying the elements into the periodic table was an important step forward. Although this was far too complicated to be the "theory of everything", it did, however, hint at some underlying, more fundamental, theory.

A decade later, in 1897, continued investigation by J. J. Thomson led to the discovery of the electron. Then came Rutherford's famous α–particle experiments which led to the discovery of the structure of the atom, ultimately leading to the identification of the proton, the neutron and the birth of nuclear physics. Then a whole plethora of hadrons were discovered in the cosmic ray experiments.

This is a very sketchy history in which a lot of important steps have been missed out; a more rigorous history can be found in [2] for example.

This now brings us to the last 100 years: the immediate history of particle physics. Particle physics has two questions to answer: the age old question "What
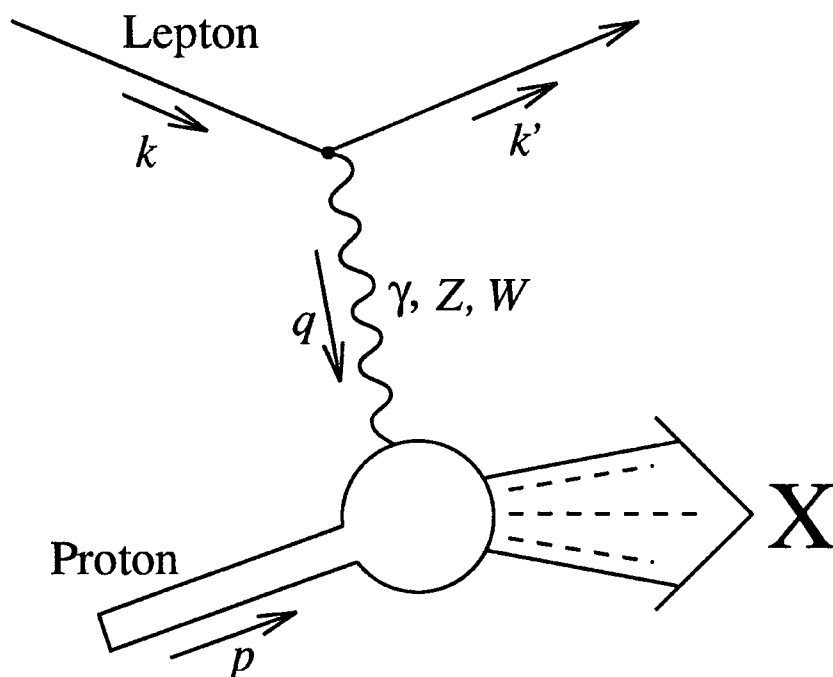
Figure 1.1: Deep inelastic experiment where a proton is hit by a lepton.

are matter's fundamental building blocks, and "How do these building blocks interact to give everything we see, i.e., what are the forces in nature?"

The particle physicists of today believe that they have gone a long way to solve these questions. Just as Rutherford and his colleagues performed experiments on the atom and found it has structure, particle physicists today perform similar experiments in principle. In these deep inelastic scattering experiments a proton is hit by a high energy lepton which emits a virtual photon, a W or a Z boson with high enough energy to probe the proton. They saw that the proton has structure. They found point–like objects that are structureless at the smallest distances probed by the highest energy particle accelerators. These were called the quarks.

The most popular theory today is that there are two types of matter units: Quarks and Leptons. They both have spin 1/2 in $\hbar$ units. The quarks are the fermionic constituents of hadrons and the building blocks for the proliferation of mesons and baryons seen in the experiments. The lepton, however, is the term used for describing the electron, the neutrino and the particles that are direct generalisations of the electron [1].

THE FUNDAMENTAL FERMIONS –

LEPTONS AND QUARKS

Particle	Symbol	Charge (e)	Mass (GeV/c^2)
Electron	e^-	-1	$5.1099906(15) \times 10^{-4}$
e-Neutrino	ν_e	0	$< 5.1 \times 10^{-9}$
Muon	μ^-	-1	$0.105658389(34)$
μ-Neutrino	ν_μ	0	$< 2.7 \times 10^{-4}$
Tau	τ^-	-1	$1.7771(5)$
τ-Neutrino	ν_τ	0	$< 3.1 \times 10^{-2}$
Down	d	$-\frac{1}{3}$	0.010 ± 0.005
Up	u	$\frac{2}{3}$	0.005 ± 0.003
Strange	s	$-\frac{1}{3}$	0.2 ± 0.1
Charm	c	$\frac{2}{3}$	1.3 ± 0.3
Bottom	b	$-\frac{1}{3}$	4.3 ± 0.2
Top	t	$\frac{2}{3}$	$176 \pm 8 \pm 10$

Table 1.1

THE FUNDAMENTAL BOSONS

Particle	Symbol	Spin	Charge (e)	Mass (GeV/c^2)
Photon	γ	1	0	0
Neutral weak boson	Z	1	0	91.1888(44)
Charged weak bosons	$W^{\pm}$	1	± 1	80.23(18)
Gluons	$g_1, ..., g_8$	1	0	0
Higgs	H	0	0	> 64.3
Graviton	G	2	0	0

Table 1.1(cont.) The fundamental particles of the Standard Model. The masses are given in the usual particle physics units of 1 GeV/c^2 = 1.782676 × 10^{-27} kg. The lepton masses are from the PDG (1994) and the quark masses are "current" masses.

Let us turn our attention now to the second question: the forces between the particles. We believe that there are four forces in the universe. One of the first forces to be discovered and to be quantified classically, by Newton, is gravity. Gravity acts on all objects and has a very large range, and although this was the case, Newton could not see how the interaction took place, i.e., "the dynamics of it" (letter from Newton to Bently) [3]. Then came electromagnetism that was quantified and described fully by Maxwell's equations and was endorsed by the discovery of the electron and its recognition as the unit of electricity. This force again acts at large distances and again the dynamical question of how the interaction could be mediated at a distance led to hypotheses such as the Ether (an amazing medium for transferring the mechanical motion). In Newtonian physics the equations of motion are postulated and the forces are inputs in the equations. Maxwell, however, dropped all the Ether theories and allowed his equations to stand on their own. We would like an approach that incorporates both particles and fields that also explains how particles and fields interact. Later these problems were solved by the field theory approach and quantum mechanics [3].

Today particle physicists believe that there are two more forces, the weak force and the strong force. Unlike the electromagnetic interactions that have infinite range (since the photon is massless) both of these forces have a very small range, the weak force having a range of $\frac{1}{M_W}$ and the strong force a range of $\frac{1}{m_\pi}$. The weak force is what is responsible for the nucleus decaying, the familiar β decay: $n \rightarrow p + e^- + \bar{\nu}_e$ with a lifetime of 15 minutes. It is only weak with respect to the electromagnetic force if they are compared for long range and at low energies. The strong force is the force that binds the constituents of the nucleus together.

Let us now focus our attention on the dynamics question: (i.e. how are the forces mediated?). Particle physicists believe that they are mediated by gauge bosons: the photon, the Z and W particles and the gluon. Their belief was justified when the W, Z were discovered in $p\bar{p}$ colliders and the gluon in e^+e^- collisions. This turns out to be closely related to a symmetry principle which in turn is related to a conservation law which is discussed in the next chapter.

Can this be the whole picture, is this the "theory of everything"? In order to test the "Standard Model" (SM), particle physicists perform measurements of

5

the fundamental particle properties (mass, lifetime, etc.) and interactions to high precision at high energy colliders, e.g., the $p\bar{p}$, e^+e^- and ep colliders. Some of these colliders are listed in Table (1.2). The aim of these precision measurements is to look for deviations from the SM predictions. This is important since this means that precision measurements performed at low energies can test for new physics at a higher energy scale. The following are examples that are of interest with respect to this thesis.

In the SM the W boson is a fundamental particle. Due to its charge, the W boson interacts with the photon; this interaction is predicted exactly by the SM. If the W boson is not fundamental but has some structure (a composite object) this will manifest itself in the $W\gamma$ interaction since at high enough energy (small enough range) we will start to see deviations from the point–like structure. So, one way of testing this theory is by measuring the $WW\gamma$ coupling precisely. This can be done, for example, using the LEP II e^+e^- collider which is expected to be running in the next few years. In chapters four and five a description of how this can be achieved is given. Another example is the top quark which has recently been discovered by the CDF and D0 collaborations in $p\bar{p}$ collisions at 1.8 TeV[4]. It is an important discovery as the top quark was predicted before its detection. It is again crucial to measure its properties such as mass, lifetime, charge and spin to check that it is indeed the sixth SM quark as predicted. In chapter six we describe one way of doing this by analysing the radiation pattern off top quark production and decay at the future NLC.

Finally, the Higgs sector of the SM is important, as the Higgs mechanism is possibly what generates the fundamental particle masses and again Higgs discovery is crucial. A lot of effort has been and will be devoted to this for the future e^+e^- and $p\bar{p}$ experiments. Less well studied is Higgs production in ep collisions which is the subject of chapter seven.

Some High Energy Colliders		
Collider	Reaction	$\sqrt{s}$(GeV)
LEP I	e^+e^-	≈ 90
LEP II	e^+e^-	< 200
Fermilab Tevatron	$p\bar{p}$	1.8×10^3
LHC	$p\bar{p}$	$(10 - 14) \times 10^3$
HERA	ep	314
NLC	e^+e^-	300-2000

Table 1.1 Some high energy colliders which are either planned or are already running.

Chapter 2

The Standard Model

In Quantum Field Theory the field equations of a system specified by several fields $\phi_i(x)$, where x is the space–time four–vector and a Lagrangian density $\mathcal{L}$ (the kinetic term minus the potential energy per unit volume) can be derived from the action

$$S = \int d^4x \mathcal{L} \tag{2.1}$$

by imposing the principle of least action

$$\delta S = 0 , \tag{2.2}$$

which gives the equations of motion, the Euler-Lagrange equations

$$\frac{\partial \mathcal{L}}{\partial \phi_i} - \partial_\mu \frac{\partial \mathcal{L}}{\partial[\partial_\mu \phi_i]} = 0 \tag{2.3}$$

with $\partial_\mu \phi = \frac{\partial \phi}{\partial x^\mu}$.

Symmetries are very important in physics, since they manifest themselves in conservation laws which can be tested experimentally. "A symmetry operation [transformation] is what you perform on an object [wave function, field] that leaves it unchanged [invariant] under the operation." [5].

Let ϕ be one of those fields and let us vary ϕ such that

$$\phi \to \phi' = \phi + \delta\phi . \tag{2.4}$$

The change in the Lagrangian is given by

$$\delta\mathcal{L} = \frac{\partial \mathcal{L}}{\partial \phi}\delta\phi + \frac{\partial \mathcal{L}}{\partial \partial_\mu \phi}\delta\partial_\mu \phi = \partial_\mu[\frac{\partial \mathcal{L}}{\partial(\partial_\mu \phi)}\delta\phi] . \tag{2.5}$$

8

Now for the Lagrangian to stay invariant under the transformation there must be a conserved "symmetry" current J_μ such that

$$\partial^\mu J_\mu = 0 \ , \tag{2.6}$$

where

$$J^\mu = \frac{\partial \mathcal{L}}{\partial [\partial_\mu \phi]} \delta \phi \ ; \tag{2.7}$$

and the conserved quantity (charge Q) here is

$$Q = \int d^3 x J_0 \ . \tag{2.8}$$

Nature seems to make use of certain special types of symmetries and this prompted theorists to look at a class of transformations where the fields transform under a continuous unitary phase U which is a representation of some symmetry group G. In particular we require such a transformation to commute with the Hamiltonian, so $[U, H] = 0$. If G is a Lie group, then

$$U = exp[i \sum_{i=1}^{i=n} T_i \alpha_i(x)] \tag{2.9}$$

where $\alpha_i(x)$ is a continuous parameter which is a function of space–time and T_i are the generators of the group with

$$[T_i, T_j] = i C_{ijk} T_k \ , \tag{2.10}$$

where C_{ijk} are the structure constants of the group. Theories that are invariant under such transformations are called local gauge theories. If C_{ijk} is zero then we have an abelian gauge theory, otherwise the theory is called non-abelian. The groups we are interested in are the $U(1)$ abelian and $SU(2)$, $SU(3)$ non–abelian gauge groups which are related to the electroweak and the strong forces.

2.1   Gauge Invariance

If the Lagrangian[1] is invariant under a symmetry group then Noether's theorem states that the system has some conserved quantity.

---

[1] We use the term Lagrangian from now on to mean the Lagrangian density

2.1.1 Abelian Gauge

Let us consider Maxwell's theory of electromagnetism. When this theory is quantised it gives Quantum Electrodynamics or QED. In the following the $\mathcal{L}_{QED}$ will be derived from the gauge principle; and we will see that by imposing the requirement for "local" gauge invariance on a free Lagrangian we will get the interacting field theory of QED.

A free electron can be described by a wave function Ψ, under a unitary local phase change

$$\Psi \rightarrow e^{i\alpha(x)}\Psi$$
$$\bar{\Psi} \rightarrow e^{-i\alpha(x)}\bar{\Psi} \ , \tag{2.11}$$

where $\alpha(x)$ is a function of space time.

The Lagrangian for an electron with mass m (which satisfies the Dirac Equation, $(i\gamma^\mu\partial_\mu - m)\Psi = 0$) is given by

$$\mathcal{L} = \bar{\Psi}(i\gamma^\mu\partial_\mu - m)\Psi \ . \tag{2.12}$$

The above Lagrangian is invariant under the above transformation only if we introduce the covariant derivative D_μ to replace ∂_μ such that

$$D_\mu = \partial_\mu - ieA_\mu \tag{2.13}$$

with the covariant derivative transforming as

$$D_\mu\Psi \rightarrow e^{i\alpha(x)}D_\mu\Psi \tag{2.14}$$

and the field A_μ transforming as

$$A_\mu \rightarrow A_\mu + \frac{1}{e}\partial_\mu\alpha \ . \tag{2.15}$$

This group of transformations is called the $U(1)$ group and the field A_μ is the gauge field. The Lagrangian becomes

$$\mathcal{L} = \bar{\Psi}(i\gamma^\mu(\partial_\mu - ieA_\mu) - m)\Psi \tag{2.16}$$

which can also be written as

$$\mathcal{L} = \bar{\Psi}(i\gamma^\mu\partial_\mu - m)\Psi - A_\mu J^\mu \ . \tag{2.17}$$

10

The presence of the gauge field A_μ and its coupling to the electron is only due to requiring the invariance of the above Lagrangian under the $U(1)$ gauge group.

Treating the above field as a physical field of the photon, we have to introduce a kinetic term which is in turn invariant under the above transformation. Consider

$$(D_\mu D_\nu - D_\nu D_\mu) = ieF_{\mu\nu} \tag{2.18}$$

with

$$F_{\mu\nu} = \partial_\mu A_\nu - \partial_\nu A_\mu . \tag{2.19}$$

We introduce the gauge invariant kinetic term

$$\mathcal{L}_A = -\frac{1}{4}F_{\mu\nu}F^{\mu\nu} \tag{2.20}$$

such that the above choice enables Maxwell's equations to be derived from the following QED Lagrangian:

$$\mathcal{L}_{QED} = \bar{\Psi}(i\gamma^\mu D_\mu - m)\Psi - \frac{1}{4}F_{\mu\nu}F^{\mu\nu} . \tag{2.21}$$

Note here that we do not have a mass term for the field A_μ of the form

$$\mathcal{L}_m = \frac{1}{2}M_A^2 A_\mu A^\mu , \tag{2.22}$$

as such a mass term will not be invariant under the above gauge transformation (2.15).

For this Lagrangian to describe all the quark and lepton electromagnetic interactions we must consider the fermion wave function under the following local gauge transformation

$$\Psi \rightarrow \Psi' = e^{i\alpha(x)Q}\Psi . \tag{2.23}$$

Now Q is the generator of the $U(1)$ group and is identified as the electric charge. The interaction term now reads

$$J^\mu A_\mu = -e\bar{\Psi}\gamma^\mu Q\Psi A_\mu . \tag{2.24}$$

This, however, is not the whole story: the above field A_μ has four degrees of freedom; the physical photon however has only two. In practice we have to add gauge fixing terms to reduce the degrees of freedom to the physical ones such that the Feynman rules can be defined and we can then calculate scattering amplitudes, decay widths etc., see for example [6].

11

2.1.2 Non-Abelian Gauge

Let us now consider the $SU(2)$ gauge group. Let the fermion wave function be Ψ where Ψ is a column vector. The transformation is then

$$\Psi \rightarrow \Psi' = exp[i \sum_{i=1}^{3} \alpha_i(x) T_i] \Psi \ . \qquad (2.25)$$

The free fermion's Lagrangian is again

$$\mathcal{L}_f = i\bar{\Psi}\gamma^\mu \partial_\mu \Psi - m\bar{\Psi}\Psi \ . \qquad (2.26)$$

We proceed in a similar manner to that for the abelian case but now we consider infinitesimal phase transformations of the field

$$\Psi' = [1 + i\alpha_i(x) T_i]\Psi \ . \qquad (2.27)$$

Under the above transformation the change in the Lagrangian is

$$\delta\mathcal{L} = -\bar{\Psi}\gamma^\mu \sum_{i=1}^{3} T_i \partial_\mu \alpha_i \Psi \ . \qquad (2.28)$$

Again, as in the previous case, we introduce the covariant derivative D_μ which transforms as

$$D_\mu \rightarrow D'_\mu(\Psi') = e^{[i \sum_{i=1}^{3} \alpha_i(x) T_i]} D_\mu \Psi \ , \qquad (2.29)$$

where

$$D_\mu = \partial_\mu + ig \sum_{i=1}^{3} T_i W_\mu^i \ . \qquad (2.30)$$

Here g is the coupling and we have introduced the three gauge fields W_μ. The above fields under the above phase change transform according to

$$\vec{W}_\mu \rightarrow \vec{W}_\mu - \frac{i}{g}\partial_\mu\vec{\alpha} - \vec{\alpha} \times \vec{W}_\mu \ . \qquad (2.31)$$

Treating the above fields as physical fields, we will define the field strength $W_{\mu\nu}$ exactly as in QED so that

$$[D_\mu, D_\nu] = ig\vec{T}.\vec{W}_{\mu\nu} \qquad (2.32)$$

where the $SU(2)$ field strength is

$$\vec{W}_{\mu\nu} = \partial_\mu\vec{W}_\nu - \partial_\nu\vec{W}_\mu - g\vec{W}_\mu \times \vec{W}_\nu \ . \qquad (2.33)$$

12

Note the extra term due to the non–abelian nature of $SU(2)$. Thus the interaction Lagrangian is

$$\mathcal{L}_W = -\frac{1}{4} W^i_{\mu\nu} W^{\mu\nu}_i \ . \tag{2.34}$$

Expanding the above interaction term gives

$$\begin{aligned}
\mathcal{L}_W = & -\frac{1}{4}(\partial_\mu W^i_\nu - \partial_\nu W^i_\mu)(\partial^\mu W^\nu_i - \partial^\nu W^\mu_i) \\
& +\frac{g}{2}(\partial_\mu W^i_\nu - \partial_\nu W^i_\mu)\epsilon_{ijk} W^\mu_j W^\nu_k \\
& -\frac{g^2}{4}\epsilon_{ijk} W^\mu_j W^\nu_k \epsilon_{ilm} W^l_\mu W^m_\nu \ .
\end{aligned} \tag{2.35}$$

Here we have two more interactions that are not present in the QED case; the second term in the above interaction Lagrangian gives rise to the triple W vertex and the third term gives rise to the quartic W interaction vertex. Note that all of the W interactions have a universal coupling strength g. Here again the field is massless because a mass term of the form (2.22) is not invariant under the above gauge transformation.

So finally, the $SU(2)$ invariant Lagrangian is

$$\begin{aligned}
\mathcal{L} = & \ i\bar{\Psi}\gamma^\mu\partial_\mu\Psi - m\bar{\Psi}\Psi \\
& -g\sum_{i=1}^{3}\bar{\Psi}\gamma^\mu T_i W^i_\mu \Psi \\
& -\frac{1}{4}W^i_{\mu\nu} W^{\mu\nu}_i \ .
\end{aligned} \tag{2.36}$$

2.2 Weak Interactions

The ultimate aim of investigating the previous gauge groups is to arrive at a theory that describes the weak interactions as well as the electromagnetic ones. We have thus far established the suitability of the $U(1)$ gauge group for QED. Unfortunately $SU(2)$ as it stands is of no use for weak interactions. This is due to two reasons that will become clear in the following discussion. First, $SU(2)$ couples both left and right handed particles equally, thus conserving parity (spatial inversion $x \rightarrow -x$); and secondly, the gauge bosons in the above theory are still massless.

The earliest attempt to treat weak interactions was Fermi's four–point interaction. Fermi postulated in 1934 that β decay can be written in terms of an

13

interaction Lagrangian of the form

$$\mathcal{L}_{Fermi} = \frac{4}{\sqrt{2}} G_{fermi} J_\mu J^{+\mu} \qquad (2.37)$$

where the current J^μ can be written as

$$J^\mu \sim \bar{\Psi}\gamma^\mu\Psi \qquad (2.38)$$

where $G_{fermi} \approx 1.16 \times 10^{-5}~GeV^{-2}$ is a dimensionful constant. In this case the neutrino–electron pair act as single photon–like emission occurring at a single space–time point (the same as the electromagnetic current). By 1956, experiments on Co^{60} showed that parity is maximally violated in weak interactions [1] and that the four–point interaction only couple to left handed particles. Hence the form of the current should be changed to

$$J^\mu = \bar{\nu}_e\gamma^\mu(\frac{1-\gamma_5}{2})e + \cdots , \qquad (2.39)$$

where ... implies the sum over all fermionic families.

From the gauge theory perspective this means that the $SU(2)$ gauge transformations will only act on the left handed fields and not on the right handed ones[2].

This, however, is not enough, as $SU(2)$, even with the above modifications, still leaves us with massless gauge fields, while, experimentally it was found that Z, W fields are massive.

Fermi's four–point interaction, even with the previous changes, has major problems: it has bad high energy behaviour as it violates unitarity (which requires that physical observables such as cross sections have conserved probabilities). This is to say that the four–point interaction is non-renormalizable so, if one considers loop corrections, the addition to the lowest order cross-section will have the following behaviour [3]

$$G_{fermi}^2 \int \frac{d^4k}{k^2} . \qquad (2.40)$$

Now, if we introduce an ultra violet cut-off Λ, the integral will diverge as $G_{fermi}^2\Lambda^2$ and the situation will get even worse at each order of perturbation theory, as we will need an infinite number of parameters (from experiments) to cope with the divergences. This is therefore a very good reason to reject the four–point interaction as a fundamental process.

---

[2]see Electroweak Theory

14

2.3 The Standard Model

2.3.1 Electroweak Theory

A gauge theory for Electroweak interactions was proposed by Glashow, Salam and Weinberg [7]. It unifies both $SU(2)$ and $U(1)$ gauge groups with the following gauge transformations

$$\Psi_L \rightarrow \Psi'_L = exp\left[\ i\ g\ \alpha_i(x)T_i +\ i\ g'\beta(x)Y\right]\ \Psi_L$$
$$\Psi_R \rightarrow \Psi'_R = exp\left[\ i\ g'\ \beta(x)Y\right]\ \Psi_R \qquad (2.41)$$

with

$$\Psi_L = (\frac{1-\gamma_5}{2})\Psi$$
$$\Psi_R = (\frac{1+\gamma_5}{2})\Psi\ .$$

$$(2.42)$$

The left handed fermions form isospin doublets Ψ_L and the right handed fermions are isospin singlets Ψ_R. For example, $\begin{pmatrix} u \\ d \end{pmatrix}_L$ and $\begin{pmatrix} \nu \\ e \end{pmatrix}_L$ are in the doublet representation, while the right handed fermions u_R, d_R, and e_R, for example, are in the singlet representation. Note that the neutrino is only left handed and therefore is massless in the SM.

The fermions must therefore be massless in order to satisfy the above symmetry (2.41) [8] since a mass term for the fermion f of the form

$$m\bar{f}f = m(\bar{f}_L f_R + \bar{f}_R f_L) \qquad (2.43)$$

is not $SU(2)$ invariant as a product of a doublet and a singlet is not invariant under $SU(2)$ rotations. The operators T and Y are the generators of the $SU_L(2)$ and $U_Y(1)$ groups and g, g' are the respective couplings. They are related to the electromagnetic charge Q by

$$Q = T_3 + \frac{Y}{2}\ . \qquad (2.44)$$

The electroweak Lagrangian that is invariant under $(SU_L(2) \times U_Y(1))$ is then

$$\mathcal{L}_{EW} = \sum_{l,q} (i\bar{\Psi}_L \gamma^\mu [\partial_\mu + ig\vec{T}.\vec{W}_\mu + ig'\frac{Y}{2}B_\mu]\Psi_L$$

$$+ i\bar{\Psi}_R \gamma^\mu [\partial_\mu + ig'\frac{Y}{2}B_\mu]\Psi_R)$$

$$-\frac{1}{4}W^i_{\mu\nu}W^{\mu\nu}_i - \frac{1}{4}B_{\mu\nu}B^{\mu\nu} \qquad (2.45)$$

where B_μ is the field associated with $U_Y(1)$. The covariant derivative that is invariant under the $(SU_L(2) \times U_Y(1))$ is then

$$D_\mu = \partial_\mu + ig\vec{T}.\vec{W}_\mu + ig'\frac{Y}{2}B_\mu . \qquad (2.46)$$

This Lagrangian leaves us with the gauge fields and the fermions still massless, even though we know from experiments that they are massive.

2.4   Higgs Sector

There is a mechanism that will generate mass for both the gauge fields and the fermions while keeping the photon massless without spoiling the results we obtained from the gauge theories. This is called the Higgs mechanism [9]. It occurs whenever a vacuum of a quantum field theory does not respect a symmetry in the theory.

2.4.1   Spontaneous Symmetry Breaking

To illustrate the concept of Spontaneous Symmetry Breaking (SSB) and how the Higgs mechanism generates mass for the gauge bosons let us consider a local $U(1)$ gauge theory with a complex scalar field $\phi = \frac{1}{\sqrt{2}}(\phi_1 + i\phi_2)$. The Lagrangian is then

$$\mathcal{L} = \mathcal{L}_H = (D_\mu\phi)^\dagger (D^\mu\phi) - \mu^2\phi^\dagger\phi - \lambda(\phi^\dagger\phi)^2 - \frac{1}{4}F_{\mu\nu}F^{\mu\nu} . \qquad (2.47)$$

The above Lagrangian is symmetric when $\phi \to -\phi$. Let us now consider the potential

$$V(\phi) = \mu^2\phi^\dagger\phi + \lambda(\phi^\dagger\phi)^2 . \qquad (2.48)$$

For $\mu^2 > 0$ and $\lambda > 0$ the minimum of the potential is at $|\phi| = 0$ and the Lagrangian (2.47) is just the Lagrangian for a charged particle of mass μ. Now

consider $\mu^2 < 0$. In this case the minimum of the potential occurs when

$$|\phi| = \frac{v}{\sqrt{2}} = \sqrt{\frac{-\mu^2}{2\lambda}} . \qquad (2.49)$$

The vacuum has a non–zero expectation value and we have a ring of minima in the (ϕ_1, ϕ_2) plane with the same expectation values. The system, however, chooses one of these minima $\Phi(x)$ at random. Thus the vacuum of the theory no longer respects a symmetry of the theory, namely $\phi \to -\phi$. This is called SSB. In order to see how this will give rise to mass terms consider expanding around this minimum[3]

$$\Phi(x) = \frac{1}{\sqrt{2}}(v + \eta(x) + i\xi(x)) . \qquad (2.50)$$

This is, however, equivalent to a gauge transformation such that

$$
\begin{aligned}
\Phi(x) &\approx \frac{1}{\sqrt{2}}(v + \eta)exp\,[i\frac{\xi}{v}] \\
&= \frac{1}{\sqrt{2}}(v + h(x))exp\,[i\frac{\theta(x)}{v}] ,
\end{aligned}
\qquad (2.51)
$$

where $\theta(x)$ is chosen such that $h(x)$ is a real field. The field A_μ transforms as

$$A_\mu \to A_\mu + \frac{1}{ev}\partial_\mu\theta(x) . \qquad (2.52)$$

Now substituting the above into (2.47) gives

$$
\begin{aligned}
\mathcal{L} &= \frac{1}{2}(\partial_\mu h)^2 - \lambda v^2 h^2 + \frac{1}{2}e^2 v^2 A_\mu^2 - \lambda v h^3 - \frac{1}{4}\lambda h^4 \\
&\quad + \frac{1}{2}e^2 A_\mu^2 h^2 + v e^2 A_\mu^2 h - \frac{1}{4}F_{\mu\nu}F^{\mu\nu} .
\end{aligned}
\qquad (2.53)
$$

This Lagrangian describes two interacting massive particles: a vector gauge boson A_μ and a massive scalar h which is called the Higgs particle, with mass

$$M_h = \sqrt{2\lambda v^2} . \qquad (2.54)$$

Turning back to the case in hand, the Glashow–Salam–Weinberg model utilises the above Higgs mechanism. Thus a combination of ideas of gauge invariance plus SSB led to a unified theory of weak and electromagnetic interactions.

---

[3]as perturbative calculations involve expansions around a stable point.

2.4.2 Glashow–Salam–Weinberg Model

The $(SU(2) \times U(1))$ gauge invariant Higgs Lagrangian is

$$\mathcal{L}_H = (D_\mu \phi)^\dagger (D^\mu \phi) - \mu^2 \phi^\dagger \phi - \lambda (\phi^\dagger \phi)^2 \, , \tag{2.55}$$

where ϕ is a complex scalar SU(2) doublet of the form

$$\phi = \frac{1}{\sqrt{2}} \begin{pmatrix} \phi_1 + i\phi_2 \\ \phi_3 + i\phi_4 \end{pmatrix} \, . \tag{2.56}$$

We are interested in the case where $\mu^2 < 0$ and $\lambda > 0$; the potential then has a minimum at $|\phi|$ such that

$$|\phi| = \frac{v}{\sqrt{2}} = (\frac{-\mu^2}{2\lambda})^{\frac{1}{2}} \, . \tag{2.57}$$

Thus we can choose the particular vacuum to be

$$\Phi = \frac{1}{\sqrt{2}} \begin{pmatrix} 0 \\ v \end{pmatrix} \tag{2.58}$$

The above choice is a very special choice; it is chosen such that the vacuum does not break the $U(1)_{em}$ symmetry. The above choice has $T_3 = -\frac{1}{2}$ and $Y = 1$ so the generator of $U(1)_{em} Q$ remains unbroken and $Q\Phi = 0$. In order to see how this SSB gives rise to gauge boson masses and coupling to the Higgs, we expand around the minimum

$$\phi(x) = \begin{pmatrix} 0 \\ v + h(x) \end{pmatrix} \tag{2.59}$$

and substitute into the Lagrangian. The relevant terms are

$$
\begin{aligned}
|D_\mu \phi|^2 &= \left| (ig\vec{T}.\vec{W}_\mu + ig'\frac{Y}{2}B_\mu)\frac{1}{\sqrt{2}} \begin{pmatrix} 0 \\ v + h \end{pmatrix} \right|^2 \\
&= \frac{g^2 v^2}{8}(W_\mu^1 W_1^\mu + W_\mu^2 W_2^\mu) + \frac{v^2(g^2 + g'^2)}{8} \left| \frac{W_\mu^3 g - g' B_\mu}{\sqrt{g^2 + g'^2}} \right|^2 \\
&\quad + interaction\ term \\
&\equiv \frac{1}{2}M_W^2 W_\mu^+ W_-^\mu + \frac{1}{2}M_Z^2 Z_\mu Z^\mu + \frac{1}{2}M_A^2 A_\mu A^\mu \\
&\quad + interaction\ term
\end{aligned}
\tag{2.60}
$$

18

where

$$W_\mu^+ = \frac{1}{\sqrt{2}}(W_\mu^1 - iW_\mu^2) \ ,$$

$$W_\mu^- = \frac{1}{\sqrt{2}}(W_\mu^1 + iW_\mu^2) \ ,$$

$$Z_\mu = \frac{W_\mu^3 g - g' B_\mu}{\sqrt{g^2 + g'^2}}$$

$$= W_\mu^3 \cos\theta_w - B_\mu \sin\theta_w \ ,$$

$$A_\mu = \frac{W_\mu^3 g' + g B_\mu}{\sqrt{(g^2 + g'^2)}}$$

$$= W_\mu^3 \sin\theta_w + B_\mu \cos\theta_w \ , \tag{2.61}$$

with

$$M_W = \frac{gv}{2} \ ,$$

$$M_Z = \frac{v}{2}\sqrt{g^2 + g'^2} \ ,$$

$$M_A = 0 \ . \tag{2.62}$$

Note that $M_A = 0$ is a consequence of the vacuum choice as the gauge bosons related to an unbroken symmetry remain massless and the electric charge operator leaves the vacuum unchanged.

The Weinberg angle θ_w is defined as

$$\frac{g'}{g} = \tan\theta_w \ . \tag{2.63}$$

The interaction terms are

$$interaction\ terms = gM_W h W_\mu^+ W_-^\mu + (g^2 + g'^2)\frac{M_Z}{2} h Z_\mu Z^\mu$$

$$+ \frac{g^2}{4} h^2 W_\mu^+ W_-^\mu + \frac{\sqrt{(g^2 + g'^2)}}{8} h^2 Z_\mu Z^\mu \ , \tag{2.64}$$

with the first two terms giving rise to the triple HWW, HZZ vertices respectively and the third and last term giving rise to the quartic ones. Next, we want to see how the fermion masses are generated and what the fermion couplings to the Higgs and the gauge bosons are. Let us start with the fermionic masses and couplings

19

to the Higgs: the relevant part of the Lagrangian after SSB is then

$$\frac{-H_f}{\sqrt{2}}\left[\bar{\Psi}_L(v+h)\Psi_R + \bar{\Psi}_R(v+h)\Psi_L\right] =$$

$$\frac{-H_f v}{\sqrt{2}}(\bar{\Psi}_L\Psi_R + \bar{\Psi}_R\Psi_L) + \frac{-H_f h}{\sqrt{2}}(\bar{\Psi}_L\Psi_R + \bar{\Psi}_R\Psi_L) \ , \qquad (2.65)$$

where H_f is an arbitrary coupling constant, so the mass of the fermion is now

$$m_f = \frac{H_f v}{\sqrt{2}} \qquad (2.66)$$

and the coupling of the Higgs to the fermion is now proportional to the mass of the fermion. Finally, let us see what the boson coupling is to the fermions. The relevant part of the Lagrangian is

$$\begin{aligned}
\mathcal{L} &= \sum_{l,q}\left(i\bar{\Psi}_L\gamma^\mu\left[\partial_\mu + ig\vec{T}.\vec{W}_\mu + ig'\frac{Y}{2}B_\mu\right]\Psi_L\right.\\
&\quad \left. + i\bar{\Psi}_R\gamma^\mu\left[\partial_\mu + ig'\frac{Y}{2}B_\mu\right]\Psi_R\right)\\
&= \frac{-g}{\sqrt{2}}\bar{u}_L\gamma^\mu W_\mu^+ d_L + \frac{g}{\sqrt{2}}\bar{d}_L\gamma^\mu W_\mu^- u_L\\
&\quad - g\bar{\Psi}_L\gamma^\mu T_3(\cos\theta_w Z_\mu + \sin\theta_w A_\mu)\Psi_L\\
&\quad - g'\bar{\Psi}_L\gamma^\mu(Q - T_3)(-\sin\theta_w Z_\mu + \cos\theta_w A_\mu)\Psi_L\\
&\quad - g'\bar{\Psi}_R\gamma^\mu(Q - T_3)(-\sin\theta_w Z_\mu + \cos\theta_w A_\mu)\Psi_R \ , \qquad (2.67)
\end{aligned}$$

with the first two terms being the flavour changing charged currents and the last three are neutral currents. The Z boson interaction, for example, can be written as

$$\mathcal{L}_{Zff} = \frac{-g}{\cos\theta_w}\bar{\Psi}\gamma^\mu Z_\mu(V + A\gamma_5)\Psi \qquad (2.68)$$

with

$$\begin{aligned}
V &= \frac{T_3}{2} - Q\sin^2\theta_w \ ,\\
A &= -\frac{T_3}{2} \ , \qquad (2.69)
\end{aligned}$$

where V is called the vector coupling and A the axial vector coupling.

Finally, all the masses and couplings have been generated in the GSW model. The only sector that has not been mentioned yet is the strong interactions sector, QCD. The gauge group relevant to this sector is $SU(3)$. This is a non–abelian

20

gauge group with eight massless gauge bosons, the gluons. Let the fermion wave function transfer as follows under a rotation in colour space:

$$\Psi \rightarrow exp\ [i\vec{T}.\vec{\alpha(x)}]\Psi \qquad (2.70)$$

with the generators of the group obeying

$$[T_i, T_j] = i\ f_{ijk}T_k \ . \qquad (2.71)$$

Again, in order to restore gauge invariance for the free fermion Lagrangian (see (2.12)), we need to introduce the covariant derivative

$$D_\mu = \partial_\mu + i\ g_s \sum_{i=1}^{8} T_i G_\mu^i \ , \qquad (2.72)$$

where g_s is the strong coupling constant and G_μ^i are the eight gluon fields with

$$G_\mu^i \rightarrow G_\mu^i - \frac{1}{g_s}\partial_\mu \alpha_i - f_{ijk}\alpha_j G_\mu^k \ . \qquad (2.73)$$

Treating the above as a physical field, we introduce a kinetic term as before such that

$$G_{\mu\nu}^i = \partial_\mu G_\nu^i - \partial_\nu G_\mu^i - g_s f_{ijk}G_\mu^j G_\nu^k \ ; \qquad (2.74)$$

so now

$$
\begin{aligned}
\mathcal{L}_{QCD} &= \bar{\Psi}(i\gamma^\mu \partial_\mu - m)\Psi \\
&\quad -g_s \sum_{i=1}^{8} \bar{\Psi}\gamma^\mu T_i G_\mu^i \Psi \\
&\quad -\frac{1}{4}G_{\mu\nu}^i G_i^{\mu\nu} \ .
\end{aligned}
\qquad (2.75)
$$

The above Lagrangian describes a self interacting theory with three and four gluon vertices.

The gluons hold quarks together into colourless hadrons by mediating the colour force. Due to the fact that the renormalised coupling $g_s^2(\mu^2) \rightarrow 0$ as μ^2 (the renormalisation scale) $\rightarrow \infty$ as we probe the hadrons at high energies the quarks behave as if they are free (asymptotic freedom). At large distances (effectively $\mu^2 \rightarrow 0$) we have $g_s^2(\mu^2) \rightarrow \infty$ which leads to the confinement of quarks and gluons inside the hadrons (infra–red slavery). This is to be contrasted with QED where $e_{em}^2(\mu^2) \rightarrow \infty$ as $\mu^2 \rightarrow \infty$, i.e., the coupling gets stronger at short distances.

21

The Standard Model of Particle Physics is then a partially unified quantum gauge field theory for the electromagnetic and the weak interactions which exhibits a broken $SU(2)_L \times U(1)$ symmetry together with $SU(3)$ symmetric QCD for strong interactions.

2.5   Beyond the SM

Although the SM has so far predicted the outcome of experiments successfully, the prevailing wisdom is that it cannot be the whole story. Sooner or later a more elegant theory will replace the SM. The motivations for going beyond the SM are abundant and we will only list some of them. The most obvious is the fact that the SM has a large number of arbitrary parameters, including the masses of the particles and the strength of their interactions, which are inputs to the theory and therefore must be obtained from the experiments. The SM does not explain the repetition in the fermionic families. Other criticisms of the SM are the facts that the Higgs sector is added by hand and that gravitational interactions are not included in the theory. Some theories are proposed as alternatives to the SM, such as SUSY, technicolour and compositeness. There are two ways to test for physics beyond the SM and thus test these theories, the most obvious of these being the discovery of new particles. There is, however, another way: performing precision measurements on the couplings, the mass and other particle properties will also at least hint at the existence of new physics beyond the SM. For example, the LEP I e^+e^- collider has been running for a few years as a Z factory through the reaction $e^+e^- \rightarrow Z \rightarrow f\bar{f}$, which has enabled tests to be performed on the $Zf\bar{f}$ couplings. So far, there is no evidence of new physics beyond the SM (the mass of the top from radiative corrections is in beautiful agreement with the measured CDF and D0 value). In the same way that LEP I is a Z factory, LEP II will be a W factory through the reaction $e^+e^- \rightarrow W^+W^-$ and again W couplings to γ and Z will be able to be measured to high precision. Anomalous couplings are a model independent way of performing this measurement, where the most general $W^+W^-\gamma$ vertex is assumed and the experimental result is compared to the SM prediction.

2.6 This Thesis

Throughout this thesis we test aspects of the Standard Model (SM) at future high energy colliders. We start by examining the SU(2)× U(1) non–abelian nature of the SM. We consider the effect of anomalous couplings on the reaction $e^+e^- \rightarrow W^+W^-\gamma$, at $\sqrt{s} = 200$ GeV, where the photon is soft. We show that the dependence on the anomalous couplings is of the same order as, but different from, the dependence of the leading order $e^+e^- \rightarrow W^+W^-$ cross section. We therefore argue that the two processes are complementary in providing precision tests of the Standard Model electroweak vertices. We also study the same process, $e^+e^- \rightarrow W^+W^-\gamma$, at high-energy e^+e^- colliders to investigate the effect of genuine quartic $W^+W^-\gamma\gamma$ and $W^+W^-Z\gamma$ anomalous couplings on the cross section. Deviations from the Standard Model predictions are quantified. We show how bounds on the anomalous couplings can be improved by choosing specific initial state helicity combinations. The dependence of the anomalous contributions on the collider energy is studied.

It is important to establish that the quark recently discovered by the CDF and D0 experiments is indeed the sixth quark of the SM. One way of doing this is to perform precision measurements which are sensitive to its mass, width, charge, etc. An example is provided by the study of soft photon radiation in $e^+e^- \rightarrow t\bar{t} \rightarrow bW^+\bar{b}W^-$. The radiation pattern is shown to depend sensitively on the top mass, width and energy, as well as the relative orientation of the initial and final state particles. Optimum conditions, in which initial state radiation is minimised and the radiation pattern has the richest structure, are discussed. Finally, we visit the Higgs sector of the SM, where the production of the SM Higgs ϕ with intermediate mass at the next proposed CERN LEP⊗LHC ep collider in $\gamma q(\bar{q}) \rightarrow W^\pm \phi q'(\bar{q}')$, $\gamma q(\bar{q}) \rightarrow Z^0 \phi q(\bar{q})$ and $g\gamma \rightarrow q\bar{q}\phi$ events is studied. This is done for all possible (massive) flavours of the quarks $q(q')$ and using photons generated via Compton back–scattering of laser light. We study signatures in which the Higgs decays to $b\bar{b}$–pairs and the electroweak vector bosons $W^\pm$ and Z^0 decay either hadronically or leptonically. All possible backgrounds to these signals are also computed.

Chapter 3

W Physics

The discovery in 1983 of the W and Z weak bosons provided dramatic confirmation of the GSW model. This led to an increased interest in W and Z physics. The aim of this chapter is to introduce W phenomenology, the essence of which is to test the SM predictions, where the W properties are measured to high precision. This includes, first, measuring the mass of the W and comparing the predicted mass with the precise measurement, as well as performing precision tests on the structure of the $W f \bar{f}$ interactions in both W production and decay; and, secondly, testing the trilinear and quadrilinear $WW\gamma$, WWZ, $WW\gamma\gamma$ and $WWZ\gamma$ interaction vertices. The mass and the coupling are already very well tested at $p\bar{p}$ colliders, for example, but so far there have been no precision tests of the W interaction with the other gauge bosons. Let us start by considering the Electroweak Lagrangian(2.67). This can be written as

$$\mathcal{L} = i\bar{\Psi}\gamma^\mu [\, eQA_\mu \;+\; \frac{e(1-\gamma_5)}{2\sqrt{2}\sin\theta_W}(T^+W_\mu^+ + T^-W_\mu^-)$$
$$+\; \frac{e}{\sin\theta_W \cos\theta_W}(\frac{1}{2}(1-\gamma_5)T^3 - Q\sin^2\theta_W)Z_\mu \,]\,\Psi \; . \quad (3.1)$$

From the above Lagrangian, the coupling of the W to the fermions is the same for all flavours. It has a distinctive feature in that it exhibits a V–A structure:

$$\frac{e}{\sqrt{2}\sin\theta_W}\left[W_\mu^-\bar{u}_e\gamma^\mu\frac{(1-\gamma_5)}{2}u_\nu + W_\mu^+\bar{u}_\nu\gamma^\mu\frac{(1-\gamma_5)}{2}u_e\right] \; . \quad (3.2)$$

This is very well tested in $p\bar{p}$ colliders where the dominant W production mechanism is

$$u\bar{d} \to W^+ \; ,$$

$$d\bar{u} \to W^- \; .$$

Then the W decays either leptonically or hadronically into its various decay channels:

$$W \to l\nu_l \ ,$$

$$W \to q\bar{q}' \ .$$

The cleanest W detection signal comes from the following leptonic decay modes

$$W \to e\nu_e \ ,$$

$$W \to \mu\nu_\mu \ .$$

The W signature from the above decay modes is a single charged lepton balanced by missing transverse energy from the undetected neutrino. From the lepton spectrum the mass of the M_W is fitted and the result is in excellent agreement with the prediction. This is important as measuring the mass of the W boson (M_W) is a test of the radiative corrections to the electroweak theory [10], since in the SM

$$
\begin{aligned}
M_W &= M_Z \cos\theta_w \\
&= \frac{M_Z}{\sqrt{2}} \left[1 + (1 - \frac{4\pi\alpha_{em}}{\sqrt{2}M_Z^2 G_{fermi}(1 - \Delta r)})^{\frac{1}{2}} \right]^{\frac{1}{2}} \ ,
\end{aligned}
\tag{3.3}
$$

where Δr is the term that arises from the radiative corrections. It depends strongly on the mass of the top and weakly on the mass of the Higgs, see for example [11].

Another important measurement that can be performed on the reaction $d\bar{u} \to e\nu_e$ is to do with testing the V–A structure of the coupling. In the SM the W couples to negative helicity fermions and positive helicity anti–fermions. Thus the conservation of angular momentum, for instance, implies that the electron prefers the direction of the incoming quark. This forward backward asymmetry will show up in the angular distribution of the outgoing lepton. The data turn out to be consistent with the V–A hypothesis [11].

The other important issue in W phenomenology is the triple and quartic gauge boson vertices. Since the non–abelian nature of the $SU(2) \times U(1)$ gauge group

not only predicts but also fixes the above vertices, these couplings stem from the kinetic term in the Lagrangian and are all proportional to one overall coupling g. Fig. (3.1) shows some of the SM vertices and their coupling constants. As we have already mentioned, the first three of these are very well tested at LEP I and at the $p\bar{p}$ colliders, for example, whereas the others are not directly tested yet. The direct measurement is important in order to verify the nature of the coupling, and this is the purpose of the next two chapters.

The CERN e^+e^- machines are excellent colliders with which to investigate W and Z physics. LEP II will act as a W factory through the reaction $e^+e^- \rightarrow W^+W^-$ in the same way that LEP I is a Z factory. One of the main physics objectives of LEP II is to investigate the reaction $e^+e^- \rightarrow W^+W^-$ to study the W mass, width and decay channels but, most importantly, the γWW and the ZWW couplings in order to confirm (or reject) the non-abelian nature of the electro-weak interactions directly [12]. This study of the three boson interaction is a very important test of the non-abelian nature of the gauge group, independently of all other tests. Fig. (3.2) shows the three Feynman diagrams that contribute to the production cross-section. The non-abelian nature of $SU(2) \times U(1)$ predicts definite relations between the above s- and t-channel diagrams, since it predicts the exact nature of the couplings. Each of these diagrams is divergent on its own (i.e., $s \rightarrow \infty$), with the ν_e exchange diagram giving the largest contribution [12]. The lowest order production cross-section σ_0 is given by [13]

$$
\begin{aligned}
\sigma_0 =\; & \frac{\pi\alpha^2}{4s\sin^4\theta_w}\left[W_1(r_w) + \frac{1 - 2\sin^2\theta_w}{r_z - 1}W_2(r_w) \right. \\
& \left. +\; \frac{1 - 4\sin^2\theta_w + 8\sin^4\theta_w}{(r_z - 1)^2}W_3(r_w) \right]
\end{aligned}
\tag{3.4}
$$

with

$$
\begin{aligned}
s &= (p_1 + p_2)^2, \\
r_w &\equiv \frac{s}{M_W^2}, \\
r_z &\equiv \frac{s}{M_Z^2}, \\
W_1 &\equiv (1 + \frac{2}{r_w} + \frac{2}{r_w^2})ln(\frac{1+\beta}{1-\beta}) - \frac{5}{4}\beta, \\
W_2 &\equiv \frac{4}{r_w}(1 + \frac{1}{2r_w})ln(\frac{1+\beta}{1-\beta}) - \frac{1}{12}\beta r_w(1 + \frac{20}{r_w} + \frac{12}{r_w^2}),
\end{aligned}
$$

26

$$W_3 \equiv \frac{1}{48}\beta^3 r_w^2 (1 + \frac{20}{r_w} + \frac{12}{r_w{}^2}) \, ,$$

$$\beta \equiv \sqrt{(1 - \frac{4M_W^2}{s})} \, , \qquad\qquad (3.5)$$

where p_1, p_2 are the W^+, W^- momenta. In fact the cancellations among these diagrams [12] mean that the W production cross-section has good high energy behaviour. The above cross-section then directly tests the gauge structure of the relevant vertices.

3.1 The Anomalous Vertex

The magnetic moment of a particle shows up in its scattering in a magnetic field. In field theory this is reduced to evaluating a tree level Feynman diagram [5]. Fig. (3.3) shows the diagram for evaluating the magnetic moment of the W boson. In the SM the magnetic moment of the W is $\mu = e/M_W$. The loop diagrams of Fig. (3.4) give the higher order corrections to μ, see section(4.1). Deviations from the SM value, the so called "anomalous magnetic moment" could signal new physics beyond the SM. One method of calculating the anomalous magnetic moment is the effective Lagrangian method, in which the tree level diagram is evaluated, but new interaction terms, which modify the SM ones, have to be added to the Lagrangian [14]. This is a model independent way of introducing such effects.

Anomalous couplings are conventionally introduced by considering the most general Lorentz-, C- , P- and $U(1)$ gauge invariant electroweak boson interaction Lagrangian. Details can be found, for example in Ref. [15]. The anomalous couplings are then defined by

$$g_{WWV}^{-1} \, \Delta\mathcal{L}_{\text{anom}} = i(\kappa_v - 1)\mathcal{W}_\mu^+ \mathcal{W}_\nu \mathcal{V}^{\mu\nu} + i\frac{\lambda_v}{M_W^2} G_{\lambda\mu} G^{+\mu\nu} \mathcal{V}_\nu^\lambda \, , \qquad (3.6)$$

where $\mathcal{V}^\mu$ is either the Z or the γ field, $\mathcal{W}^\mu$ is the W^- field, $\mathcal{W}_{\mu\nu} = \partial_\mu \mathcal{W}_\nu - \partial_\nu \mathcal{W}_\mu$, $\mathcal{V}_{\mu\nu} = \partial_\mu \mathcal{V}_\nu - \partial_\nu \mathcal{V}_\mu$ are the corresponding field strengths and $G_{\mu\nu} = \mathcal{W}_{\mu\nu} - ie(A_\mu \mathcal{W}_\nu - \mathcal{W}_\mu A_\nu)$, with A_μ being the photon field. The above Lagrangian has operators of dimensions four and six.

The overall coupling constants can be fixed such that the W charge is defined.

Without loss of generality, the couplings are

$$g_{WW\gamma} = -e ,$$
$$g_{WWZ} = -e \cot\theta_W , \tag{3.7}$$

where e denotes the positron charge and θ_w the Weinberg angle.

The SM values of the parameters are

$$\kappa_z = \kappa_\gamma = 1 ,$$
$$\lambda_z = \lambda_\gamma = 0 , \tag{3.8}$$

κ_γ is conventionally called the anomalous magnetic moment of the W. The couplings κ_γ and λ_γ are related to the magnetic moment μ_W and the electric quadrupole moment Q_W of the W^+ by

$$\mu_W = \frac{e}{2M_W}(1 + \kappa_\gamma + \lambda_\gamma) ,$$
$$Q_W = -\frac{e}{M_W^2}(\kappa_\gamma - \lambda_\gamma) . \tag{3.9}$$

In the next chapter we will examine the above triple vertex as well as the anomalous ZWW one using a general coupling of two charged vector bosons with a neutral vector boson .
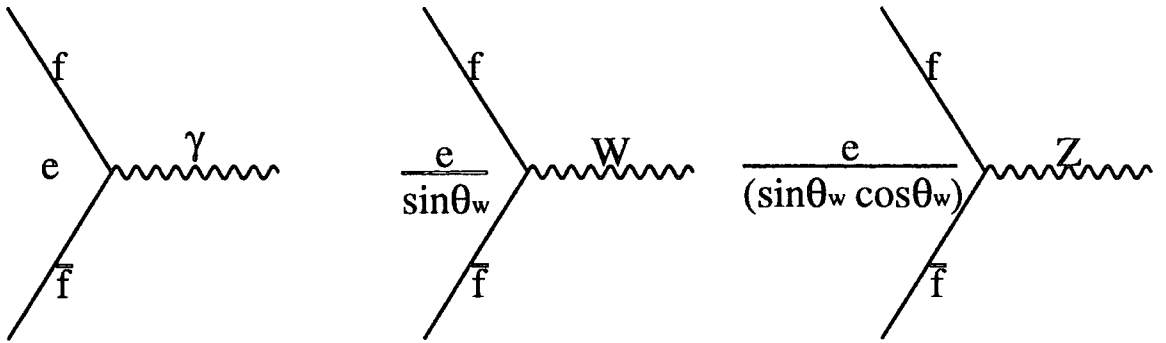
The above are very well tested
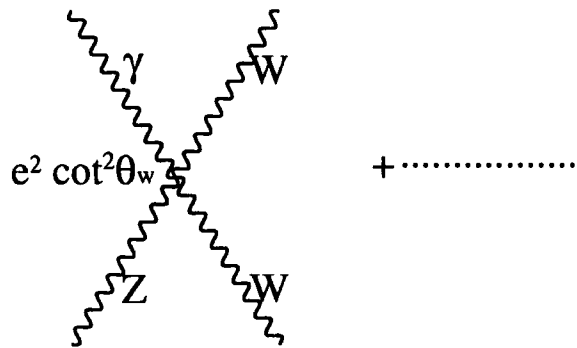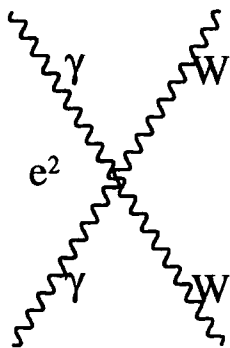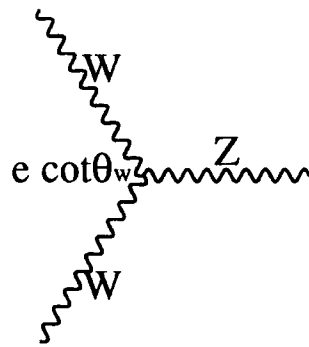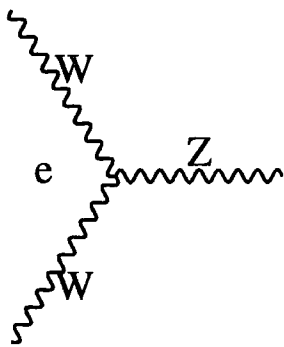
Not yet tested directly

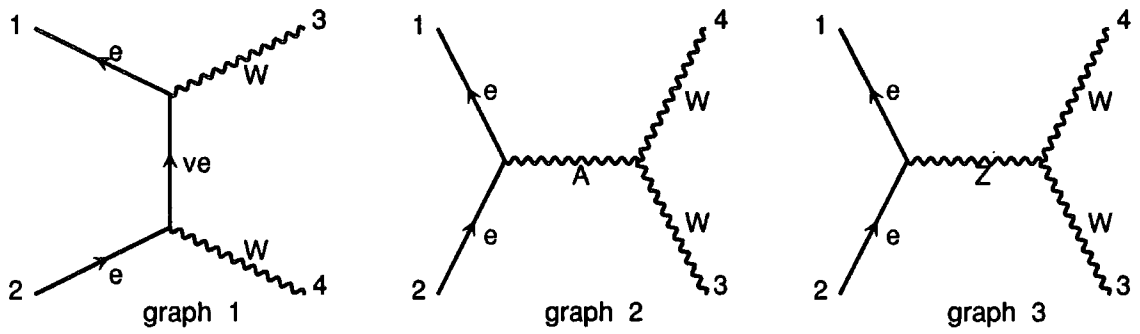Figure 3.1: SM couplings for f, γ, W and Z.

Figure 3.2: Feynman diagrams contributing to the process $e^+e^- \rightarrow W^+W^-$ at tree level, A stands for photon.
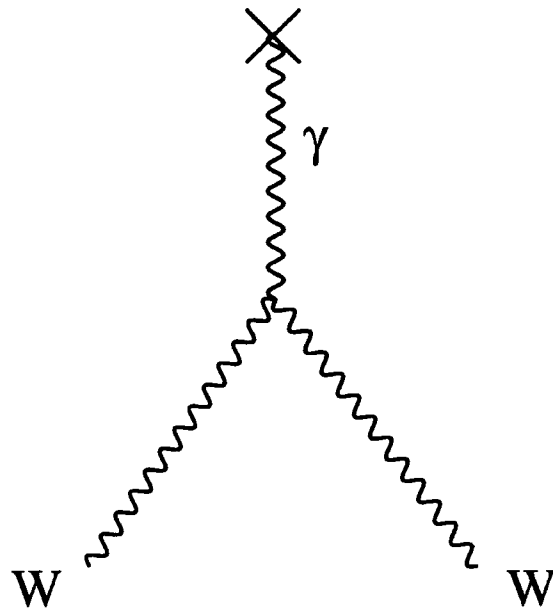

Figure 3.3: Feynman diagram that needs to be evaluated to calculate the magnetic moment.
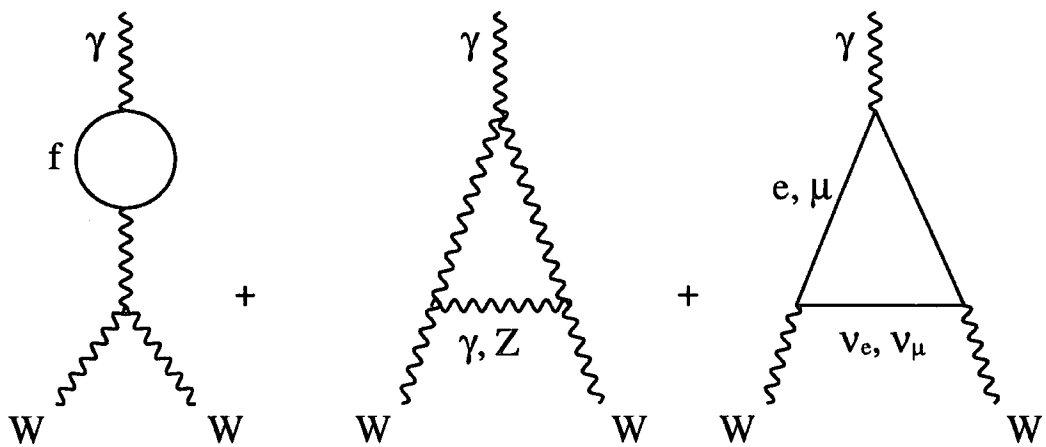
Figure 3.4: Feynman diagrams that need to be evaluated in the SM to calculate the corrections to the magnetic moment.

Chapter 4

Soft Photon Radiation and Anomalous Couplings in $e^+e^- \rightarrow W^+W^-$ at LEP II

4.1 Introduction

In the Standard Model (SM) of electroweak interactions, the SU(2)×U(1) non-abelian nature of the gauge symmetry fixes the tri-linear and quadri-linear electroweak gauge boson vertices. The LEP-II e^+e^- collider will be able to test these vertices with high precision, principally from the reaction $e^+e^- \rightarrow W^+W^-$. In particular, tests can be performed for the presence of 'anomalous couplings', arising for example from compositeness structure and other new physics see for example [12]. The process $e^+e^- \rightarrow W^+W^-$ is sensitive to anomalous tri-linear couplings through the $s-$channel photon and Z exchange diagrams. The unitarity cancellation between these and the $t-$channel neutrino exchange diagram ensures good high-energy behaviour. Any small deviations from the SM couplings will spoil this cancellation and should therefore be revealed by cross-section measurements at LEP-II.

In contrast, the process $e^+e^- \rightarrow W^+W^-\gamma$ receives contributions from quadri-linear as well as tri-linear couplings, and therefore probes a different combination of anomalous couplings. In [16] this process was studied in the context of future high-energy linear colliders. To avoid the infra-red region, a 'hard-photon' cut of $E_\gamma > 0.05\sqrt{s}$ was used. The problem with this is that at LEP-II there are very few such events, with most emitted photons being soft. Here we investigate the

dependence of the *soft-photon* cross section on the anomalous couplings, and to extend the work of [16] to include a more general set of anomalous couplings.

Current limits on κ_γ and λ_γ, obtained from $W\gamma$ production in $p\bar{p}$ collisions, are not very stringent; the most recent values from the CDF and D0 experiments are [17]

$$
-0.11 < \kappa_\gamma < 2.27 \ ,
$$
$$
-0.81 < \lambda_\gamma < 0.84 \ . \tag{4.1}
$$

There are no limits on κ_Z and λ_Z. In the Standard Model, non-zero values of $(\kappa-1)$ and λ are generated at the one-loop level, see figure (3.4). The exact values depend on the top and Higgs masses, but typical sizes are $(\kappa_\gamma - 1) \sim 5 \times 10^{-3}$ and $\lambda_\gamma \sim -5 \times 10^{-4}$ [18]. It is straightforward to extract from the Lagrangian (3.6) the modifications to the form of the triple and quartic interaction vertices [14]. For example, for the case of the ZWW and γWW vertices which contribute to the lowest order $e^+e^- \rightarrow W^+W^-$ cross section we have (see Figure (4.1))

$$
\begin{aligned}
\Gamma^V_{\mu\alpha\beta}(p, q_1, q_2) &= ig_{WWV}[(q_2 - q_1)_\mu \left((1 + \frac{\lambda_v p^2}{2M_W^2})g_{\alpha\beta} - \lambda_v \frac{p_\alpha p_\beta}{M_W^2} \right) \\
&+ (p_\beta g_{\mu\alpha} - p_\alpha g_{\mu\beta})(1 + \kappa_v + \lambda_v)] \ .
\end{aligned} \tag{4.2}
$$

As mentioned above, the $e^+e^- \rightarrow W^+W^-$ amplitude contains at most one tri-linear coupling, and the cross section therefore depends *quadratically* on the anomalous couplings. In contrast, the $e^+e^- \rightarrow W^+W^-\gamma$ cross section receives contributions from diagrams with up to two three-boson vertices and one four-boson vertex, and so the dependence on the anomalous couplings is *quartic* in κ. In principle, therefore, this process provides increased sensitivity, at the expense of course of fewer events [16]. In Section (4.2) we calculate the photon energy dependence of this cross section, and introduce the soft-photon approximation. Section (4.3) contains our numerical results and conclusions.

4.2 The Soft-Photon Cross Section

We begin by studying the photon energy dependence of the SM $W^+W^-\gamma$ cross section at $\sqrt{s} = 200$ GeV, with a view to establishing the region of validity of

the soft approximation. In order to obtain a finite cross section, we must impose energy and angular cuts on the photon. For purposes of illustration, we choose

$$\omega > 2.5 \text{ GeV} ,$$

$$|\eta_\gamma| < 1 \quad (40° < \theta_\gamma < 140°) , \qquad (4.3)$$

where ω and η_γ are the photon energy and pseudorapidity respectively and θ_γ is the photon angle relative to the beam direction. In all the results presented below we use $M_W = 80$ GeV, $M_Z = 91$ GeV, $\sin^2 \theta_W = 0.23$ and $\Gamma_Z = 2.55$ GeV. Figure (4.2) (solid histogram) shows the distribution $d\sigma_{WW\gamma}/d\omega$. Note that the total $W^+W^-\gamma$ cross section for these cuts is 0.26 pb, which is roughly 1.5% of the total W^+W^- cross section.

When the photon is soft, the cross section can be approximated by a simple analytic form. The details can be found, for example, in [19, 20] and in chapter 6, and will only be summarised here. Let $\mathcal{M}$ be the matrix element for the process $e^-(p_1)e^+(p_2) \to W^+(q_1)W^-(q_2)\gamma(k)$. When the photon momentum k^μ is much smaller than any of the other momenta, we can write

$$|\mathcal{M}|^2 \simeq |\mathcal{M}_0|^2 \, e^2 \, \mathcal{F} , \qquad (4.4)$$

where $\mathcal{M}_0$ is the matrix element without the photon emission, and

$$\begin{aligned}
\mathcal{F} = &-\frac{M_W^2}{(q_1.k)^2} - \frac{M_W^2}{(q_2.k)^2} + \frac{2q_1.q_2}{q_1.k \; q_2.k} - \frac{m_e^2}{(p_1.k)^2} - \frac{m_e^2}{(p_2.k)^2} + \frac{2p_1.p_2}{p_1.k \; p_2.k} \\
&-\frac{2q_2.p_1}{q_2.k \; p_1.k} - \frac{2q_1.p_2}{q_1.k \, p_2.k} + \frac{2q_1.p_1}{q_1.k \; p_1.k} + \frac{2q_2.p_2}{q_2.k \; p_2.k} .
\end{aligned} \qquad (4.5)$$

To obtain the cross section we integrate over the phase space of the final state particles:

$$\sigma(W^+W^-\gamma) = \frac{1}{2F} \int |\mathcal{M}|^2 d\Phi_3 \simeq \frac{1}{2F} \int |\mathcal{M}_0|^2 d\Phi_2 \, \frac{e^2}{16\pi^3} \, \mathcal{F} \, \omega \, d\omega \, d\cos\theta_\gamma \, d\phi_\gamma \qquad (4.6)$$

where $d\Phi_n$ denotes the phase space integration and F is the flux factor. Now suppose that the W^+ is emitted at angle θ_w to the beam in the e^+e^- centre-of-mass frame. If we integrate over all ϕ_γ and over photon polar angles such that $|\eta_\gamma| < \eta$, then the inclusive photon energy distribution is

$$\omega \, \frac{d\sigma}{d\omega} \simeq \int \frac{d\sigma_0}{d\cos\theta_w} \, S(\eta, \cos\theta_w) \, d\cos\theta_w \equiv C_s , \qquad (4.7)$$

where the soft-photon emission probability is

$$S(\eta, \cos\theta_w) = \frac{e^2}{16\pi^3} \int \omega^2 \mathcal{F} \, \mathrm{d}\cos\theta_\gamma \, \mathrm{d}\phi_\gamma \, . \qquad (4.8)$$

This soft approximation is compared to the exact distribution in Figure (4.2). We see clearly that the approximation is good for $\omega \lesssim (10-15)$ GeV but, as expected, breaks down for more energetic photons.

The next step is to study the effect of introducing anomalous couplings. It can readily be shown that in the limit that the photon is soft, the dependence on the anomalous couplings drops out of the $W^+W^-\gamma$ and $W^+W^-\gamma\gamma$ vertices. *Therefore, the distribution of soft photon emission, $\mathcal{F}$, is independent of such couplings.* However, this does *not* imply that the soft photon cross section is simply proportional to the lowest order cross section. If this were the case, the (κ, λ) dependence would simply cancel in the ratio $\sigma_0^{-1}\mathrm{d}\sigma/\mathrm{d}\omega$. The key point to note is that the soft-photon factor S in (4.7) has a non-trivial θ_w dependence, and therefore weights the (κ, λ)-dependent W^+W^- angular distribution differently from the lowest order cross section. In [16] it was noted that in order to explore the origin of the anomalous contributions which have a similar effect on the total cross-section, the differential distributions—for example the $\cos\theta_w$ spectrum— could be exploited. Our analysis using soft photons provides another method of probing this distribution.

Note, also, that we treat the $W^\pm$ bosons as on-shell, stable particles. It would be straightforward to include the additional contributions to $\mathcal{F}$ which arise from emission off the decay products in $W \rightarrow f\bar{f}'$; the details can be found in [20], for example. These additional contributions have, of course, no dependence on the anomalous couplings and can in practice be largely removed by requiring the photons to be isolated from the final state fermions (*i.e.* leptons and jets), in analogy to the rapidity cut already introduced.

4.3   Dependence on the Anomalous Couplings

We wish to study how the fraction of events containing a soft photon within a certain energy and pseudorapidity range (which is taken to be $\omega_0 < \omega < \omega_1$ and $|\eta_\gamma| < 1$ respectively) depends on the anomalous κ and λ couplings defined in

Section (3.1). We therefore define the ratio

$$r(\kappa, \lambda) = \frac{1}{\sigma_0(\kappa, \lambda)} \int_{\omega_0}^{\omega_1} d\omega \, \frac{d\sigma(\kappa, \lambda)}{d\omega} \simeq \frac{C_s(\kappa, \lambda)}{\sigma_0(\kappa, \lambda)} \log\left(\frac{\omega_1}{\omega_0}\right) . \tag{4.9}$$

With Standard Model couplings and $\omega_0 = 2.5$ GeV, $\omega_1 = 10$ GeV we find $r \equiv r_{\rm SM} = 8.7 \times 10^{-3}$. Figures (4.3(a-d)) (dashed lines) shows the ratio

$$R(\kappa, \lambda) = \frac{r(\kappa, \lambda)}{r_{\rm SM}} \tag{4.10}$$

as a function of the anomalous couplings $(\kappa_\gamma, \kappa_Z, \lambda_\gamma, \lambda_Z)$ as each is varied with the other three kept at their SM values. Note that within the soft approximation, the quantity R is independent of the photon energy range, since the logarithm in (4.9) cancels in the ratio. For comparison, the figure also shows (solid lines) the corresponding ratio of the lowest order $e^+e^- \to W^+W^-$ cross sections without photon emission, $i.e.$

$$R_0 = \frac{\sigma_0(\kappa, \lambda)}{\sigma_0(1, 0)} . \tag{4.11}$$

The fact that the solid and dashed curves are *different* means that the soft photon and total cross sections provide independent and complementary information on the anomalous couplings. For example, with only the total cross section measurement, there can be a two-fold degeneracy in the extraction of the coupling value (the R_0 curves are quadratic), which can be resolved with additional information from R.

Finally, we study how the dependence of the $W^+W^-\gamma$ cross section on the anomalous couplings varies with the photon energy. Figures (4.4(a,b)) show the inclusive photon energy distribution

$$\frac{1}{\sigma_0(\kappa, \lambda)} \frac{d\sigma(\kappa, \lambda)}{d\omega} . \tag{4.12}$$

normalised to the corresponding SM distribution (*i.e.* the solid histogram in Figure (4.2). In Figure (4.4(a)), κ_γ is fixed at its SM value and κ_Z is varied, and *vice versa* for Figure (4.4(b)). Also shown on the vertical axis are the soft-photon limits of these ratios obtained from Figure (4.3). It is interesting that the qualitative behaviour of the ratios in the two cases are very different. The very hard photon cross section is almost independent of κ_γ, while being maximally sensitive to κ_Z. The soft-photon variation is, on the other hand, comparable in the two

cases. Unfortunately, it is unlikely that the overall event rate will allow a detailed quantitative study of the hard photon region. In conclusion, we have shown that at LEP-II energies, the cross section for $W^+W^-\gamma$ production, where the photon is soft, is sensitive to the standard set of anomalous couplings used to parameterise the general form of the electroweak boson interaction Lagrangian. The dependence on these couplings is comparable in magnitude to, but qualitatively different from, the corresponding behaviour of the total W^+W^- cross section. Events with soft photons could therefore provide complementary information on the form of the electroweak boson interactions.
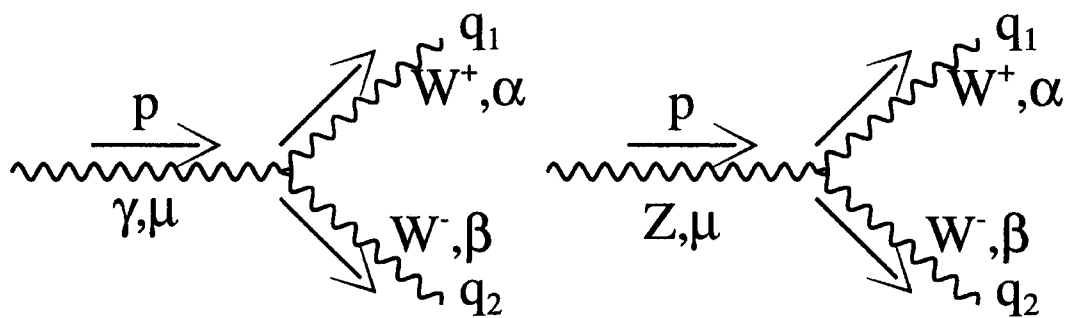
The three boson interaction vertex

Figure 4.1: The γW^+W^- and ZW^+W^- vertices $\Gamma^V_{\mu,\alpha,\beta}(P, q_1, q_2)$.
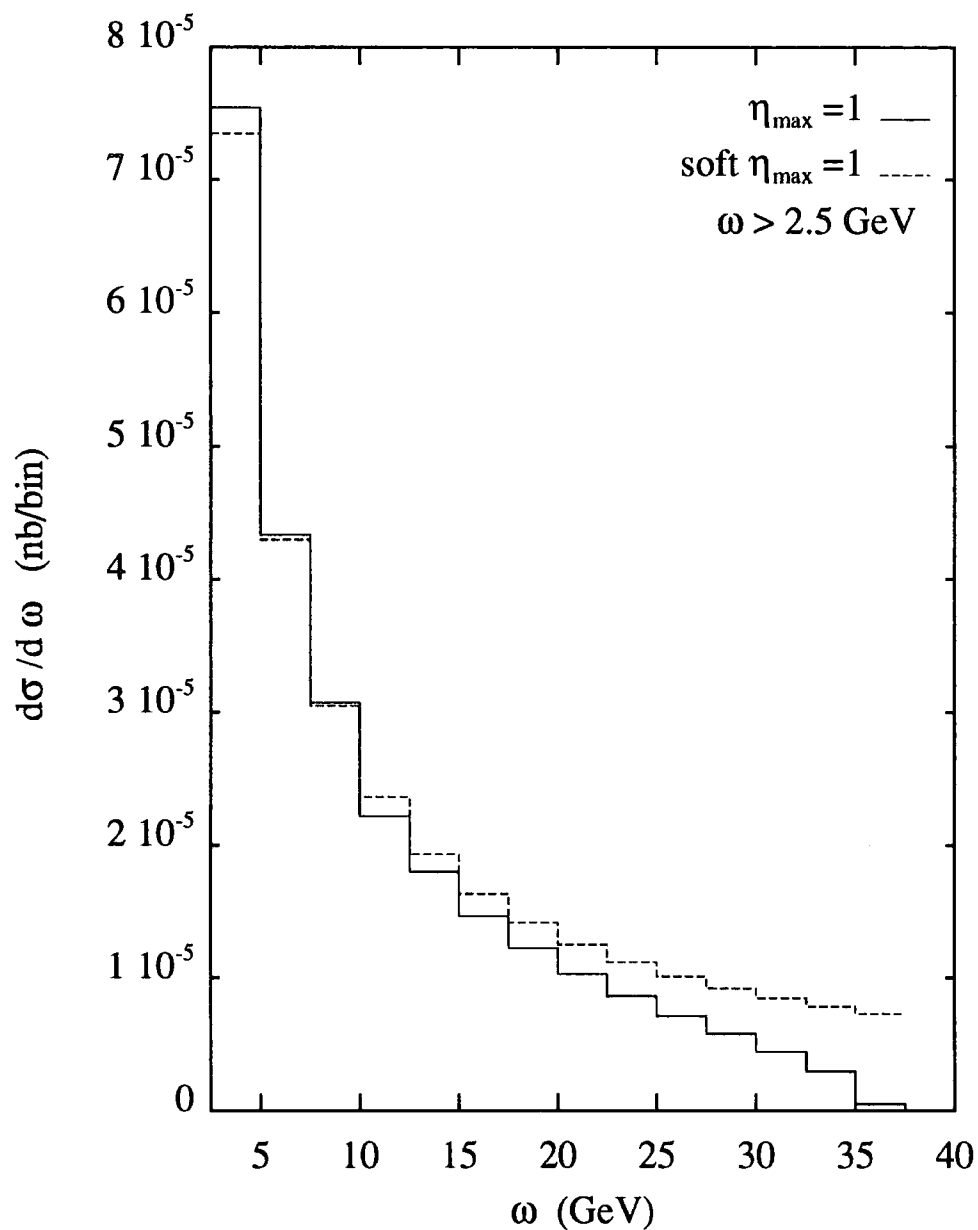
Figure 4.2: The photon energy distribution $d\sigma(W^+W^-\gamma)/d\omega$ at $\sqrt{s} = 200$ GeV with $|\eta_\gamma| < 1$, in the Standard Model. The solid histogram is the result of the exact calculation and the dashed histogram is the soft approximation defined in (4.7).
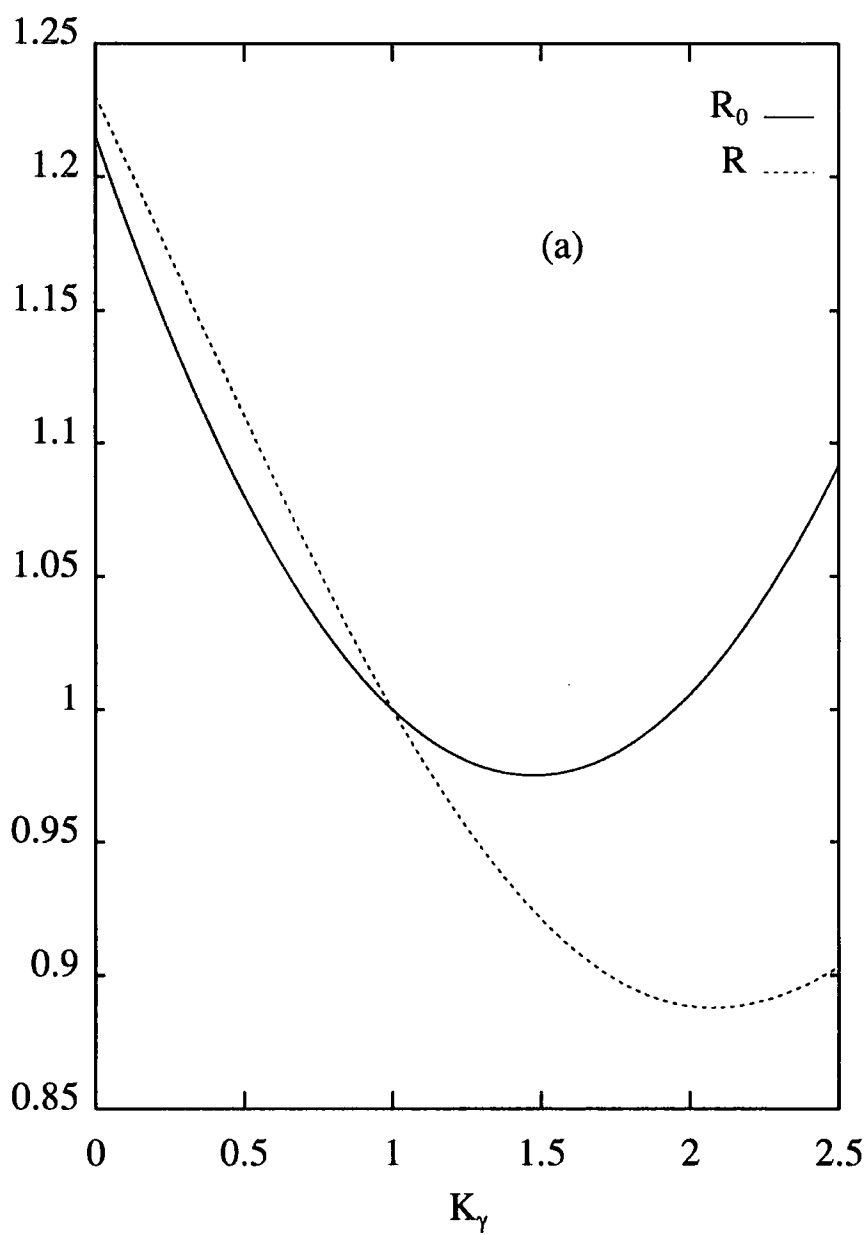
Figure 4.3(a)The ratios R (dashed lines) and R_0 defined in (4.10) and (4.11) respectively, as a function of the anomalous couplings defined in (3.6). κ_γ is varied while the others are kept fixed at their SM values.

Figure 4.3(b) The ratios R (dashed lines) and R_0 defined in (4.10) and (4.11) respectively, as a function of the anomalous couplings defined in (3.6). κ_Z is varied while the others are kept fixed at their SM values.

Figure 4.3(c) The ratios R (dashed lines) and R_0 defined in (4.10) and (4.11) respectively, as a function of the anomalous couplings defined in (3.6). λ_γ is varied while the others are kept fixed at their SM values.
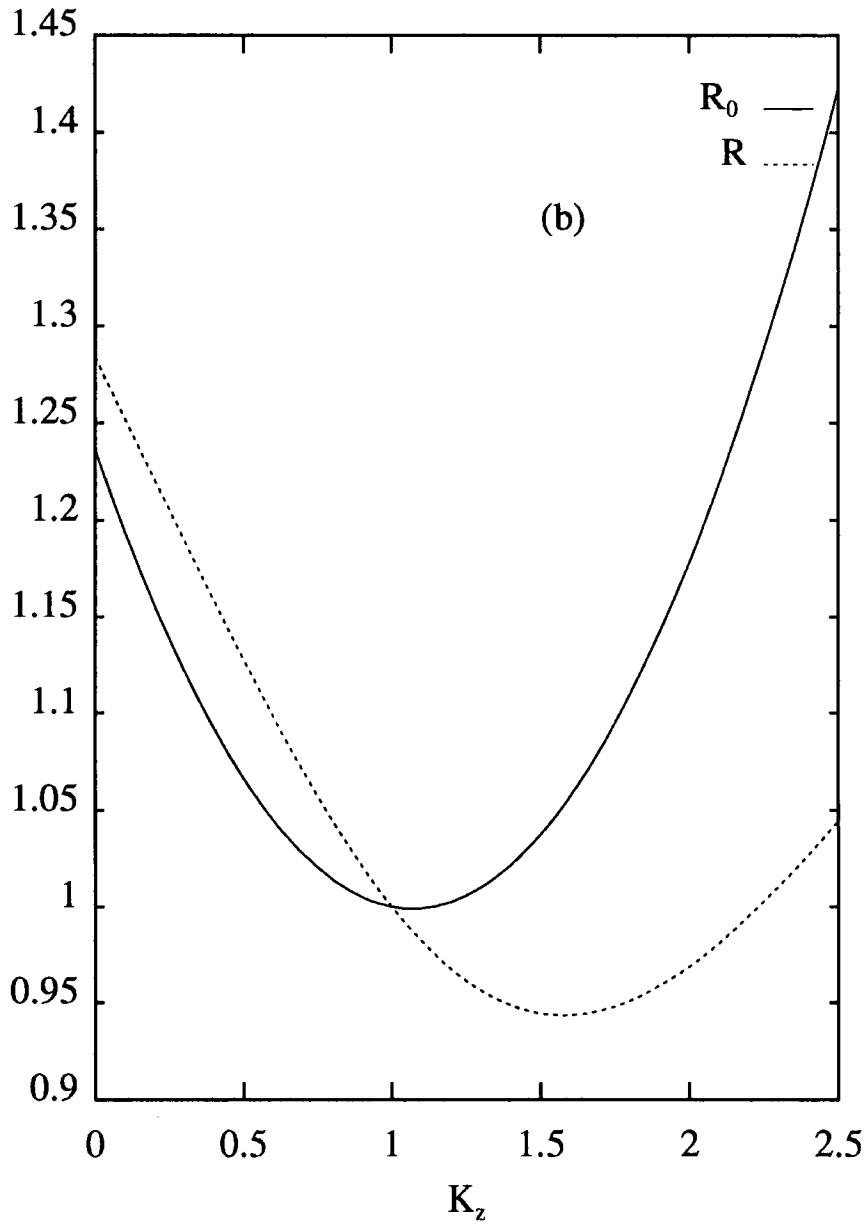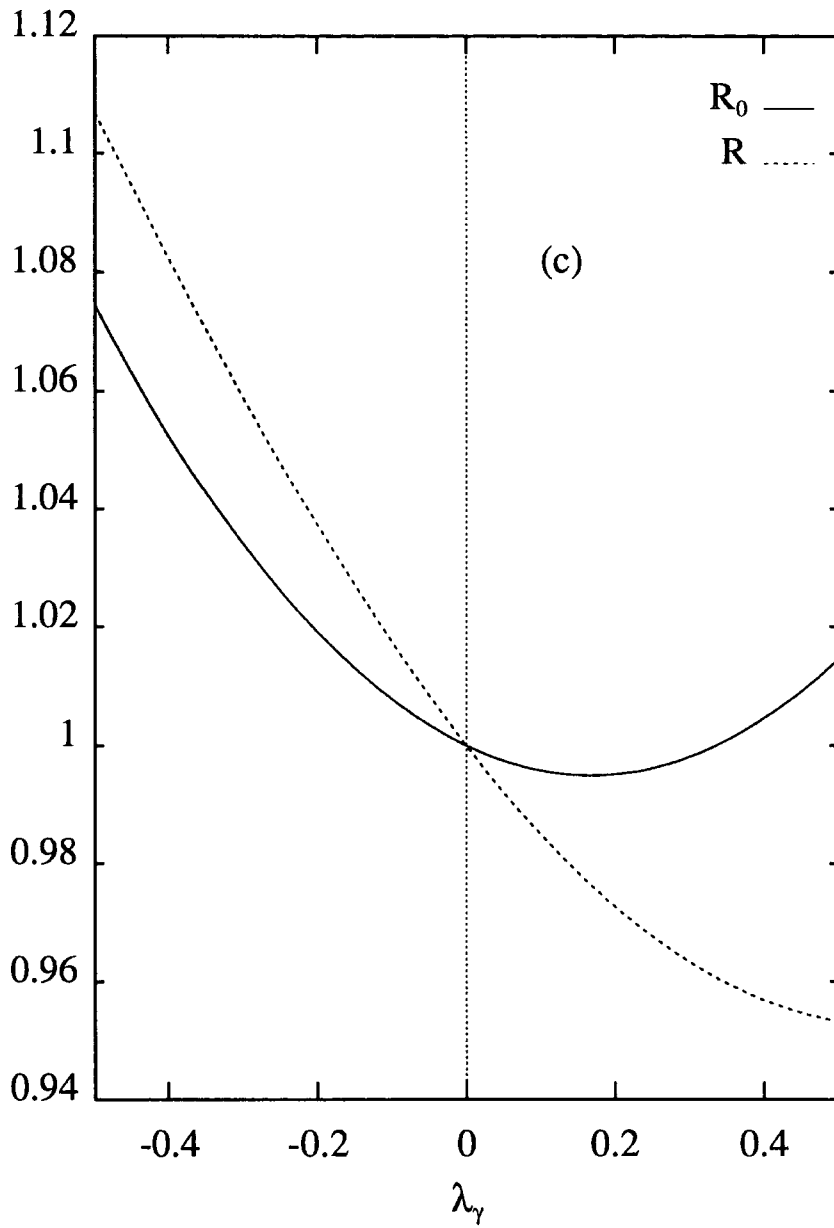
42
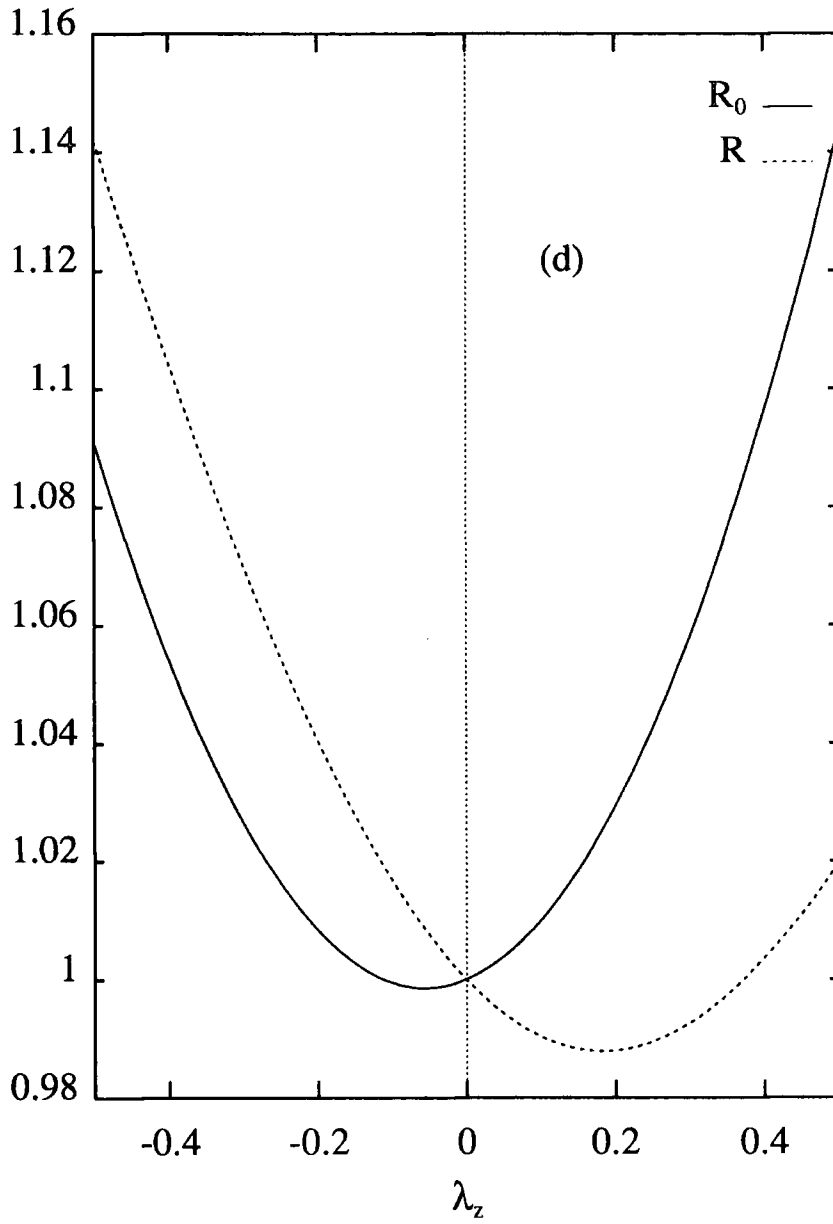
Figure 4.3(d) The ratios R (dashed lines) and R_0 defined in (4.10) and (4.11) respectively, as a function of the anomalous couplings defined in (3.6). λ_Z is varied while the others are kept fixed at their SM values.

Figure 4.4(a) The inclusive photon energy distribution defined in (4.12), normalised to the SM distribution for different κ_γ with $(\kappa_Z, \lambda_\gamma, \lambda_Z)$ fixed at their SM values.

Figure 4.4(b) The inclusive photon energy distribution defined in (4.12), normalised to the SM distribution for different κ_Z with $(\kappa_\gamma, \lambda_\gamma, \lambda_Z)$ fixed at their SM values.

Chapter 5

Anomalous Quartic Couplings in $W^+W^-\gamma$ production at e^+e^- Colliders
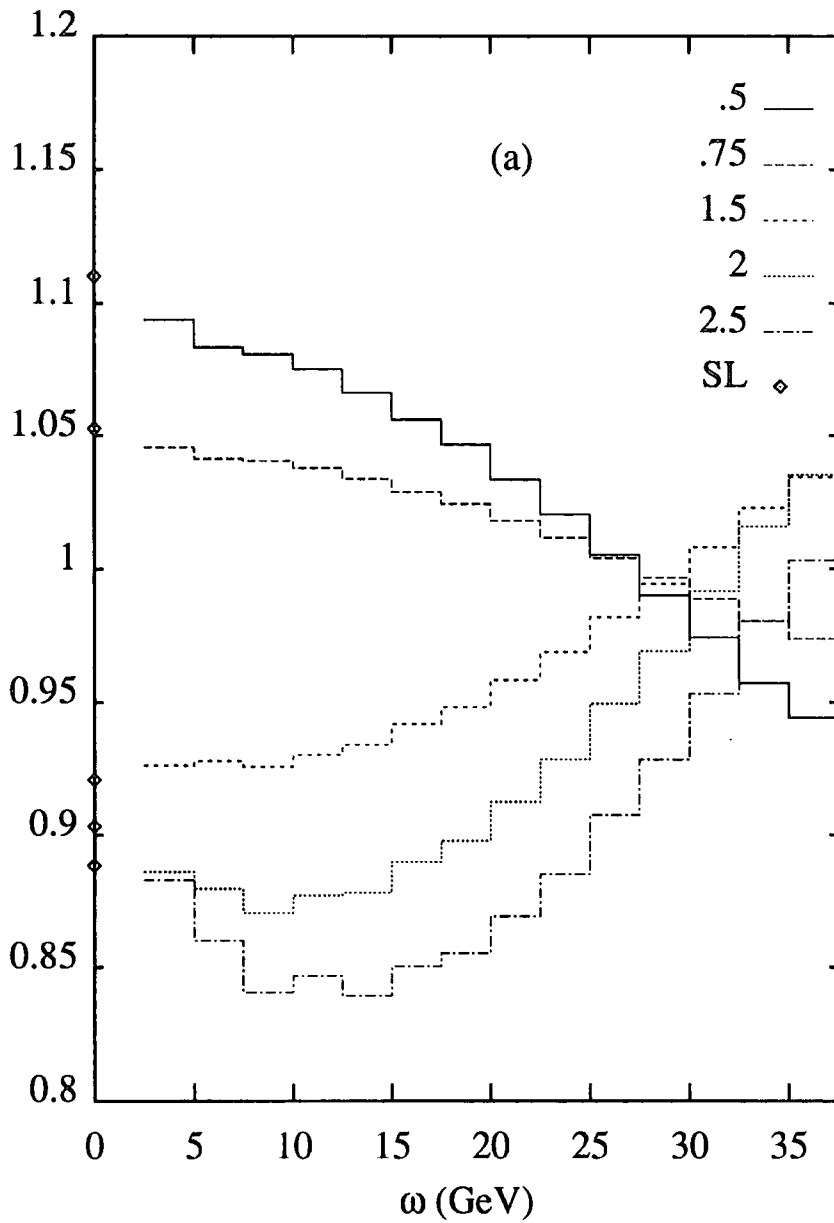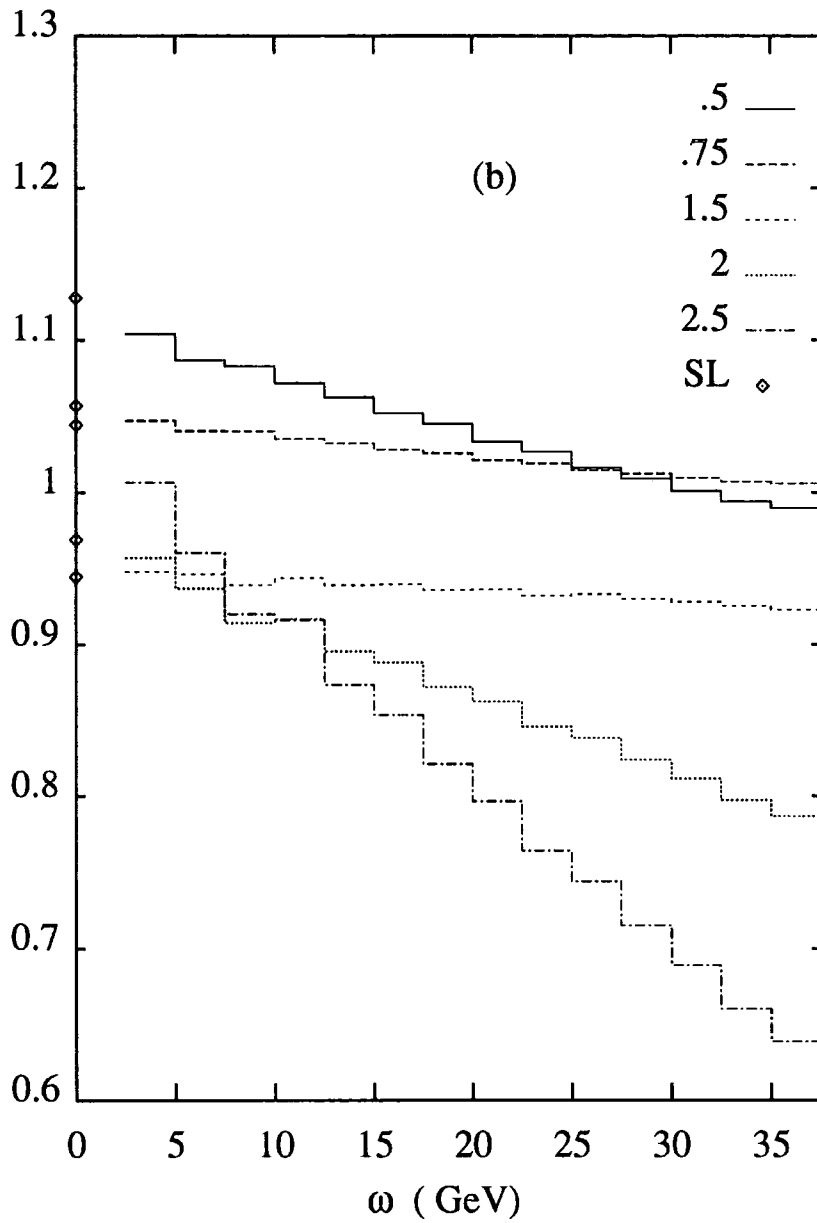
5.1 Introduction

As stressed in chapters three and four, in the Standard Model (SM) of electroweak interactions, the $SU_L(2) \times U_Y(1)$ non-abelian nature of the gauge symmetry relates the trilinear and quadrilinear vertices to the universal SU(2) gauge coupling, g. At tree level there are only two trilinear vertices, $W^+W^-\gamma$ and W^+W^-Z, and four quartic vertices $W^+W^-\gamma\gamma$, $W^+W^-\gamma Z$, W^+W^-ZZ and $W^+W^-W^+W^-$. Only recently have experiments begun to test these vertices directly. At the CERN and FNAL $p\bar{p}$ colliders, a handful of $W^\pm\gamma$ events have been used to place limits on the anomalous $W^+W^-\gamma$ trilinear couplings. The LEP II e^+e^- collider will also test the trilinear vertices through the total W^+W^- cross section [12]. However, independent tests of the *quartic* couplings require more complicated processes. One of the most accessible in the short term is the process $e^+e^- \rightarrow W^+W^-\gamma$, and it is this which provides the focus of the study in this chapter.

Studying the gauge boson interactions (of the W boson in particular) will help our understanding of the mechanism of spontaneous symmetry breaking. The gauge-boson interaction originates in the kinetic term of the Lagrangian, see Section (2.1.2). It is also directly related to the Goldstone modes and the Higgs particle, see Section (2.4.1) and [1]. The quartic couplings in particular will provide a way of testing the Higgs mechanism, either verifying the local gauge

46

invariance or signaling the existence of new physics beyond the Standard Model. A review of the importance of quartic couplings in probing new physics can be found in [21].

There is an important distinction between anomalous trilinear and genuine anomalous quartic couplings, *i.e.* those which give no contribution to the trilinear vertices [22]. Whereas the trilinear couplings involving W's are essentially form factors where massive fields are integrated out at the one-loop level, the anomalous quartic couplings are contact interactions – manifestations of the exchange of heavy particles. One can therefore imagine a theory in which the trilinear couplings have their Standard Model values, but the quartic couplings are modified by any number of independent anomalous contact interactions.

In this chapter we study the effect of anomalous quartic couplings in the process $e^+e^- \to W^+W^-\gamma$ at high energy. Our work builds on and extends the analysis of [21, 22], in that we investigate the collider energy and polarization dependence of the anomalous effects. In Section (5.2) we discuss the contributions of the anomalous operators in the context of $W^+W^-\gamma$ production and in Section (5.3) the numerical results are presented.

5.2 The Interaction Lagrangian

In this section we discuss the lowest dimension operators which lead to genuine quartic couplings. These operators must of course have the proper Lorentz structure, and should also respect the custodial SU(2) symmetry in order to evade experimental bounds on the ρ parameter [23]. The phenomenological Lagrangian should also respect the full U(1) gauge invariance, as at least one of the fields is a photon. For simplicity, we restrict the study to C- and P-conserving operators. The lowest dimension operators that satisfy the above constraints are of dimension 6, since the U(1)$_{em}$ symmetry requires derivatives [22]. These operators[1] are:

$$\mathcal{L}^0 = -\frac{\pi\alpha}{4\Lambda^2}a_0 F_{\alpha\beta}F^{\alpha\beta}(\vec{W}_\mu \cdot \vec{W}^\mu) \tag{5.1}$$

$$\mathcal{L}^c = -\frac{\pi\alpha}{4\Lambda^2}a_c F_{\alpha\mu}F^{\alpha\nu}(\vec{W}^\mu \cdot \vec{W}_\nu) \tag{5.2}$$

$$\mathcal{L}^n = i\frac{\pi\alpha}{4\Lambda^2}a_n \epsilon_{ijk}W_{\mu\alpha}^{(i)}W_\nu^{(j)}W^{(k)\alpha}F^{\mu\nu} \tag{5.3}$$

---

[1]Note that the operator $\mathcal{L}^0$ can be parametrized by the exchange of a neutral scalar particle.

where $\vec{W}_\mu$ is an SU(2) triplet, and $F^{\mu\nu}$ and $\vec{W}^{\mu\nu}$ are the U(1)$_{em}$ and the SU(2) field strengths respectively. The parameter Λ is an unknown 'new-physics' scale which, following convention, we take to be M_W.

The physical Lagrangians are obtained when the above are written in terms of the physical fields W^+, W^- and $Z^0 = W^3 \cos\theta_w$. The physical basis for $\mathcal{L}^0$ and $\mathcal{L}^c$ is obtained by the substitution [22]

$$\vec{W}_\mu \cdot \vec{W}_\nu \rightarrow 2W_\mu^+ W_\nu^- + \frac{1}{\cos\theta_w^2} Z_\mu Z_\nu \tag{5.4}$$

while the physical basis for the part of $\mathcal{L}^n$ which gives rise to quartic couplings is

$$\begin{aligned}
\vec{W}_{\mu\alpha} \cdot (\vec{W}_\nu \times \vec{W}^\alpha) \rightarrow \frac{i}{\cos\theta_w} &\left[(\partial_\mu W_\alpha^+ - \partial_\alpha W_\mu^+)(Z_\nu W^{-\alpha} - Z^\alpha W_\nu^-) \right. \\
&+ (\partial_\mu W_\alpha^- - \partial_\alpha W_\mu^-)(Z^\alpha W_\nu^+ - Z_\nu W^{\alpha+}) \\
&\left. + (\partial_\mu Z_\alpha - \partial_\alpha Z_\mu)(W_\nu^- W^{+\alpha} - W_\nu^+ W^{-\alpha}) \right]
\end{aligned} \tag{5.5}$$

The effective Lagrangians $\mathcal{L}^0$ and $\mathcal{L}^c$ give rise to an anomalous $W^+ W^- \gamma\gamma$ coupling, whereas $\mathcal{L}^n$ gives rise to an anomalous $W^+ W^- Z\gamma$ coupling. The corresponding Feynman rules for the above interactions where all the momenta are incoming to the vertex such that $W^+(p_+)$, $W^-(p_-)$, $\gamma^\alpha(p_1)$ and $\gamma^\beta(p_2)$ (or $Z^\beta(p_2)$ for $\mathcal{L}^n$) are

$$i\frac{2\pi\alpha}{\Lambda^2} a_0 g_{\mu\nu}[g_{\alpha\beta}(p_1 \cdot p_2) - p_{2\alpha}p_{1\beta}] \tag{5.6}$$

and

$$\begin{aligned}
i\frac{\pi\alpha}{2\Lambda^2} a_c \quad &[(p_1 \cdot p_2)(g_{\mu\alpha}g_{\nu\beta} + g_{\mu\beta}g_{\alpha\nu}) + g_{\alpha\beta}(p_{1\mu}p_{2\nu} + p_{2\mu}p_{1\nu}) \\
&- p_{1\beta}(g_{\alpha\mu}p_{2\nu} + g_{\alpha\nu}p_{2\mu}) - p_{2\alpha}(g_{\beta\mu}p_{1\nu} + g_{\beta\nu}p_{1\mu})\,]\ .
\end{aligned} \tag{5.7}$$

Finally,

$$\begin{aligned}
i\frac{\pi\alpha}{4\cos\theta_w\Lambda^2} a_n \quad &[g_{\mu\beta}[g_{\nu\alpha}p_1 \cdot (p_2 - p_+) - p_{1\nu}(p_2 - p_+)_\alpha] \\
&- g_{\nu\beta}[g_{\mu\alpha}p_1 \cdot (p_2 - p_-) - p_{1\mu}(p_2 - p_-)_\alpha] \\
&+ g_{\mu\nu}[g_{\alpha\beta}p_1 \cdot (p_+ - p_-) - p_{1\beta}(p_+ - p_-)_\alpha] \\
&- p_{2\mu}(g_{\alpha\nu}p_{1\beta} - g_{\alpha\beta}p_{1\nu}) + p_{2\nu}(g_{\alpha\mu}p_{1\beta} - g_{\alpha\beta}p_{1\mu}) \\
&- p_{-\beta}(g_{\alpha\mu}p_{1\nu} - g_{\alpha\nu}p_{1\mu}) + p_{+\beta}(g_{\alpha\nu}p_{1\mu} - g_{\alpha\mu}p_{1\nu}) \\
&+ p_{+\nu}(g_{\alpha\beta}p_{1\mu} - g_{\alpha\mu}p_{1\beta}) + p_{-\mu}(g_{\alpha\beta}p_{1\nu} - g_{\alpha\nu}p_{1\beta})\,]\ .
\end{aligned} \tag{5.8}$$

Note that the operators studied here do not respect the full *local* $SU_L(2) \times U_Y(1)$ gauge invariance. The Lagrangians $\mathcal{L}^0$ and $\mathcal{L}^c$ should be regarded as effective Lagrangians at the scale of the experiments. They can always be re-written in a gauge-invariant form by introducing the appropriate covariant derivatives. A more detailed discussion can be found in [24].

5.3 Numerical Results and Conclusions

We begin this section by analysing the effect of the anomalous couplings a_0, a_c and a_n on the total $W^+W^-\gamma$ production cross section at a 500 GeV e^+e^- collider [21]. The anomalous cross sections are quadratic functions of the parameters a_0, a_c and a_n. Fig. (5.1) shows the total cross-sections with one parameter being different from zero at any one time. In order to avoid collinear singularities caused by the massless photon the following rapidity and energy cuts are implemented

$$|\eta_\gamma| \le 2 \ , \qquad E_\gamma \ge 20 \text{ GeV} \tag{5.9}$$

In addition, all the initial and final particles are separated by at least 15°. Other parameter values are $M_W = 80$ GeV/c^2, $\sin^2 \theta_W = 0.23$ and $\Gamma_Z = 2.55$ GeV. With these parameters, the Standard Model total cross section ($a_0 = a_c = a_n = 0$) is 123.4 fb, which corresponds to a total of $N(W^+W^-\gamma) = 1234$ events for an integrated luminosity of $\mathcal{L} = 10$ fb^{-1}. The two horizontal lines in Fig. (5.1) correspond to a $\pm 3\sigma$ statistical variation of the Standard Model result, *i.e.*

$$\delta\sigma_{SM} = \pm 3 \sqrt{\frac{\sigma_{SM}}{\mathcal{L}}} \tag{5.10}$$

where the integrated luminosity is again taken to be $\mathcal{L} = 10$ fb^{-1}. The $\pm 3\sigma$ band corresponds to the following variation in the anomalous couplings:

$$-0.64 \le \ a_0 \ \le 0.42$$
$$-1.38 \le \ a_c \ \le 0.65$$
$$-3.9 \le \ a_n \ \le 4.25 \ , \tag{5.11}$$

indicating that the sensitivity is greatest for the a_0 parameter and least for the a_n parameter.[2] We next investigate the dependence of the cross sections on the

---

[2]In deriving these limits we are of course assuming that the statistical error dominates the overall experimental error, as in the case, for example, in [17].

photon energy. Fig. (5.2) shows the E_γ distribution at $\sqrt{s} = 500$ GeV, with the same cuts and parameters as before. Fig. (5.2(a)) shows the distributions for $a_0 = 0$ (Standard Model, solid line), $a_0 = \pm 1$ (dashed lines) and $a_0 = 0.42$ (the 3σ value, dotted line), the other anomalous couplings being set to zero. Evidently the bulk of the sensitivity comes from the hard photon end of the spectrum. This is not unexpected, since the additional contributions do not give rise to infra-red singularities as $E_\gamma \to 0$. Similar remarks apply to the other parameters. Figs. (5.2(b)) and (5.2(c)) show the effect on the photon energy distribution of varying a_c and a_n respectively.

In an attempt to improve the sensitivity to the anomalous couplings, we consider next the helicity decomposition of the cross section. The amplitude for $e^+ e^- \to W^+ W^-$ contains two different types of contribution: s-channel Z, γ exchange and t-channel neutrino exchange. The anomalous quartic coupling contributions to $W^+ W^- \gamma$ production, however, only receive contributions from the former, i.e. $e^+ e^- \to Z^*, \gamma^* \to W^+ W^- \gamma$. It follows that the effects will be largest in the *positive helicity* initial-state configuration, $\lambda_{e^-} \lambda_{e^+} = +1$, since this receives no contribution from the 'Standard Model background' neutrino-exchange diagrams. Fig. (5.3) shows the distribution $d\sigma^\pm(a_i)/dE_\gamma$ ($i = 0, c$) at 500 GeV for (a) the positive helicity $\lambda_{e^-} \lambda_{e^+} = +1$ cross section (σ^+) and (b) the negative helicity $\lambda_{e^-} \lambda_{e^+} = -1$ cross section (σ^-). For the same variation in the a_i, the effect is indeed much larger in the former.

Unfortunately, at these energies the positive helicity cross section is in absolute terms much smaller than the negative helicity cross section. This is illustrated in Fig. (5.4), which shows the spin decomposition of the total $W^+ W^- \gamma$ Standard Model cross section as a function of E_{beam}. There is a difference of some two orders of magnitude between σ^- and σ^+.

Finally, we address the question of whether there is any possibility of seeing an effect in $W^+ W^- \gamma$ production at lower $e^+ e^-$ collider energies. We consider variations in a_0 only – similar remarks apply to the other couplings. The problem at lower energies is that phase space restricts the photon to be soft, which is where the sensitivity to the anomalous couplings is least. This is illustrated in Fig. (5.5), which shows the ratio of σ, σ^+ and σ^- for $a_0 = 1$ to that of the corresponding

Standard Model cross section, as a function of E_{beam}, with the same photon cuts as before. Below $E_{\text{beam}} = 150$ GeV the effects are negligible. The increased sensitivity to a_0 in σ^+ is partially offset by the much smaller cross section in this channel. Taking $\mathcal{L} = 10$ fb^{-1} for both the positive and negative helicity channels, we calculate from Fig. (5.5) that at 500 GeV, $a_0 = 1$ gives a 7.5σ increase of σ^- and a 47σ increase of σ^+. The corresponding numbers for 300 GeV collisions are 0.4σ and 1.0σ respectively.

Of course we do expect to obtain a handful of $W^+W^-\gamma$ events even at LEP II, and from these it will be possible to derive very crude limits on the anomalous quartic couplings. Fig. (5.6) shows the total $W^+W^-\gamma$ cross sections for $E_\gamma > 20$ GeV, $|\eta_\gamma| < 2$ photons in e^+e^- collisions at 200 GeV, as a function of a_0 and a_c.[3] Again, the dependence is quadratic. Note the vastly expanded horizontal scale compared to Fig. (5.1).

In conclusion, quartic couplings can provide a window on new physics beyond the Standard Model. We have quantified the effect of various types of anomalous operators on the $W^+W^-\gamma$ production cross section in e^+e^- collisions. The effects are largest in the positive helicity cross section, although this represents only a small fraction of the total cross section. This type of physics is best suited to high energy colliders – there is an enormous increase in sensitivity in going from $\sqrt{s} = 300$ GeV to $\sqrt{s} = 500$ GeV – although some crude limits should be possible even from a handful of events at LEP II.
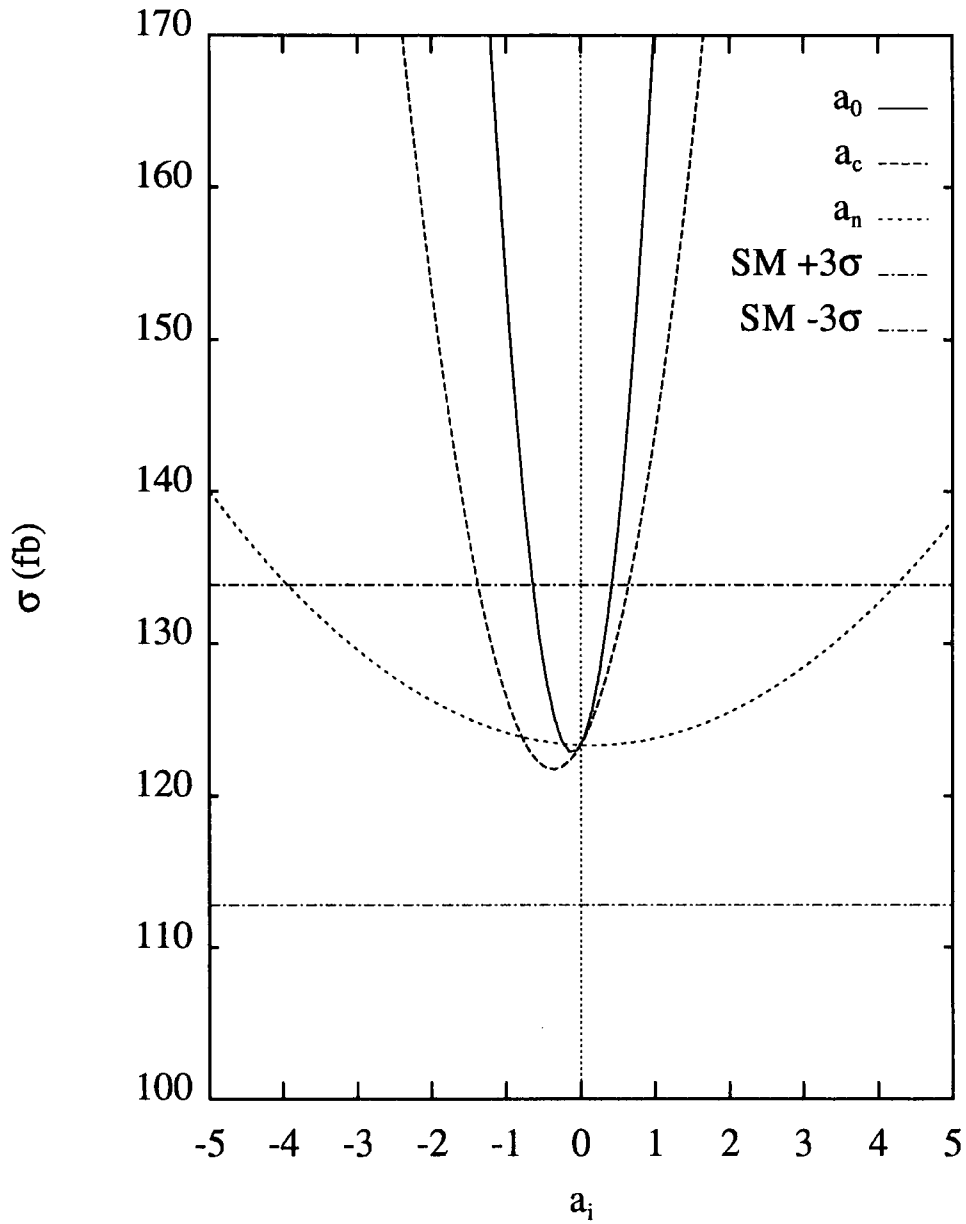
---

[3]the dependence on a_n is negligible at this energy

51

Figure 5.1: The total cross section for the process $e^+e^- \to W^+W^-\gamma$ at $\sqrt{s} = 500$ GeV as a function of the anomalous couplings a_0, a_c and a_n. The $\pm 3\sigma$ variation about the SM cross-section is indicated by the horizontal lines.

Figure 5.2(a)The photon energy distribution $d\sigma/dE_\gamma$ for different values of the a_0 parameter, at $\sqrt{s} = 500$ GeV.

Figure 5.2(b) The photon energy distribution $d\sigma/dE_\gamma$ for different values of the a_c parameter, at $\sqrt{s} = 500$ GeV.
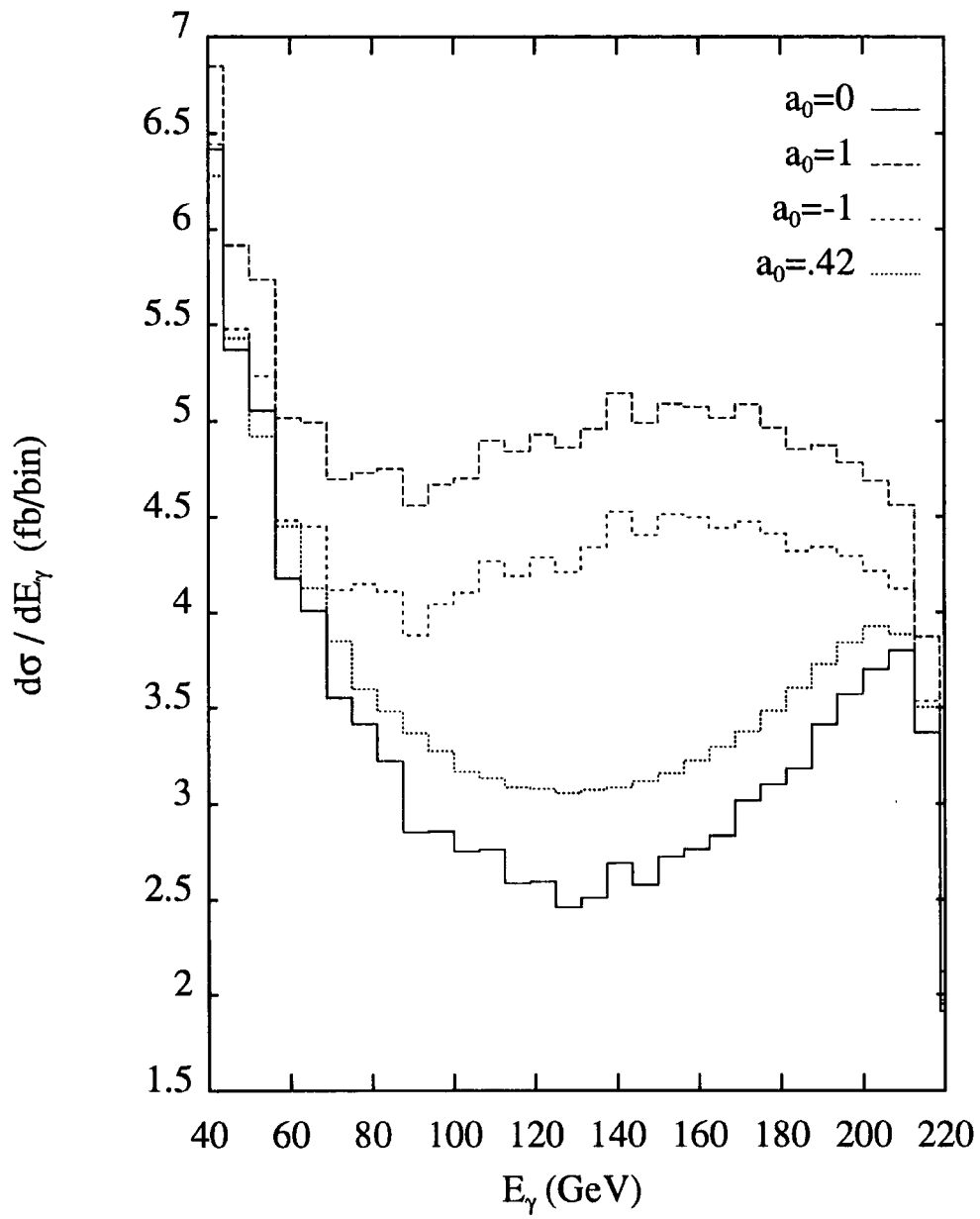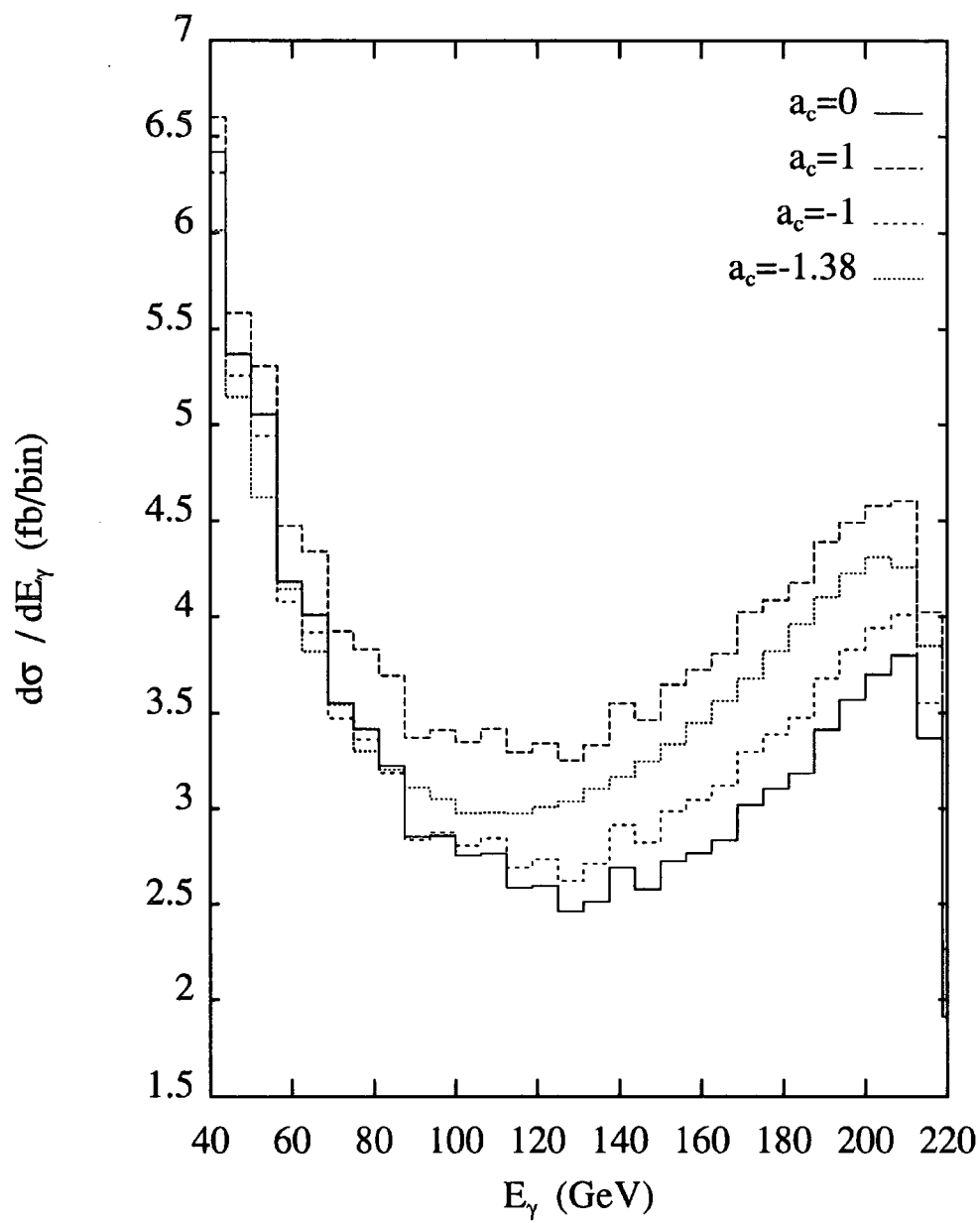
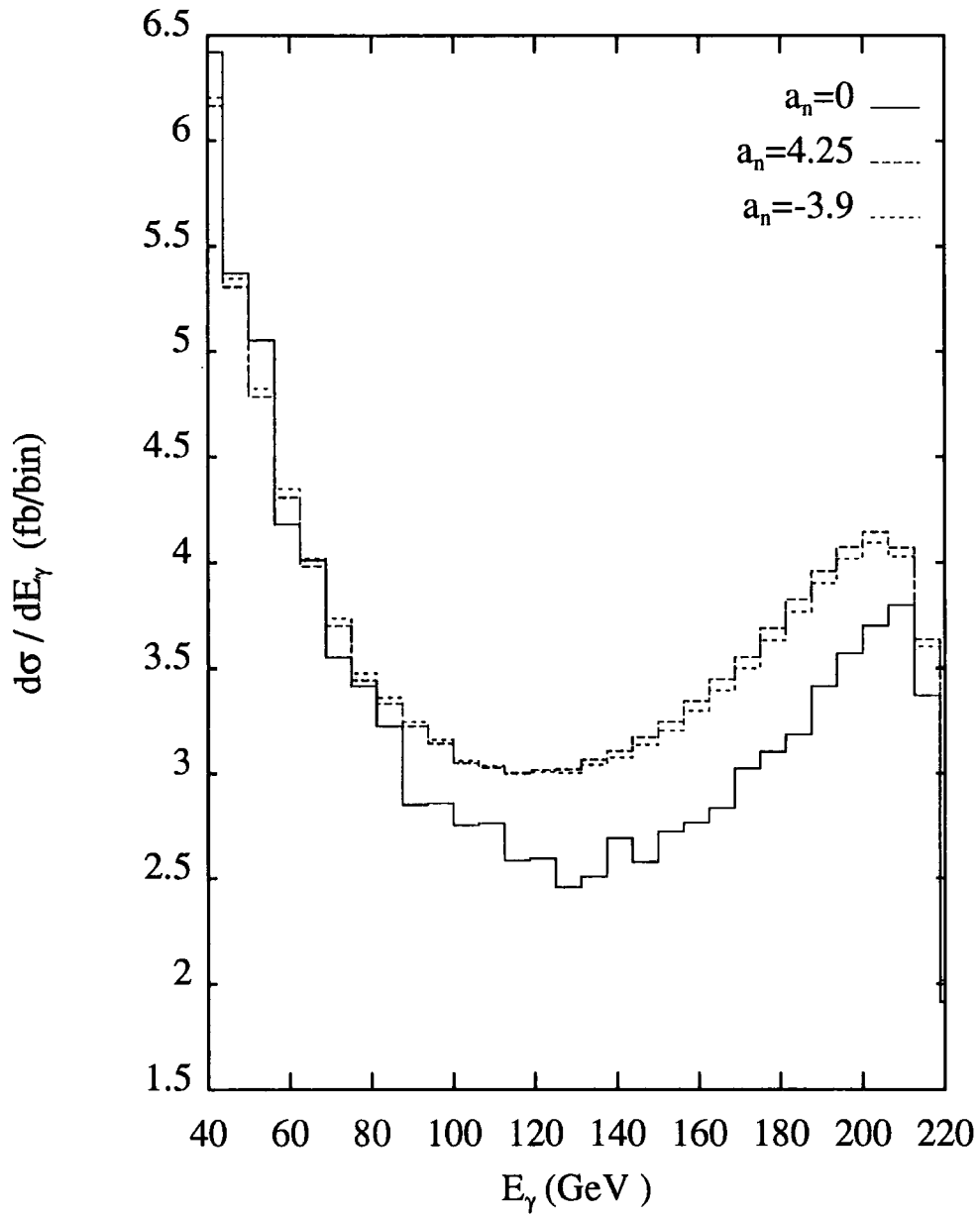Figure 5.2(c)The photon energy distribution $d\sigma/dE_\gamma$ for different values of the a_n parameter, at $\sqrt{s} = 500$ GeV.
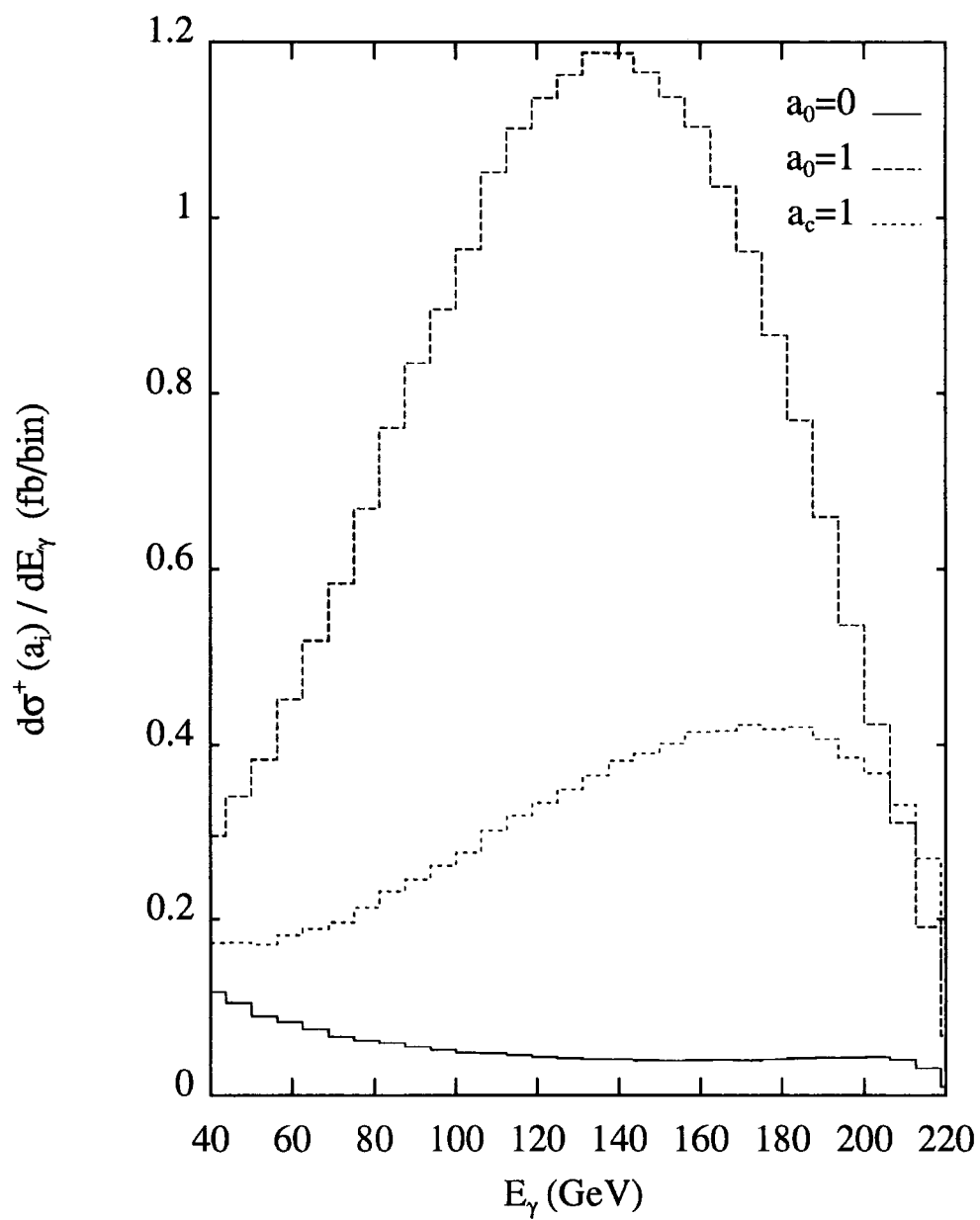
Figure 5.3(a) The positive-helicity cross sections $d\sigma^{\pm}(a_i)/dE_\gamma$ as a function of the photon energy, at $\sqrt{s} = 500$ GeV.
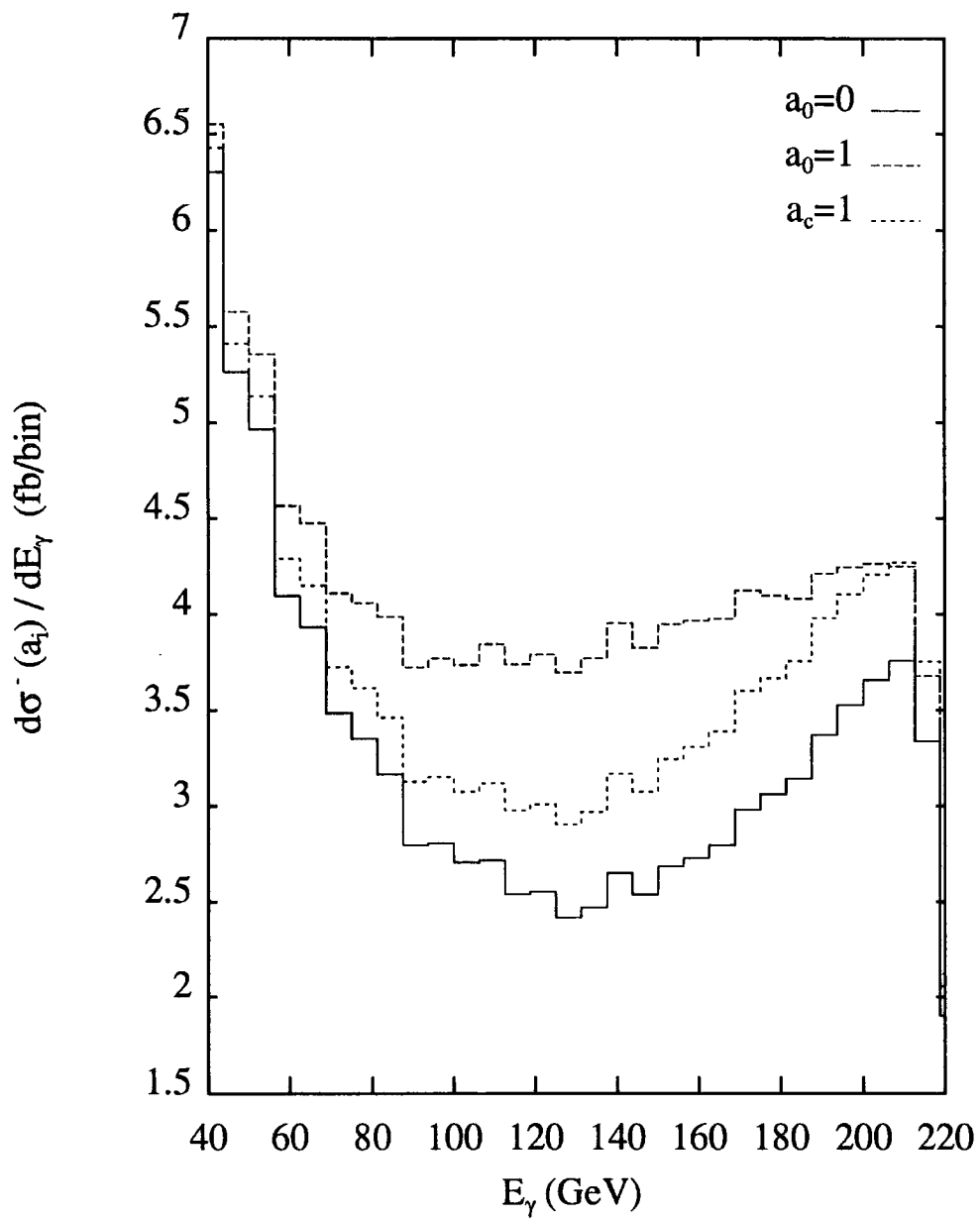
Figure 5.3(b) The negative-helicity cross sections $d\sigma^{\pm}(a_i)/dE_{\gamma}$ as a function of the photon energy, at $\sqrt{s} = 500$ GeV.
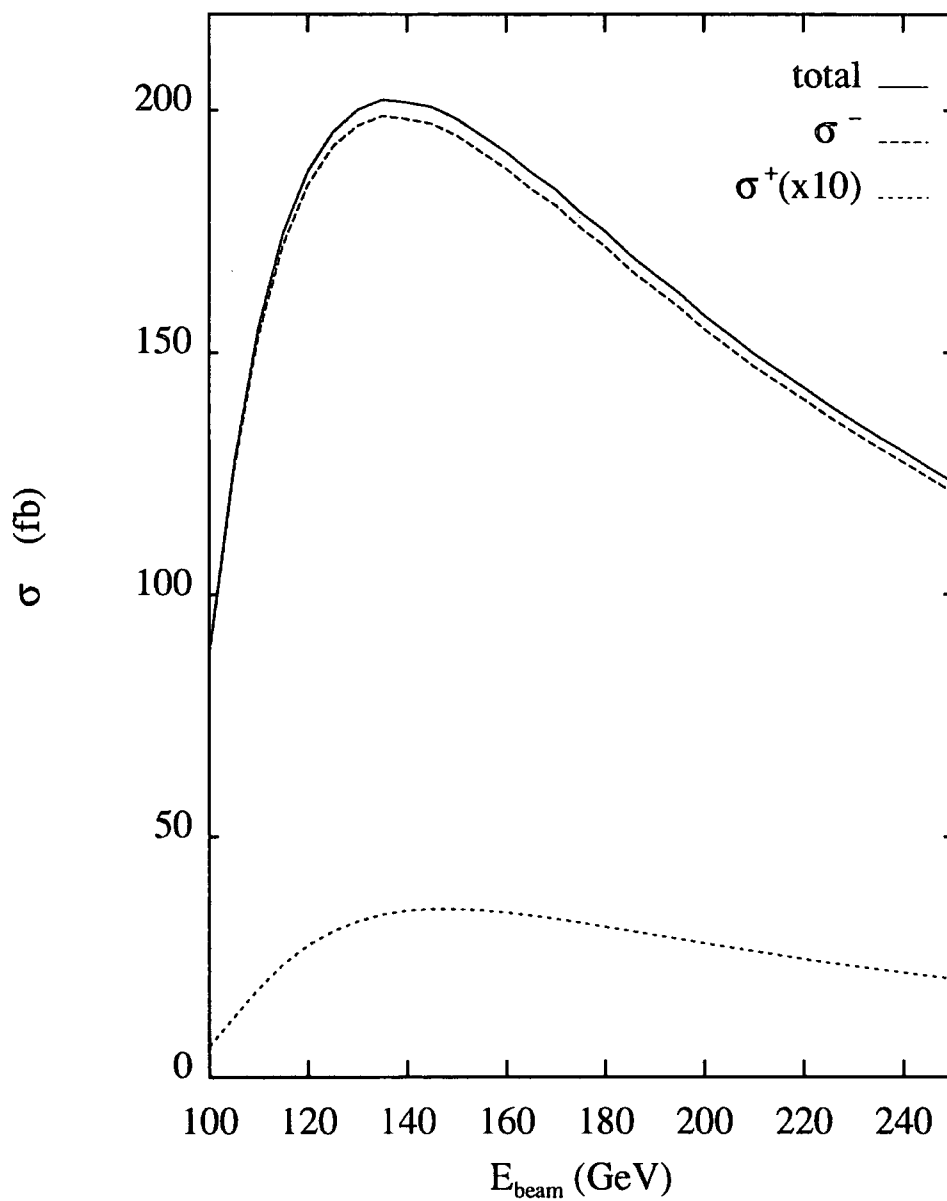
Figure 5.4: The positive- and negative-helicity contributions to the Standard Model $e^+e^- \rightarrow W^+W^-\gamma$ cross section as a function of the beam energy.
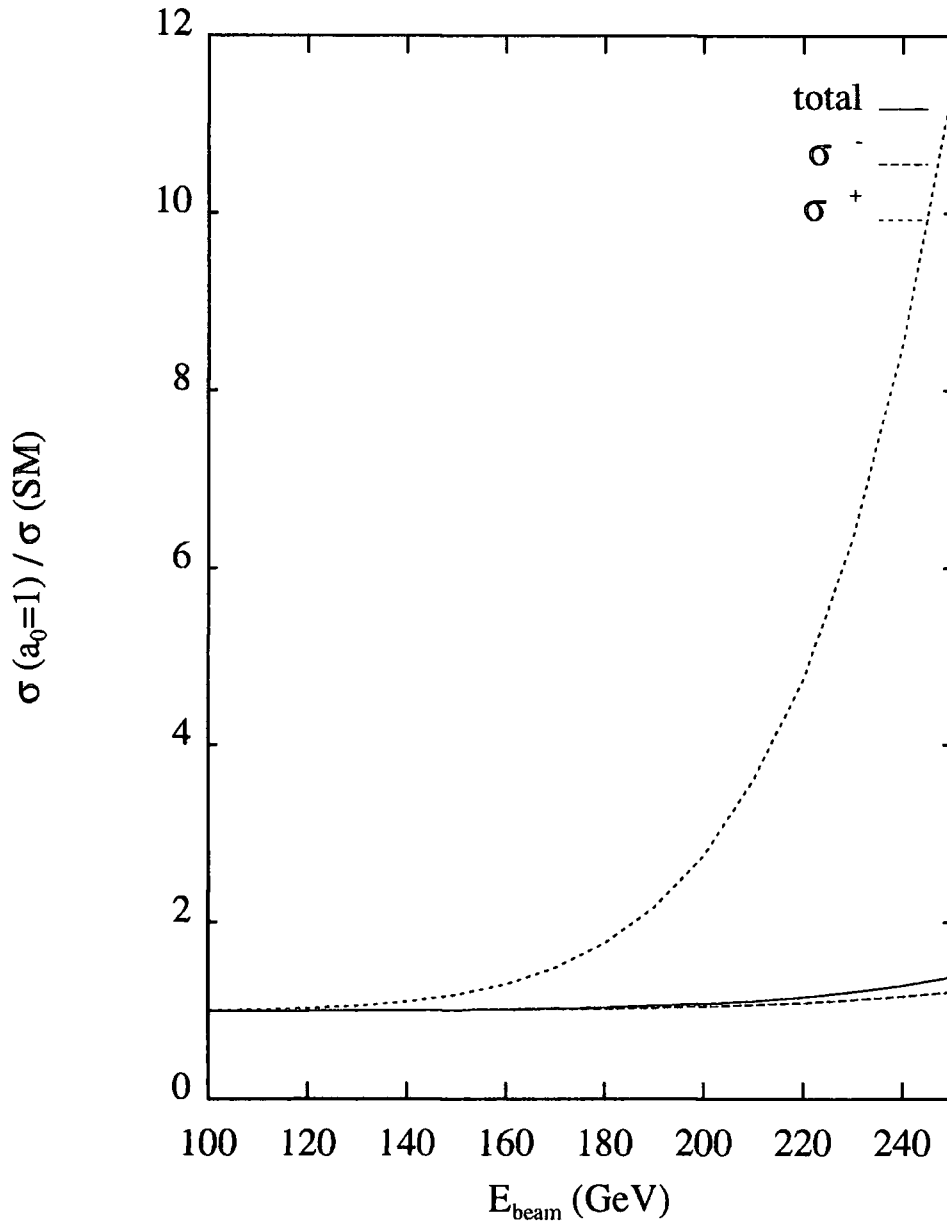
Figure 5.5: The ratio of the total, negative-helicity and positive-helicity cross sections for $a_0 = 1$ to those of the Standard Model ($a_0 = 0$), as a function of the beam energy.
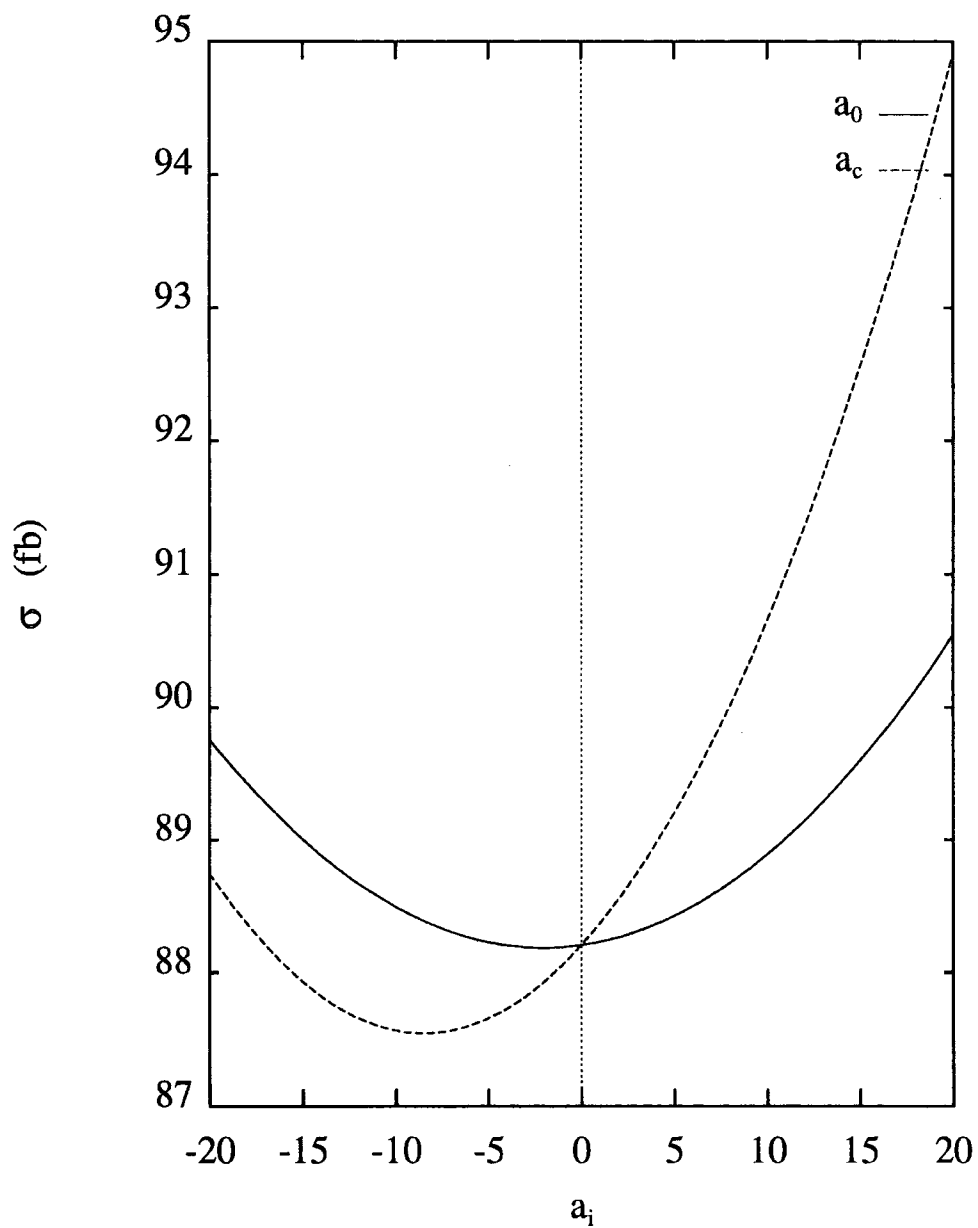
Figure 5.6: The dependence of the total $e^+e^- \rightarrow W^+W^-\gamma$ cross section on the anomalous couplings a_0 and a_c at LEP II ($\sqrt{s} = 200$ GeV).

Chapter 6

Soft Photon Radiation in $e^+e^- \to t\bar{t} \to b\bar{b}W^+W^-$

This chapter presents a detailed analysis of soft photon emission in top quark production and decay. In particular, the radiation pattern in the process $e^+e^- \to t\bar{t} \to bW^+\bar{b}W^-$ at high scattering energies (of order 600 GeV) is considered. The motivation behind this is as follows. The recent results from the D0 and CDF experiments places the mass of the top [150–200] GeV, thus suggesting an exciting possibility of a great experimental input from the next generation of linear e^+e^- colliders. Previous work on the subject [25, 26] with soft gluons (*i.e.* gluons with energy $\omega \sim \Gamma$ where Γ is the top width) shows that the radiation pattern depends sensitively on the top mass and width. Similar effects should be observed in soft photon radiation as well. Although the rate is smaller, photons are probably easier to detect and measure than soft gluon jets. An apparent disadvantage however, is that for photons initial state radiation is a potentially important background to the interesting effects due to radiation off the top quarks and their decay products. In this chapter we present the analogous calculation to [25] for soft photon radiation, taking the initial state radiation contribution fully into account. We shall see that for certain configurations of initial and final state particles, the radiation pattern does indeed have a very rich structure, depending on the top mass, width and energy as well as on the orientation of the b quark and the W boson with respect to the parent t's and to each other. The conditions under which initial state radiation is minimised are investigated.

Consider the production of a stable heavy quark pair in e^+e^- annihilation at

high collision energy 2E. The soft photon emission probability is

$$
\frac{1}{\sigma_0}d\sigma = \; - \; e^2\left[e_Q^2\left(\frac{M^2}{(q_1.k)^2} + \frac{M^2}{(q_2.k)^2} - 2\frac{q_1.q_2}{(q_1.k)(q_2.k)}\right)\right.
$$
$$
+ \; \left(e_e^2\left[\frac{m_e^2}{(P_1.k)^2} + \frac{m_e^2}{(P_2.k)^2} - 2\frac{P_1.P_2}{(P_1.k)(P_2.k)}\right]\right)
$$
$$
+ \; 2e_Q e_e\left(\frac{q_2.P_1}{(q_2.k)(P_1.k)} + \frac{q_1.P_2}{(q_1.k)(P_2.k)}\right.
$$
$$
\left.\left. - \; \frac{q_1.P_1}{(q_1.k)(P_1.k)} - \frac{q_2.P_2}{(q_2.k)(P_2.k)}\right)\right] \tag{6.1}
$$

where e is the electromagnetic coupling constant, P_1 is the e^- momentum, P_2 is the e^+ momentum, q_i are the quark momenta, k is the photon momentum and M is the quark mass.

The result for soft *gluon* emission is obtained from (6.1) by setting $e_Q = 1$, $e_e = 0$ and $e^2 = C_F\,g_s^2$, where g_s is the strong coupling constant. For emission angles θ close to the quark direction and ignoring photon emission from the electron lines, this reduces to

$$
\frac{1}{\sigma_0}d\sigma = e_Q^2\frac{\alpha_{em}}{\pi}\frac{d\omega}{\omega}\frac{\theta^2 d\theta^2}{[\theta^2 + (M/E)^2]^2} \tag{6.2}
$$

where E is the energy of the quark in the quark centre of mass frame and ω is the photon energy. In the high energy limit $E/M \gg 1$, (6.2) exhibits the 'dead-cone' effect: the emission is suppressed for angles $\theta \lesssim \theta_0 = M/E$ [27]. As the energy increases, the cone becomes more narrow.

If the top quark is then allowed to decay, a simple modification of the above equation taking the top width into consideration leads to [25]

$$
\frac{1}{\sigma_0}d\sigma = e_Q^2\frac{\alpha_{em}}{\pi}\frac{d\omega}{\omega}\frac{\theta^2 d\theta^2}{[\theta^2 + \theta_0^2]^2 + (M\Gamma/E\omega)^2} \; . \tag{6.3}
$$

The above equation now exhibits the dead-cone effect in an angular region dependent on Γ and the mass of the top. However, it ignores emissions off the b quarks and the W bosons. Depending on the orientation of these particles, these emissions may lie within the top dead-cone, thus deforming the cone and exhibiting

dead-cone effects themselves in their directions. The orientation of these particles (which can be controlled experimentally) has a major effect on the radiation pattern as we shall see.

In Section (6.1) we shall derive from first principles the soft photon radiation pattern in $e^+e^- \rightarrow t\bar{t} \rightarrow b\bar{b}W^+W^-$. In Section (6.2) we present some numerical results that can be realized in the next generation of e^+e^- colliders. In Section (6.3) we present the conclusions.

6.1 Calculation of the Radiation Pattern

In this section we describe the calculation of the soft photon radiation pattern in $e^+e^- \rightarrow t\bar{t} \rightarrow b\bar{b}W^+W^-$.

6.1.1 Lowest Order Cross-Section

We consider photon radiation in the process $e^+e^- \rightarrow t\bar{t} \rightarrow bW^+\bar{b}W^-$ at high energies, well above the $t\bar{t}$ threshold. First we define some variables: W is the centre of mass energy, E =W/2 is the energy of the t and $\bar{t}$, M is the mass of the top quark, Γ is the total decay width of the top quark, $d\Omega_t$ is the solid angle element of the $t\bar{t}$ pair in the lab (e^+e^- centre of mass) frame, and $\theta_b(\theta_{\bar{b}})$ are the polar angles of the $b(\bar{b})$ quarks with respect to the $t(\bar{t})$ direction. The momenta of the particles are labeled by $e^-(P_1)e^+(P_2) \rightarrow b(p_1)W^+(r_1)\bar{b}(p_2)W^-(r_2)$ and $q_i = p_i + r_i$ (i=1,2). Note that the b quark and the W boson are treated as stable particles, *i.e.* we do <u>not</u> consider radiation off the W decay products. The inclusion of these extra contributions would be entirely straightforward but very cumbersome. Our focus here is rather on the interplay of initial and final state radiation. It is also worth mentioning that our analysis *is* exact for the process $e^+e^- \rightarrow W^+W^- \rightarrow l\bar{l}\nu\bar{\nu}\gamma$ where the formula derived applies totally with an appropriate modification of the charge factors (as the eikonal factor is the same for a photon coupling to a W and a photon coupling to a quark).

The lowest order cross section (no photon emission) [25] is

$$\frac{d\sigma}{d\Omega_t d\Omega_b d\Omega_{\bar{b}}} = \frac{1}{128W^2(2\pi)^8}v_t\frac{|\mathbf{r_1}||\mathbf{r_2}|}{E^2}(1 - \cos\theta_b v_t/v_b)^{-1}(1 - \cos\theta_{\bar{b}} v_t/v_{\bar{b}})^{-1}$$

63

$$\times \int \frac{dq_1^2}{(q_1^2 - M^2)^2 + M^2\Gamma^2} \frac{dq_2^2}{(q_2^2 - M^2)^2 + M^2\Gamma^2}$$

$$\times \frac{1}{4}\sum |\mathcal{M}'(e^+e^- \to b\bar{b}W^+W^-)|^2 \qquad (6.4)$$

where the sum is over the spins. The v's are the quark velocities in the lab frame: $v_t = |\mathbf{q}|/E$, $v_{b(\bar{b})} = |\mathbf{p_i}|/E_{b(\bar{b})}$ and the internal t quark propagators have been factored out of the matrix element $\mathcal{M}'$. To perform the integral over the t quark virtualities the *narrow width approximation* is used [25]

$$\int \frac{dq^2}{(q^2 - M^2)^2 + M^2\Gamma^2} = \frac{\pi}{M\Gamma} \qquad (6.5)$$

with the matrix element evaluated at $q_i^2 = M^2$.

6.1.2 Cross-Section with Photon Emission

We next consider the cross section including the emission of a single soft photon of momentum k, Fig. (6.1). In the limit $k \ll p_i, r_i$ the phase space can be written as

$$d\Phi_5 \to d\Phi_4 \, \omega \, d\omega \, d\cos\theta_\gamma \, d\Phi_\gamma/2(2\pi)^3 \qquad (6.6)$$

where θ_γ is the polar angle of the photon with respect to the top direction, Φ_γ is the azimuthal angle with respect to the top direction, ω is the photon's energy and the matrix element can be written in terms of J^μ:

$$\mathcal{M} \simeq \mathcal{M}' \, e \, J \cdot \epsilon_\lambda \qquad (6.7)$$

where ϵ_λ^μ is the photon's polarization vector and J^μ is the current.

After absorbing the internal quark propagators into the definition of the current and making use of the identity

$$\frac{1}{(q^2 - \overline{M}^2)((q+k)^2 - \overline{M}^2)} = \frac{1}{2q\cdot k}\left(\frac{1}{q^2 - \overline{M}^2} - \frac{1}{(q+k)^2 - \overline{M}^2}\right), \qquad (6.8)$$

the following result is obtained for J^μ:

$$J^\mu = \left(e_t\left[\frac{q_2^\mu}{q_2.k} - \frac{q_1^\mu}{q_1.k}\right] + e_{e^-}\left[\frac{P_1^\mu}{P_1.k} - \frac{P_2^\mu}{P_2.k}\right]\right)\frac{1}{(q_1^2 - \overline{M}^2)(q_2^2 - \overline{M}^2)}$$

$$- \left(-e_t \frac{q_1^\mu}{q_1.k} + e_b \frac{p_1^\mu}{p_1.k} + e_{W^+} \frac{r_1^\mu}{r_1.k} \right) \frac{1}{((q_1+k)^2 - \overline{M}^2)(q_2^2 - \overline{M}^2)}$$

$$+ \left(-e_t \frac{q_2^\mu}{q_2.k} + e_b \frac{p_2^\mu}{p_2.k} + e_{W^+} \frac{r_2^\mu}{r_2.k} \right) \frac{1}{(q_1^2 - \overline{M}^2)((q_2+k)^2 - \overline{M}^2)}$$

$$\equiv \quad \mathcal{A}^\mu - \mathcal{B}_1^\mu + \mathcal{B}_2^\mu \tag{6.9}$$

where $\overline{M} = M - i\Gamma/2$.

The current J'^μ for the analogous process $e^+ e^- \to W^+ W^- \gamma \to l \bar{l} \nu \bar{\nu} \gamma$ is :

$$
J'^\mu = \quad = \quad \left(\left[\frac{q_2^\mu}{q_2.k} - \frac{q_1^\mu}{q_1.k} \right] + \left[\frac{P_1^\mu}{P_1.k} - \frac{P_2^\mu}{P_2.k} \right] \right) \frac{1}{(q_1^2 - \overline{M}^2)(q_2^2 - \overline{M}^2)}
$$

$$
- \left(-\frac{q_1^\mu}{q_1.k} + \frac{p_1^\mu}{p_1.k} \right) \frac{1}{((q_1+k)^2 - \overline{M}^2)(q_2^2 - \overline{M}^2)}
$$

$$
+ \left(-\frac{q_2^\mu}{q_2.k} + \frac{p_2^\mu}{p_2.k} \right) \frac{1}{(q_1^2 - \overline{M}^2)((q_2+k)^2 - \overline{M}^2)}
$$

$$
\equiv \quad \mathcal{A}^\mu - \mathcal{B}_1^\mu + \mathcal{B}_2^\mu \tag{6.10}
$$

where the momenta of the final state particles are labeled by

$$e^-(P_1) e^+(P_2) \to W^+(q_1) W^-(q_2) \to l(p_1)\ \bar{l}(p_2)\ \nu(r_1)\ \bar{\nu}(r_2)\ \gamma(k).$$

All the individual terms are separately gauge invariant: $\mathcal{A}.k = \mathcal{B}_1.k = \mathcal{B}_2.k = 0$. In overall structure the result in (6.9) is very similar to the gluon result [25] but note the presence of extra terms which arise from the fact that photons can also be emitted off the initial e^+ and e^- and off the W boson.

The next step is to square the matrix element, summing over the spins and integrating over the q_i^2 virtualities, which gives

$$\int dq_1^2 dq_2^2 \sum |\mathcal{M}|^2 \simeq (\frac{\pi}{M\Gamma})^2 \sum |\mathcal{M}'|^2 \Big|_{q_1^2 = q_2^2 = M^2} e^2 \mathcal{F} \tag{6.11}$$

where the quantity $\mathcal{F}$ is defined by

$$\mathcal{F} \equiv (\frac{M\Gamma}{\pi})^2 \int dq_1^2 dq_2^2 [-J.J^*] . \tag{6.12}$$

Now using the above definition of J^μ, $\mathcal{F}$ is simply

$$\mathcal{F} = |\mathcal{A}|^2 + |\mathcal{B}_1|^2 + |\mathcal{B}_2|^2 - 2Re[\mathcal{B}_1 \mathcal{B}_2^*] + 2Re[\mathcal{A}(\mathcal{B}_2 - \mathcal{B}_1)^*] \tag{6.13}$$

65

with

$$|\mathcal{A}|^2 = - e_t^2 \left(\frac{M^2}{(q_1.k)^2} + \frac{M^2}{(q_2.k)^2} - 2\frac{q_1.q_2}{(q_1.k)(q_2.k)} \right)$$

$$- (e_{e-})^2 \left(\frac{m_e^2}{(P_1.k)^2} + \frac{m_e^2}{(P_2.k)^2} - 2\frac{P_1.P_2}{(P_1.k)(P_2.k)} \right)$$

$$- 2e_t e_{e-} \left(\frac{q_2.P_1}{(q_2.k)(P_1.k)} + \frac{q_1.P_2}{(q_1.k)(P_2.k)} \right.$$

$$- \left. \frac{q_1.P_1}{(q_1.k)(P_1.k)} - \frac{q_2.P_2}{(q_2.k)(P_2.k)} \right)$$

$$|\mathcal{B}_1|^2 = - \frac{e_b^2 m_b^2}{(p_1.k)^2} - \frac{e_{W+}^2 M_{W+}^2}{(r_1.k)^2} - \frac{e_t^2 M^2}{(q_1.k)^2}$$

$$- 2e_b e_{W+} \frac{p_1.r_1}{(p_1.k)(r_1.k)} + 2e_t e_b \frac{q_1.p_1}{(q_1.k)(p_1.k)}$$

$$+ 2e_t e_{W+} \frac{q_1.r_1}{(q_1.k)(r_1.k)}$$

$$|\mathcal{B}_2|^2 = - \frac{e_b^2 m_b^2}{(p_2.k)^2} - \frac{e_{W+}^2 M_{W+}^2}{(r_2.k)^2} - \frac{e_t^2 M^2}{(q_2.k)^2}$$

$$- 2e_b e_{W+} \frac{p_2.r_2}{(p_2.k)(r_2.k)} + 2e_t e_b \frac{q_2.p_2}{(q_2.k)(p_2.k)}$$

$$+ 2e_t e_{W+} \frac{q_2.r_2}{(q_2.k)(r_2.k)}$$

$$-2Re[\mathcal{B}_1\mathcal{B}_2^*] = \left(e_b^2 \frac{p_1.p_2}{(p_1.k)(p_2.k)} + e_{W+}^2 \frac{r_1.r_2}{(r_1.k)(r_2.k)} + e_t^2 \frac{q_1.q_2}{(q_1.k)(q_2.k)} \right.$$

$$+ e_b e_{W+} \left(\frac{p_1.r_2}{(p_1.k)(r_2.k)} + \frac{p_2.r_1}{(p_2.k)(r_1.k)} \right)$$

$$- e_b e_t \left(\frac{p_1.q_2}{(p_1.k)(q_2.k)} + \frac{q_1.p_2}{(q_1.k)(p_2.k)} \right)$$

$$\left. - e_t e_{W+} \left(\frac{r_1.q_2}{(r_1.k)(q_2.k)} + \frac{q_1.r_2}{(q_1.k)(r_2.k)} \right) \right)$$

$$\times 2M^2\Gamma^2 D_1 D_2 (q_1.k q_2.k + M^2\Gamma^2)$$

$$+2Re[\mathcal{A}(\mathcal{B}_2 - \mathcal{B}_1)^*] = \left[e_t^2 \left(\frac{M^2}{(q_2.k)^2} - \frac{q_1.q_2}{(q_1.k)(q_2.k)} \right) \right.$$

$$- e_t e_b \left(\frac{q_2.p_2}{(q_2.k)(p_2.k)} - \frac{q_1.p_2}{(q_1.k)(p_2.k)} \right)$$

$$- e_t e_{W+} \left(\frac{q_2.r_2}{(q_2.k)(r_2.k)} - \frac{q_1.r_2}{(q_1.k)(r_2.k)} \right)$$

$$+ e_{e-} e_t \left(\frac{P_1.q_2}{(P_1.k)(q_2.k)} - \frac{P_2.q_2}{(P_2.k)(q_2.k)} \right)$$

$$- e_{e-} e_b \left(\frac{P_1.p_2}{(P_1.k)(p_2.k)} - \frac{P_2.p_2}{(P_2.k)(p_2.k)} \right)$$

$$
\begin{aligned}
- \quad & e_{e^-}e_{W^+}\Big(\frac{P_1.r_2}{(P_1.k)(r_2.k)} - \frac{P_2.r_2}{(P_2.k)(r_2.k)}\Big)\Big] \\
\times \quad & 2M^2\Gamma^2 D_2 \\
+ \quad & \Big[e_t^2\Big(\frac{M^2}{(q_1.k)^2} - \frac{q_2.q_1}{(q_2.k)(q_1.k)}\Big) \\
+ \quad & e_t e_b\Big(\frac{q_2.p_1}{(q_2.k)(p_1.k)} - \frac{q_1.p_1}{(q_1.k)(p_1.k)}\Big) \\
+ \quad & e_t e_{W^+}\Big(\frac{q_2.r_1}{(q_2.k)(r_1.k)} - \frac{q_1.r_1}{(q_1.k)(r_1.k)}\Big) \\
+ \quad & e_{e^-}e_t\Big(\frac{P_2.q_1}{(P_2.k)(q_1.k)} - \frac{P_1.q_1}{(P_1.k)(q_1.k)}\Big) \\
+ \quad & e_{e^-}e_b\Big(\frac{P_1.p_1}{(P_1.k)(p_1.k)} - \frac{P_2.p_1}{(P_2.k)(p_1.k)}\Big) \\
+ \quad & e_{e^-}e_{W^+}\Big(\frac{P_1.r_1}{(P_1.k)(r_1.k)} - \frac{P_2.r_1}{(P_2.k)(r_1.k)}\Big)\Big] \\
\times \quad & 2M^2\Gamma^2 D_1 \tag{6.14}
\end{aligned}
$$

$$
D_i = \frac{1}{(q_i.k)^2 + M^2\Gamma^2}, \quad i = 1,2. \tag{6.15}
$$

Finally dividing through by the lowest order cross-section (6.4), we obtain the photon energy and angular distribution in the form:

$$
\frac{1}{\sigma_0}\frac{d\sigma_\gamma}{d\omega d\cos\theta_\gamma d\phi_\gamma} = \frac{\alpha_{em}}{4\pi^2}\,\omega\,\mathcal{F}. \tag{6.16}
$$

Notice that the separation of the current into three pieces can be understood as dividing the emission into a contribution which can be attributed to emission off the initial e^+e^- and a stable $t\bar{t}$ pair $(\mathcal{A}^\mu)$ and contributions $(\mathcal{B}_1^\mu\mathcal{B}_2^\mu)$ associated with the emission off the t, b quarks and the W^+ boson in the decay $t \to bW^+$ and $\bar{t}\bar{b}$ quarks and W^- boson in the decay $\bar{t} \to \bar{b}W^-$. Thus, the radiation pattern (the current squared) contributions come from three antennas $\{e^+e^-t\bar{t}, tbW^+, \bar{t}\bar{b}W^-\}$ together with interferences between them.

6.2 Numerical Analysis

In this section we present the numerical results for the photon distribution and in particular the angular distribution given by

$$
\frac{dN}{d\cos\theta_\gamma} \equiv \frac{1}{\sigma_0} \frac{d\sigma_\gamma}{d\omega \, d\cos\theta_\gamma d\phi_\gamma}\Big|_{\omega=5\text{GeV},\Phi_\gamma=0}
$$
$$
= \frac{\alpha_{em}}{4\pi^2} \, \omega \, \mathcal{F}\Big|_{\omega=5\text{GeV},\Phi_\gamma=0} \, .
$$

(6.17)

Since we assume the photon is soft, it does not change the kinematics of the basic process significantly. Obviously the most general case of the orientation of final state particles is rather complicated, and hence we focus on a special configuration which demonstrates the physics without unduly complicating the problem. Our choice is the following; the t and $\bar{t}$ momenta are back-to-back in the e^+e^- centre of mass frame, the $\bar{b} \, W^-$ are taken to be in the same plane as the $b \, W^+$ and the $b\bar{b}$ pair is taken to be back-to-back in the lab. All the angles are measured with respect to the t direction, or the tbW^+plane, i.e. $\Phi_\gamma = 0$ corresponds to photon emission in the plane of tbW^+. In all the figures shown W (the collision energy)=600 GeV, M=140 GeV[1], $\omega = 5$ GeVand α_{em} is taken to be $\frac{1}{137}$. Note that we choose $\omega = 5$ GeV not only to correspond to a potentially measurable photon but also because the greatest sensitivity to the width is for $\omega \sim \Gamma$ [25].

Fig. (6.2) shows the radiation pattern with all the particles, including the e^+e^- beam particles, located in the same plane. Although a specific configuration like this has a very small event rate, it is constructive to consider it in order to gain an understanding of the problem. The figure shows the photon's total angular (θ_γ) distribution (Tot) as given in (6.17) with $\theta_b = 45^o$, $\theta_e = 90^o$ and $\Gamma = 0.7$ GeV, the standard model value for M=140 GeV. The distribution is symmetric when $\theta_\gamma \to \theta_\gamma + 180^o$ due to the symmetric configuration chosen. The contributions according to the decomposition (6.13) are also shown. It is obvious from the figure that the biggest contribution comes from the initial state radiation $|A|^2$ (A) term in (6.17). So in order to reveal the important physics in the process

---

[1]Although this value is slightly less than the recently reported CDF value, see Table(1.1), non of the conclusions depend sensitively on the actual value.

the initial state radiation has to be minimized. This will be discussed extensively below, where the $|A^2|$ term will be examined more closely.

The remaining contributions come from the tbW^+ antenna, $|B_1|^2$ (B1) and the $\bar{t}\bar{b}W^-$ antenna $|B_2|^2$ (B2). These peak at different angles and are not symmetric on their own. However, the sum is symmetric about 180° as expected.

The interference of the final state radiation off the decay products from the decay $t \to bW^+$ and $\bar{t} \to \bar{b}W^-$ is the $-2\mathrm{Re}[B_1 B_2^*]$ (B1B2) contribution. This term is sensitive to Γ but is not the biggest interference contribution. Finally, the last contribution comes from the interference between initial and final state radiation, $2\mathrm{Re}[A(B_2 - B_1)^*]$ (AB). This is the biggest of the two interference contributions. It also has a destructive part which gives the dead-cone structure as discussed in the introduction. The above contribution depends sensitively on Γ as suggested by (6.14). However, the initial state radiation has the strongest effect on the pattern and all the other contributions are swamped by it.

Fig. (6.3) shows the photon's angular distribution (with all particles still in the same plane) for the case of $\theta_b = 45^o$, $\theta_{e^-} = 90^o$ for three values of Γ, 0.7 GeV (the standard model value), infinity and 0 GeV. As we can see the radiation pattern depends on Γ as predicted by (6.14), the small change between the pattern at 0.7 and 0 is mainly due to the fact that the dominant effect is the initial state radiation which is independent of Γ. The main features to be noticed here are:

1. Dead-cone-like distribution [25] : the emission is at a minimum in the particles' (*i.e.* b, W^+, $\bar{b}$, W^-) directions, high around them and is suppressed between them.

2. The lack of symmetry of the distribution about the b and the $\bar{b}$ direction. This depends quite sensitively on Γ, and so by changing the value of Γ one can change the shape of the curve.

3. There is a shoulder at 180° which is the direction of the $\bar{t}$. By changing the value of Γ the shape of the radiation pattern is changed, in particular the shoulder alters its shape and become less pronounced for increasing Γ. This is mainly due to the fact that the bigger the value of Γ, the bigger the interference terms and the same is true for the t direction.

4. There are singularities in the radiation pattern at 90° and 180° due to initial state radiation. Since the leptons are taken to be massless, the dot products like $(P_1.k)$ can vanish and the distribution is singular.

From the above observations it is clear that the initial state radiation should be minimized to gain greatest sensitivity to Γ.

Fig. (6.4) shows how the radiation pattern changes when the separation of the initial state and final state particles is increased. We do this by keeping all the final state particles in a plane and by rotating the initial e^+e^- beam directly out of plane by an angle ϕ_e, keeping $\theta_e = 90^o$. As we can see from the figure, the contribution from the initial state radiation dies quickly, in fact it almost has reached its minimum by the time the e^+e^- beam is at around 30° out of the tbW^+ plane. Note that fig. (6.2) is the $\phi_e = 0$ plane in the three-dimensional plot. Thus, as the e^+e^- beam moves away from the rest of the particles the initial state radiation effects die out rapidly.

The $|A|^2$ term can be written as a contribution from the $t\bar{t}$ quarks A_1, the e^+e^- beam A_2, and interferences between them A_3, $i.e.$

$$|\mathcal{A}|^2 = A_1 + A_2 + A_3 \tag{6.18}$$

where

$$
\begin{aligned}
A_1 &= -\ e_t^2 \left(\frac{M^2}{(q_1.k)^2} + \frac{M^2}{(q_2.k)^2} \right) + 2e_t^2 \frac{q_1 \cdot q_2}{(q_1.k)(q_2.k)} \\
A_2 &= -\ (e_{e^-})^2 \left(\frac{m_e^2}{(P_1.k)^2} + \frac{m_e^2}{(P_2.k)^2} - 2\frac{P_1.P_2}{(P_1.k)(P_2.k)} \right) \\
A_3 &= -\ 2e_t e_{e^-} \left[\frac{q_2.P_1}{(q_2.k)(P_1.k)} + \frac{q_1.P_2}{(q_1.k)(P_2.k)} \right. \\
&\quad -\ \left. \frac{q_1.P_1}{(q_1.k)(P_1.k)} - \frac{q_2.P_2}{(q_2.k)(P_2.k)} \right] \ .
\end{aligned}
$$

$$\tag{6.19}$$

Fig. (6.5) shows these contributions with $\theta_b = 45^o$ and $\theta_e = 90^o$. The A_1 part is identical to the gluon case within a multiplicative factor, and is independent

of the orientation with respect to the e^+e^- beam. In the case where the photon is in the tbW^+ plane, the second part (A_2 term) is largest when the e^+e^- beam is in the plane of the rest of the particles. Note that when the beam is in the transverse plane ($\phi_e = 90^o$) this term is constant *i.e.* independent of θ_γ . Note also that we have a symmetry when $\phi_e \rightarrow 180^o - \phi_e$ as can be seen in the figure. Finally, the A_3 interference term is antisymmetric when $\phi_e \rightarrow 180^o - \phi_e$ and thus is identically zero at $\phi_e = 90^o$. It is also worth mentioning that for a wide range of angle ϕ_e the A_2 term is constant and the A_3 term is very small.

Fig. (6.6) shows the angular distribution under minimum initial state radiation conditions with $\theta_b = 45^o$. It is interesting to compare this figure with fig. (6.3). The most important feature to be noticed is that the *dead-cone effect* is now well pronounced for example, in the b quark direction. In this configuration the initial state radiation does not dominate the pattern and does not fill the angular region between the final state particles.

In order to focus on the effects of the initial state radiation we have so far restricted the photon to lie in the plane of the final state particles. If we take the plane of the final state particles to be transverse to the beam direction ($\phi_e = 90^o$) and then allow the photon to be emitted out of this plane ($\Phi_\gamma > 0^o$) then we again see the influence of the initial state radiation. Fig. (6.7) shows the radiation pattern for different Φ_γ, the e^+e^- beam is in the completely transverse plane so $\phi_e = \theta_e = 90^o$, $\theta_b = 45^o$ and $\Gamma = 0.7$ GeV. The $\Phi_\gamma = 0^o$ curve is essentially identical to the $\Gamma = 0$ GeV curve in fig. (6.6) (*i.e.* the difference between the $\Gamma = 0$ GeV and the $\Gamma = 0.7$ GeV is very small). The *dead-cone* effect is again swamped by initial state radiation since the dot product terms like ($P_1.k$) are angle dependent and so the A_2 term which is the biggest contribution to the initial state radiation is not a constant, and the interference term A_3 does not vanish.

6.3 Conclusion

In this chapter the distribution of soft photon radiation in the process $e^+e^- \rightarrow t\bar{t} \rightarrow b\bar{b}W^+W^-$ is studied. We have demonstrated that the initial state radiation

71

can easily swamp the sensitivity of the radiation pattern to the top decay width. However, for the case when the final state particles are in a plane transverse to the beam direction and when the photon itself is in this plane, then the initial state radiation effects are minimized, only contributing a small constant background to the overall pattern. Thus the radiation pattern depends sensitively on the top width. For purposes of illustration we have chosen a top mass $M = 140$ GeV. Although the radiation pattern depends in detail on M (see (6.14)), qualitatively the results are unchanged if the mass is increased to the most recent CDF value of 176 GeV. It is clear from fig. (6.5) that the minimum of the initial state radiation is valid for a much wider range of angles than just 90°. Thus, in practice, simply to keep the final state particles (including the photon) well away from the initial beam should be sufficient.
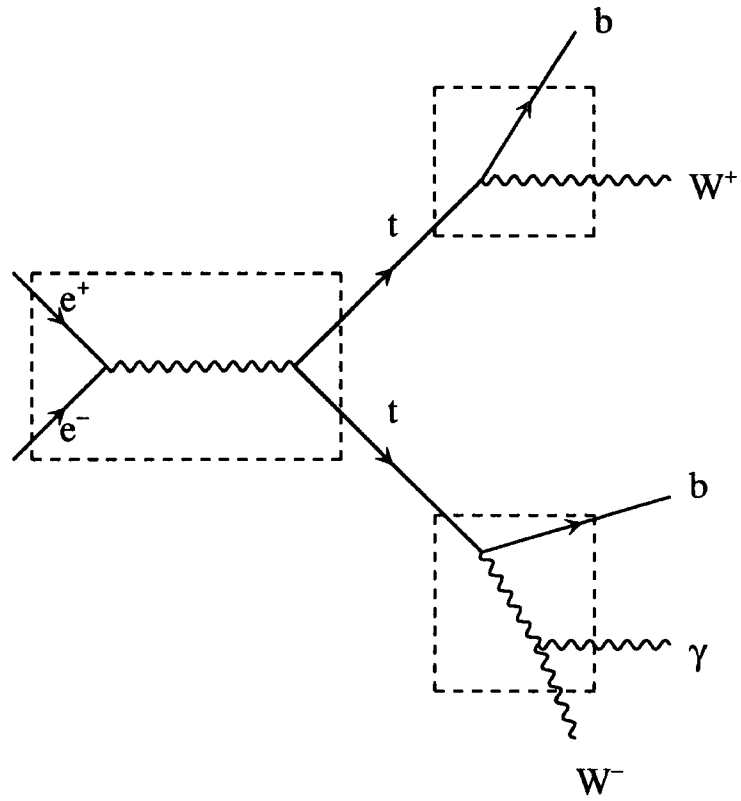
Figure 6.1: An example of a Feynman diagram for photon emission in $e^+e^- \rightarrow t\bar{t} \rightarrow bW^+\bar{b}W^-$; the decomposition corresponds to that in (6.9).
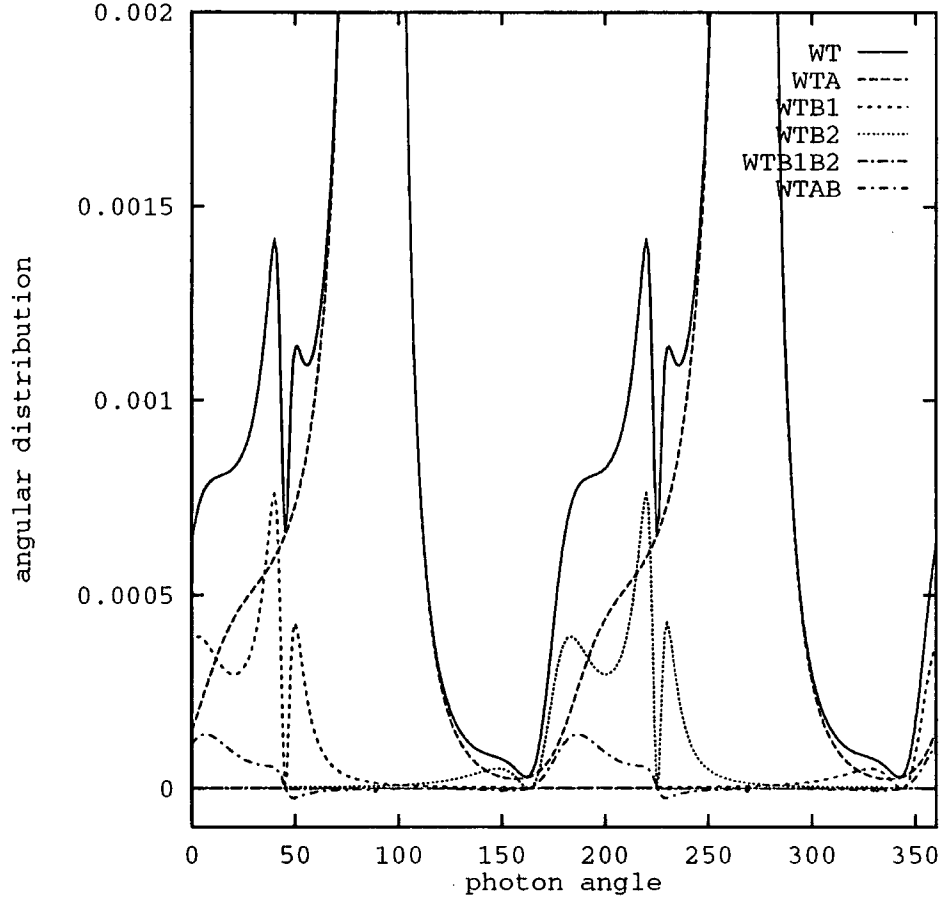
Figure 6.2: Distribution of soft photon radiation in $e^+e^- \to t\bar{t} \to bW^+\bar{b}W^-$. $dN/d\cos(\theta_\gamma)$ (defined in (6.17)) for $M = 140$ GeV, $W = 600$ GeV, $\Gamma = 0.7$ GeV and $\theta_b = 45°$ with decomposition according to (6.14). WT: total $dN/d\cos(\theta_\gamma)$. WTA: $|A|^2$ contribution. WTB1: $|B_1|^2$ contribution. WTB2: $|B_2|^2$ contribution. WTB1B2 : $B_1 - B_2$ interference. WTAB: $A - B$ interference.
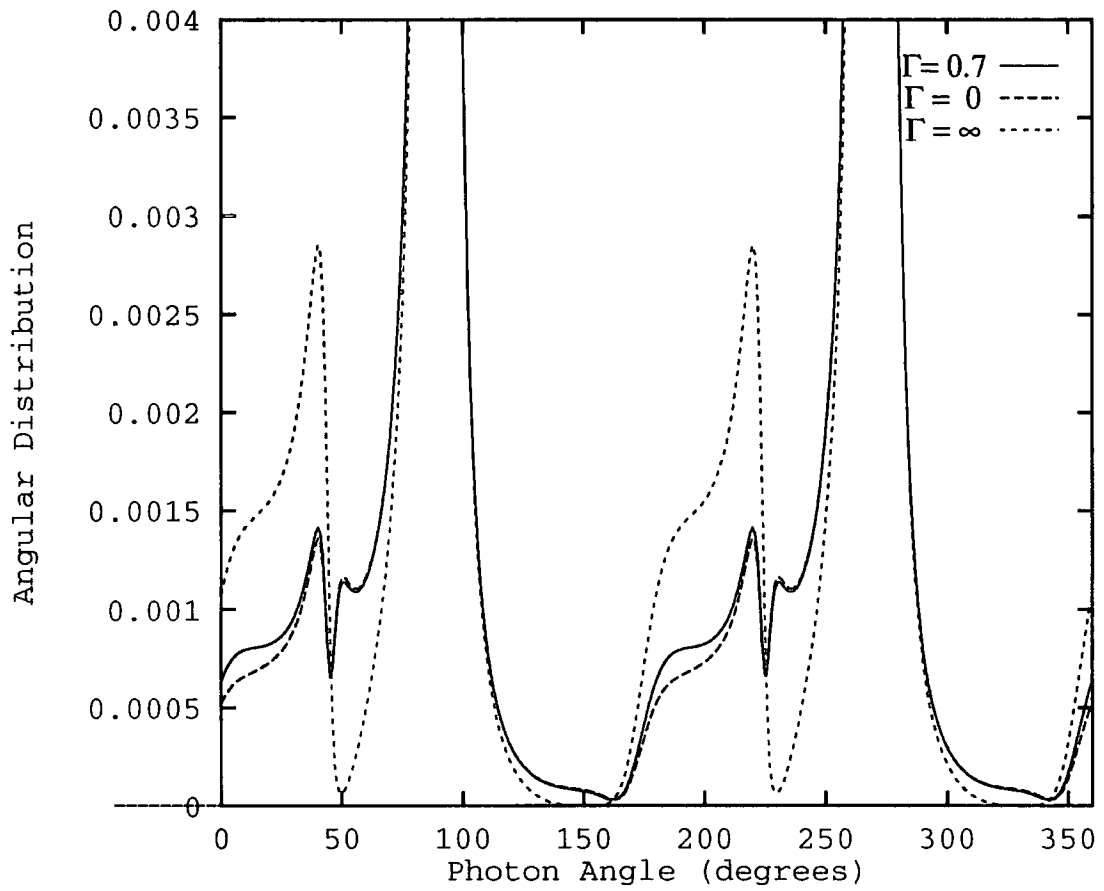
Figure 6.3: Sensitivity of the radiation pattern to Γ:
soft photon distribution $dN/d\cos(\theta_\gamma)$ for $M = 140$ GeV, $W = 600$ GeV, and $\theta_b = 45°$ for different values of Γ. Namely $\Gamma = 0.7$ GeV the standard model value, $\Gamma = 0$ GeV and $\Gamma = \infty$.
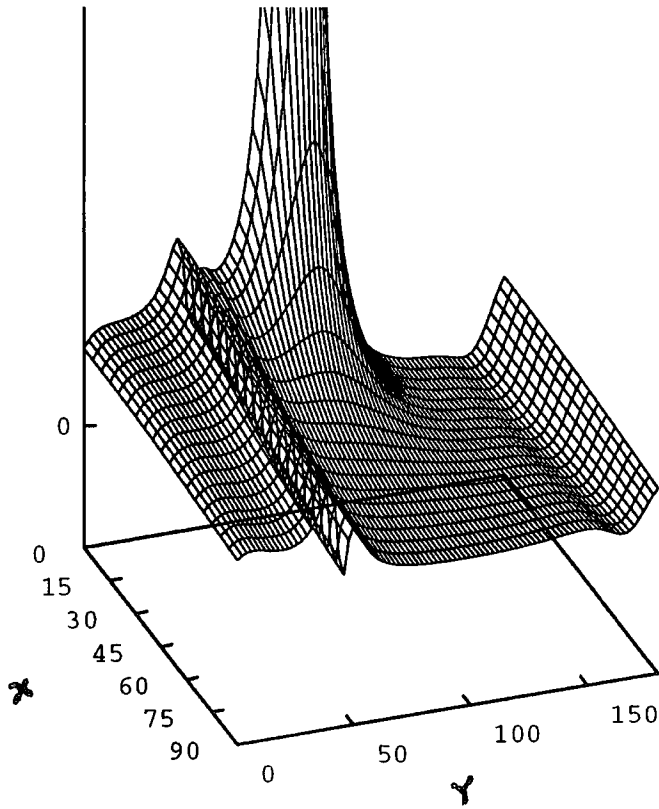
Figure 6.4: The effect of initial state radiation when the e^+e^- beam is moved away from the final state particles. The parameter values are $\theta_b = 45°$, $\Gamma = 0.7$ GeV, $M = 140$ GeV and $W = 600$ GeV. The x–axis is ϕ_e in degrees while the y-axis is θ_γ in degrees.
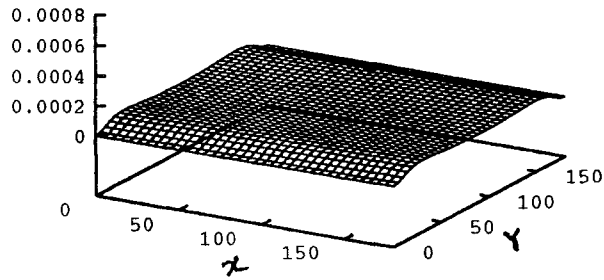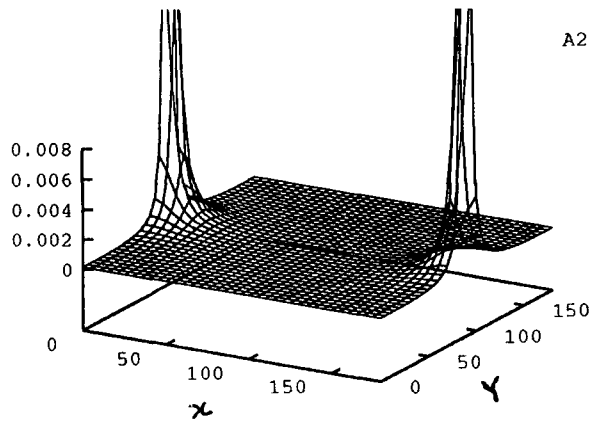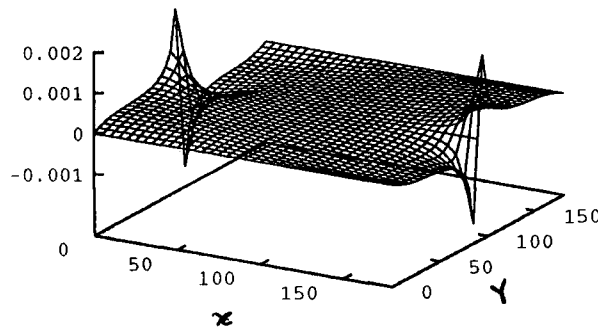
Figure 6.5: The decomposition of the initial state radiation according to contributions in $dN/d\cos(\theta_\gamma)$ defined in (6.17).

A_1 is the $t\bar{t}$ contribution, A_2 is the e^+e^- contribution, and A_3 is the interference contribution

The parameter values are $\theta_b = 45^o$, $\Gamma = 0.7$ GeV, $M = 140$ GeV and $W = 600$ GeV. The x-axis is ϕ_e in degrees while the y-axis is θ_γ in degrees.
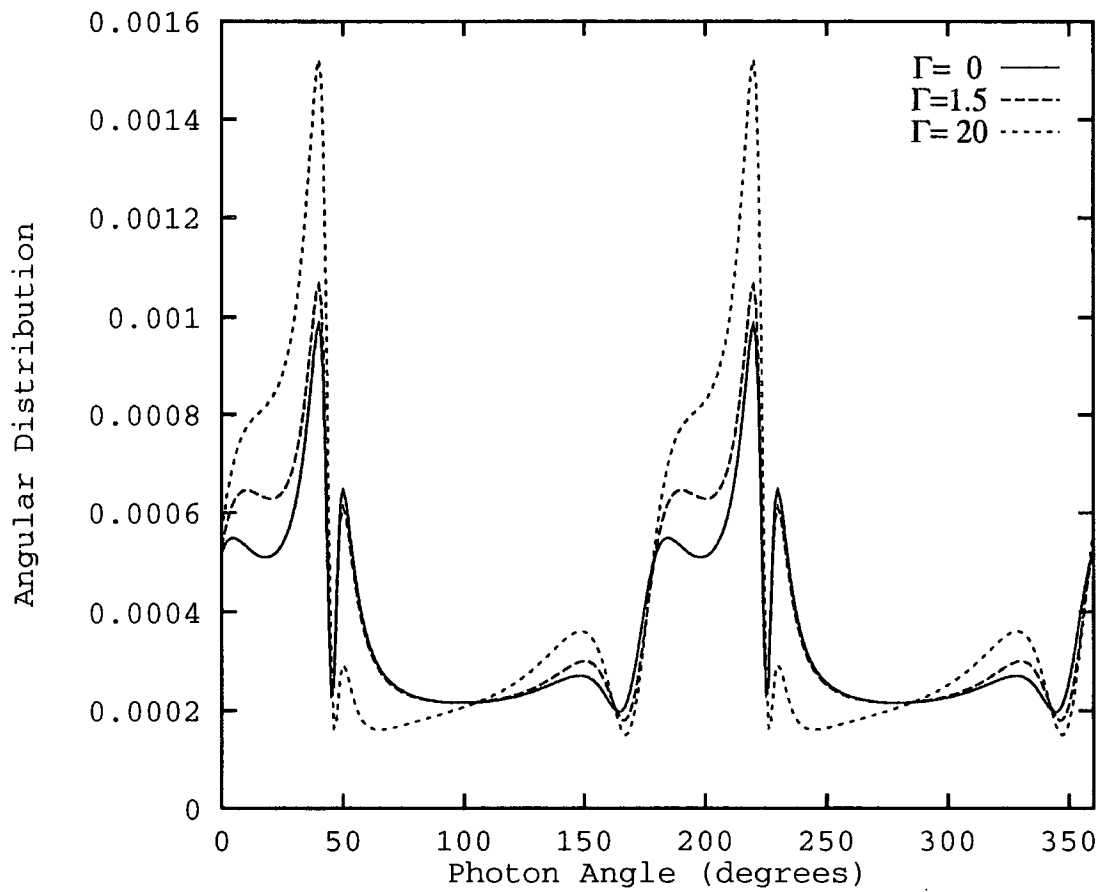
Figure 6.6: Sensitivity to Γ in the case of minimum initial state radiation. $dN/d\cos(\theta_\gamma)$ is plotted for $M = 140$ GeV, $\theta_b = 45°$, $W = 600$ GeV and Γ is as marked.
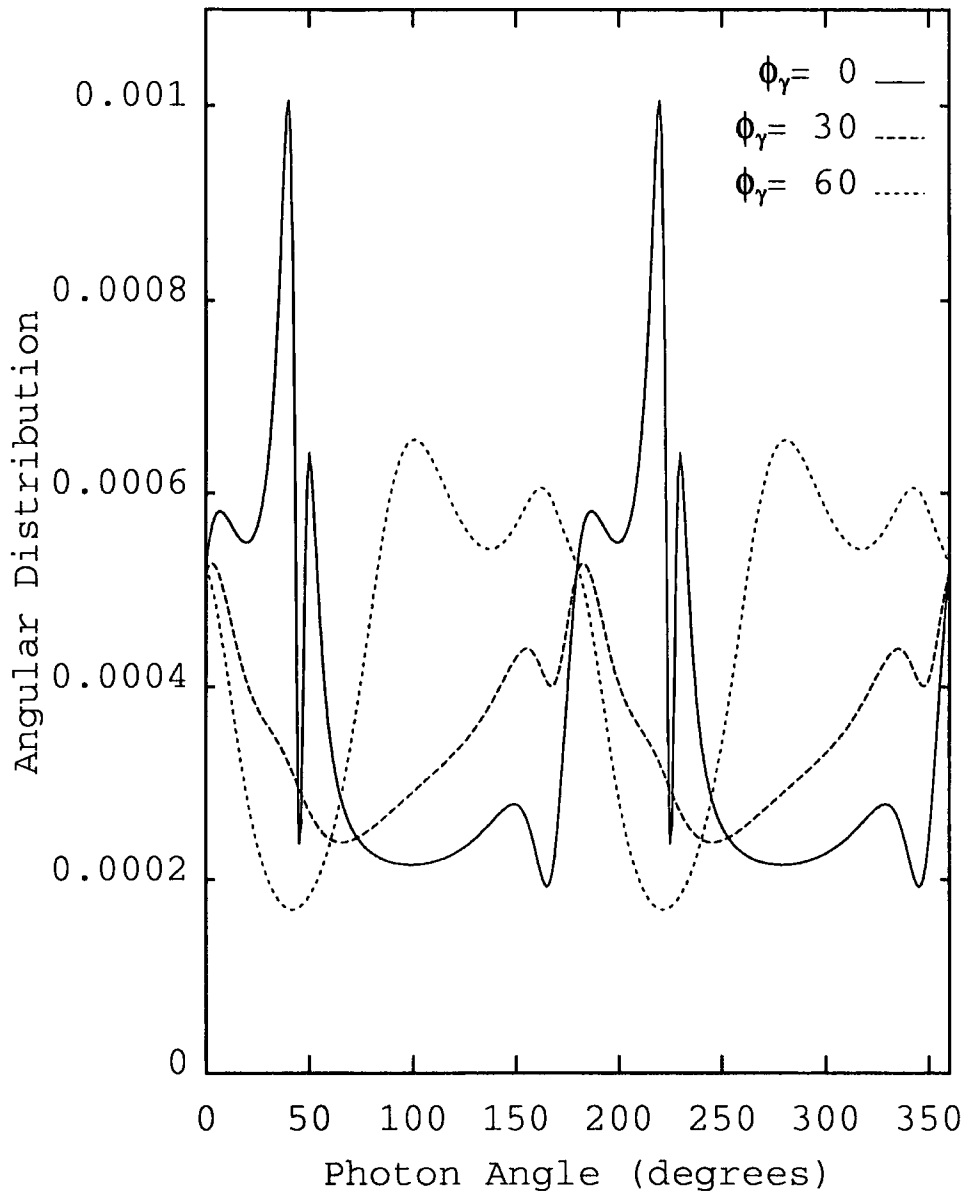
Figure 6.7: Distribution of soft photon radiation in $e^+e^- \rightarrow t\bar{t} \rightarrow bW^+\bar{b}W^-$ plotted for different Φ_γ, as marked in the figure. The parameter values are $M = 140$ GeV, $\theta_b = 45°$, $W = 600$ GeV and $\Gamma = 0.7$ GeV.

Chapter 7

The intermediate mass SM Higgs boson at LEP⊗LHC ep collider

7.1 Introduction

The Higgs sector of the Standard Model (SM) [7, 9] is one of its most investigated sectors, yet is continues to be very elusive. So far the Higgs particle has evaded all searches. Nevertheless, a lower limit on the mass of the SM Higgs ϕ of 64.3 GeV was extracted from the lack of $e^+e^- \rightarrow Z^0 \rightarrow Z^{0*}\phi$ events at LEP I [28]. An upper bound of ≈ 1 TeV is expected. This is derived by requiring the validity of perturbation theory [29] and the unitarity of the model [30]. Therefore, if the SM Higgs ϕ exists, we could expect it to be discovered by the next generation of CERN high energy colliders: LEP II ($\sqrt{s}_{ee}$ =160–200 GeV) [31] and the LHC ($\sqrt{s}_{pp} = 10, 14$ TeV)[32].

LEP II will be able to cover the mass range M_ϕ <80–100 GeV. A Higgs with a larger mass should be searched for at the LHC. At LEP II ϕ can be detected [1] through a large variety of decay channels, the most favoured being $Z^0\phi \rightarrow (\mu^+\mu^-)(b\bar{b})$. A Higgs boson with mass $M_\phi \gtrsim 130$ GeV is clearly detectable at the LHC using the four–lepton mode $\phi \rightarrow Z^{0*}Z^0 \rightarrow \ell\bar{\ell}\ell\bar{\ell}$[2]. Due to the QCD backgrounds typical of hadron colliders, it is still controversial whether it is possible to detect an intermediate mass Higgs[3] in the mass range $90 \lesssim M_\phi \lesssim 130$ GeV (where ϕ mainly decays to $b\bar{b}$ pairs). In this mass range ϕ can be searched for

---

[1] And produced via the Bjorken bremsstrahlung process $e^+e^- \rightarrow Z^{0*} \rightarrow Z^0\phi$ [33].

[2] With ϕ produced via $gg-$ [34] or $W^\pm W^\mp-$ and Z^0Z^0–fusion [35].

[3] Via the associated production with a $W^\pm$ boson (decaying leptonically to $\ell\nu$) [36, 37] or a $t\bar{t}$ pair (with one t decaying semileptonically to $b\ell\nu$) [38, 39].

through the rare $\gamma\gamma$ decay mode and this relies on the fact that both a high luminosity and a very high di–photon mass resolution must be achieved at the LHC [40]. It is also unclear whether it is possible to cleanly detect the intermediate SM Higgs in the $\phi \to b\bar{b}$ channel using the b–tagging capabilities of vertex detectors [41, 42]. The main difficulties being the expected low signal rates after reconstruction, the necessity to have an accurate control on all the possible background sources and to achieve a very high b–tagging performance [43].

In the distant future, cleaner environments for studying the Higgs boson parameters will be the e^+e^- linear accelerators ($\sqrt{s}_{ee} = 350 - 2000$ GeV) [8, 44, 45, 46, 47].

At the Next Linear Collider (NLC), with $\sqrt{s}_{ee} = 300 - 500$ GeV [46], the Higgs boson can be searched for through a large number of channels over the whole intermediate mass range [48]. The dominant production mechanism is the Bjorken reaction for $\sqrt{s}_{ee}$ below 500 GeV while the $W^{\pm}W^{\pm}-$ and Z^0Z^0–fusion processes [49] will dominate at larger energies. At $\sqrt{s}_{ee} \gtrsim 500$ GeV [45] a heavy Higgs can be detected in the four–jet modes $\phi \to W^{\pm}W^{\mp}, Z^0Z^0 \to jjjj$ [50, 51] in addition to the 4ℓ–mode. At higher energies, $\sqrt{s}_{ee} = 1 - 2$ TeV [47], the same search strategies still hold with the fusion mechanisms becoming the dominant ones.

The conversion of the linear e^+e^- NLCs into $\gamma\gamma$ and/or $e\gamma$ colliders, by photons generated via Compton back–scattering of laser light, will provide new possibilities for detecting and studying the Higgs boson [52]. In $\gamma\gamma$ collisions two of the important channels will be: the production of a heavy Higgs (up to ≈ 350 GeV) by a triangular loop of heavy fermions or $W^{\pm}$, with the detection via the decay mode $\phi \to Z^0Z^0 \to q\bar{q}\ell^+\ell^-$ at $\sqrt{s}_{ee} = 500$ GeV [53], and the process $\gamma\gamma \to t\bar{t}\phi$, which appears more useful than the corresponding e^+e^- one in measuring the *top* Yukawa coupling $t\phi$, at $\sqrt{s}_{ee} = 1 - 2$ TeV [54]. The $e\gamma$ option at linear colliders can be exploited for studying Higgs production via the process $e\gamma \to \nu_e W\phi$, at $\sqrt{s}_{ee} = 1 - 2$ TeV and over the mass range 60 GeV $\lesssim M_\phi \lesssim 150$ GeV [55, 56], using the signature $W^-\phi \to (jj)(b\bar{b})$ [57]. The cross section for the above process at such $\sqrt{s}_{ee}$'s is comparable to the fusion process $e^+e^- \to \bar{\nu}_e\nu_e W^{\pm*}W^{\mp*} \to \bar{\nu}_e\nu_e\phi$ and larger than the bremsstrahlung reaction $e^+e^- \to Z^{0*} \to Z^0\phi$. Finally, it

has been shown in [58] that the process $e\gamma \to e\gamma\gamma \to e\phi$ is the most important mechanism for ϕ–production at $\sqrt{s}_{ee} = 500$ GeV, for $M_\phi \gtrsim 140$ GeV.

Let us now consider the production of the SM Higgs boson at ep machines. This seems to be beyond the capabilities of HERA [59], which has been primarily designed for providing accurate data on the proton structure functions in the small–x region, more than for Higgs searches [60]. In the future, another ep collider is contemplated, the CERN LEP$\otimes$LHC accelerator: it will combine an electron/positron beam from LEP II and a proton beam from the LHC [32, 61]. A detailed study on the detectability of an intermediate mass SM Higgs boson at such a machine has been presented in [62]. This is based on the $W^\pm W^\mp-$ and $Z^0 Z^0-$ fusion processes [60, 63, 64], with ϕ decaying to $b\bar{b}$. It has been shown that it should be possible to detect ϕ provided that a high luminosity and/or an excellent $b-$ flavour identification can be achieved. Only recently has the possibility of resorting to back–scattered laser photons at the ep CERN collider been suggested [65], searching for, e.g., $\gamma q \to q' W^\pm \phi$ events, with $\phi \to b\bar{b}$ and $W^\pm \to \ell\nu$ or jj, which should give detectable Higgs signals if good $M_{b\bar{b}}$ invariant mass resolution can be achieved and efficient b-tagging can be performed.

The purpose of this chapter is to study the following reactions at the LEP$\otimes$LHC ep collider

$$q\gamma \to q' W^\pm \phi, \qquad (7.1)$$

$$q\gamma \to q Z^0 \phi, \qquad (7.2)$$

$$g\gamma \to q\bar{q}\phi, \qquad (7.3)$$

in the intermediate mass range of ϕ, for all possible (anti)flavours of the (anti)quarks $q(q')$, using laser back–scattered photons. We discuss their relevance to the detection of the SM Higgs and the study of its parameters, with the Higgs decaying to $b\bar{b}$–pairs and assuming flavour identification on its decay products.

Although process (7.1) has already been studied in [65], and the part of the analysis devoted to it here largely overlaps that study, we decided nevertheless to include it for completeness and since, in principle, we can slightly improve the results previously obtained. In fact, since we consider heavy quarks we include additional Higgs bremsstrahlung off quarks in the amplitudes, even though these are suppressed with respect to contributions coming from diagrams involving $\phi W^+ W^-$

vertices. We also computed all the necessary rates for all the relevant backgrounds exactly, whereas these latter contributions were only estimated in [65]. Reaction (7.3) has been analysed in [66] for MSSM neutral Higgses, b–quarks and using bremsstrahlung photons but to our knowledge, neither the larger energy option available at LEP$\otimes$LHC nor the possibility of using laser back–scattered photons has been exploited.

There are at least two important motivations for analysing processes (7.1)–(7.3) at the LEP$\otimes$LHC collider. First, if the SM Higgs boson turns out to have an intermediate mass greater than the maximum value that can be reached by LEP II and if the LHC detectors are not able to achieve the necessary performances for the predicted Higgs measurements [43], the ep CERN collider will be the first alternative option available for studying such a Higgs, as it will certainly be operating before any NLC. Second, although both the cross sections and the luminosity at LEP$\otimes$LHC are expected to be small if compared with the LHC ones, the CERN ep option will constitute the first TeV energy environment partially free from the enormous QCD background typical of purely hadronic colliders. Moreover, processes (7.1)–(7.3) have the advantage, compared to the $W^{\pm}W^{\mp}$– and Z^0Z^0–fusion mechanisms, that the additional heavy particles $W^{\pm}$ and Z^0 (and also t, in principle) can be used for tagging purposes by searching for their decays, thus increasing the signal to background ratio.

The plan of the chapter is as follows. In Section (7.2) we give details of the calculation and the numerical values adopted for the various parameters. Section (7.3) is devoted to the discussion of the results, while the conclusions are in Section (7.4).

7.2 Calculation

Fig. (7.1) shows all the Feynman diagrams at tree level contributing to the reactions (7.1) and (7.2) in the unitary gauge, where (q, q', V) represent the possible combinations (d, u, W^-), (u, d, W^+) and (q, q, Z^0) respectively (in the case of process (7.2) only the first eight diagrams of fig. (7.1) contribute). Fig. (7.2) shows the Feynman diagrams at tree level for process (7.3). All quarks have been considered massive, so diagrams with a direct coupling of ϕ to the fermion lines have

been taken into account.

The amplitudes squared have been computed by means of the spinor techniques of [67, 68][4]. The matrix elements for the processes $\bar{d}\gamma \to \bar{u}W^+\phi$ / $\bar{u}\gamma \to \bar{d}W^-\phi$ and $\bar{q}\gamma \to \bar{q}Z^0\phi$ can easily be obtained by trivial operations of charge–conjugation. All of the above amplitudes have been tested for gauge invariance. We were also able to "roughly"[5] reproduce, with appropriate couplings, hadron distributions and luminosity function of the photons, the results of [65] and of [66]. Moreover, since a simple adaptation of the implemented formulae (by changing photon couplings from quarks into leptons and setting the quark masses equal to zero) allowed us to reproduce the computation of [57], we have checked our helicity amplitudes in this way also.

As proton structure functions we adopted the HMRS set B [70] (this was done in order to make comparisons with already published work easier), setting the energy scale equal to the center–of–mass (CM) energy at the parton level (i.e. $\mu = \sqrt{\hat{s}_{\text{parton}}}$). The strong coupling constant α_s, which appears in the gluon initiated processes, has been evaluated at two loops, for $\Lambda_{QCD} = 190$ MeV, with a number $N_f = 5$ of active flavours and a scale μ equal to that used for the proton structure functions. We are confident that changing the energy scale and/or distribution function choice should not affect our results by more than a factor of two.

For the energy spectrum of the back–scattered (unpolarized) photon we have used [71]

$$F_{\gamma/e}(x) = \frac{1}{D(\xi)}\left[1 - x + \frac{1}{1-x} - \frac{4x}{\xi(1-x)} + \frac{4x^2}{\xi^2(1-x)^2}\right], \qquad (7.4)$$

where $D(\xi)$ is the normalisation factor

$$D(\xi) = \left(1 - \frac{4}{\xi} - \frac{8}{\xi^2}\right)\ln(1+\xi) + \frac{1}{2} + \frac{8}{\xi} - \frac{1}{2(1+\xi)^2}, \qquad (7.5)$$

and $\xi = 4E_0\omega_0/m_e^2$, ω_0 is the incoming laser photon energy and E_0 the (unpolarized) electron/positron energy. In (7.4) $x = \omega/E_0$ is the fraction of the energy

---

[4]We do not present here the corresponding helicity amplitudes, since they can be obtained by appropriate changes of couplings as a subset of those to be given in [69] for the case of MSSM Higgs bosons.

[5]See footnote 10 below.

of the incident electron/positron carried by the back–scattered photon, with a maximum value

$$x_{\text{max}} = \frac{\xi}{1 + \xi}. \tag{7.6}$$

In order to maximise ω while avoiding e^+e^- pair creation, one takes ω_0 such that $\xi = 2(1 + \sqrt{2})$ and one gets the typical values $\xi \simeq 4.8$, $x_{\text{max}} \simeq 0.83$, $D(\xi) \simeq 1.8$.

In the case of $q(g)\gamma$ scattering from ep collisions, the total cross section σ is obtained by folding the subprocess cross section $\hat{\sigma}$ with the photon $F_{\gamma/e}$ and hadron $F_{q(g)/p}$ luminosities:

$$\sigma(s_{ep}) = \int_{x^\gamma_{\text{min}}}^{x^\gamma_{\text{max}}} dx^\gamma \int_{x^{q(g)}_{\text{min}}}^{1 - x^\gamma} dx^{q(g)} F_{\gamma/e}(x^\gamma) F_{q(g)/p}(x^{q(g)}) \hat{\sigma}(\hat{s}_{q(g)\gamma} = x^\gamma x^{q(g)} s_{ep}), \tag{7.7}$$

where $\hat{s}_{q(g)\gamma}$ is the CM energy at parton (i.e., $q(g)\gamma$) level, while

$$x^\gamma_{\text{min}} x^{q(g)}_{\text{min}} = \frac{(M_{\text{final}})^2}{s_{ep}}, \tag{7.8}$$

where M_{final} is the sum of the final state particle masses.

The multidimensional integrations have been performed numerically using the Monte Carlo routine VEGAS [72].

To our knowledge, a detailed study, as for the cases of $e\gamma$ and $\gamma\gamma$ collisions [71], on the efficiency of the laser back–scattering method in converting $e \rightarrow \gamma$ at ep colliders does not exist. In this chapter we assume for the effective γp luminosity a conservative estimate of half the ep one. For the discussion of the results we have adopted an overall total integrated luminosity $\mathcal{L} = 3$ fb^{-1} per year, adopting the value of [65].

For the numerical part of our work, we have taken $\alpha_{em} = 1/128$ and $\sin^2 \theta_W \equiv s^2_W = 0.23$, while for the gauge boson masses and widths: $M_{Z^0} = 91.175$ GeV, $\Gamma_{Z^0} = 2.5$ GeV, $M_{W^\pm} = M_{Z^0} \cos \theta_W \equiv M_{Z^0} c_W$ and $\Gamma_{W^\pm} = 2.2$ GeV. For the fermions we have: $m_e = 0.511 \times 10^{-3}$ GeV, $m_\mu = 0.105$ GeV, $m_\tau = 1.78$ GeV, $m_u = 8.0 \times 10^{-3}$ GeV, $m_d = 15.0 \times 10^{-3}$ GeV, $m_s = 0.3$ GeV, $m_c = 1.7$ GeV, $m_b = 5.0$ GeV and $m_t = 175$ GeV, with all widths equal to zero apart from $\Gamma_t \approx 1.58$ GeV, adopting its tree–level expression). All neutrinos have been considered massless: i.e., $m_{\nu_e} = m_{\nu_\mu} = m_{\nu_\tau} = 0$. The branching ratios (BRs) of the Higgs boson were extracted from [73].

We have analysed the processes (7.1)–(7.3) over the mass range 60 GeV $\lesssim$ M_ϕ $\lesssim$ 140 GeV and for ep CM energy ranging from 0.5 to 3.0 TeV, with special attention devoted to the case $\sqrt{s}_{ep}$ = 1.36 TeV, corresponding to the collision of an electron/positron beam from LEP II and a proton beam from LHC [65].

7.3 Results

In figs. (7.3)–(7.5) we present the dependence of processes (7.1)–(7.3) on the collider CM energy, for a selection of Higgs masses: M_ϕ = 60, 80, 100, 120 and 140 GeV. Summations over all possible combinations of (anti)flavours have been performed (the *top* contributions in the final states are included[6]), as well as the integration over the initial $g/q(\bar{q})$– and γ–structure functions. A general feature in figs. (7.3) and (7.5) is the rapid increase of all the plots with $\sqrt{s}_{ep}$, especially for $\sqrt{s}_{ep}$ $\gtrsim$ 1 TeV. This is because for $\sqrt{s}_{ep}$ much larger than the final particle masses, phase space effects are quantitatively unimportant. The same effect is less evident in fig. (7.4), since process (7.2) is affected by the s–channel structure of the corresponding Feynman diagrams, whereas [part of] these are in t–channel for process [(7.1)](7.3). We also notice that the cross section for the process $ep \rightarrow W^{\pm}\phi X$ is much larger than that of $ep \rightarrow Z^0\phi X$. This is due to two reasons: first, the coupling ϕW^+W^- is larger than $\phi Z^0 Z^0$ and second, in process (7.1) there are additional diagrams (i.e., # 9–12 in fig. (7.1)), some of which (i.e., # 11 and 12) are not suppressed by Yukawa couplings.

In Table (7.1) we give the cross sections at the LEP$\otimes$LHC CM energy $\sqrt{s}_{ep}$ = 1.36 TeV. To show the importance of the relative contributions of the various flavours entering in the subprocesses (7.1)–(7.3), we give their separate rates in Table (7.2) at M_ϕ = 60 GeV. For reaction (7.1) at a fixed $\sqrt{s}_{ep}$, increasing the Higgs mass reduces the *top* quark contributions, this is due to the limited phase space available, while the light flavours contributions (i.e., q = u, d, s, c and b) do not change significantly. For example, the *top* contribution to process (7.1) diminishes from 1.4% to 0.12% when M_ϕ increases from 60 to 140 GeV, whereas the contributions from *up* (*down*) [*strange*] {*charm*}–initiated processes vary from

---

[6]As a first approximation only combinations of two flavours within the same quark doublet have been computed for process (7.1), setting all Cabibbo–Kobayashi–Maskawa terms equal to one.

86

≈ 53 (35) [8] {3}% to ≈ 64 (29) [5] {2}%. For process (7.2) there is no substantial phase space effect of this kind, since we cannot have *top* contributions here. Thus the numbers do not differ as much: they are ≈ 74 (16) [4] {5} < 0.6 > % to ≈ 80 (14) [3] {3} < 0.33 >%, with the numbers in the "brackets" <> corresponding to *b*-contributions. For reaction (7.3), things change dramatically because, on the one hand, *top*-lines are not connected to the initial state as in (7.1) and the phase space suppression due to the large *top* mass is important only if $\sqrt{s}_{ep} \lesssim 1$ TeV, and on the other hand, the Higgs always couples to the very massive *top*-quark through the ($\sim m_t$) Yukawa coupling, in all Feynman diagrams at tree–level. Because of this $\sim m_q$ coupling the very light flavours $q = u, d$ and s give here completely negligible contributions, while c– and b–fractions are suppressed by a factor of $\approx (m_t/m_c)^2 \approx 10^4$ and $\approx (m_t/m_b)^2 \approx 1225$, respectively with respect to the top ones. Therefore, for process (7.3), the *top*–contribution is by far the dominant one for $\sqrt{s}_{ep} \gtrsim 1$ TeV and all ϕ–masses[7]. The corresponding numbers at the LEP⊗LHC energy, varying M_ϕ in the range $60 - 140$ GeV, are: $\approx$0.0016–0.0013% for u–, $\approx$0.0013–0.0011% for d–, $\approx$0.29–0.28% for s–, $\approx$17–20% for c–, $\approx$14–21% for b– and $\approx$69–58% for t–quarks.

Next, we checked if neglecting diagrams 1-6 [and 9-10] of process (7.2)[(7.1)] inside the matrix elements, as done in [65], where all quark masses were set equal to zero, could be a source of error[8]. In doing this we needed to apply some cuts to avoid collinear and soft singularities (in the couplings of the incoming photon to the outgoing quark q_{out}) that would otherwise make our amplitudes divergent. To do this, we require, e.g., $|\cos\theta_{\gamma q_{out}}| < 0.95$ and $|p_{q_{out}}| > 3$ GeV: restrictions which are reasonably compatible with eventual requirements from the detectors[9]. Setting again $\sqrt{s}_{ep} = 1.36$ TeV and $M_\phi = 60$ GeV, we have found percentage differences only of the order of 1 in 1000 in the case of light flavour final states, and of $\approx$2% for the contribution $b\gamma \to tW^-\phi$ + c.c., in process (7.1). For reaction (7.2), differences are appreciable only in the case of c– and b–quarks,

---

[7]Whereas for $\sqrt{s}_{ep} \lesssim 1$ TeV the c–contribution is the largest one: in this case the effect of the $q\gamma$ electromagnetic coupling, which favours c–quarks, is dominant on the Yukawa $q\phi$ electroweak one, which favours b–quarks.

[8]We expect differences coming from phase space and propagator effects to be negligible for the light flavours u, d, s, c and b, since $m_q << \sqrt{s}_{ep}$ for all of them.

[9]Since similar cuts were not listed in [65], we were unable to reproduce exactly the numbers there computed.

these being $\approx 3\%$ and $\approx 13\%$, respectively. These mass effects are approximately the same over the whole intermediate M_ϕ range. However, due to the relative flavour contributions of Tables (7.2(a,b)), when one sums over all of these the effects are largely washed out. We also notice that the errors due to neglecting the quark masses are larger for process (7.2) than for (7.1), since in the latter there are also contributions (dominant with respect to the Higgs bremsstrahlung) coming from $\gamma \to W^+ W^-$ splitting whereas at tree–level there is no corresponding $\gamma \to Z^0 Z^0$ coupling. Obviously, taking into account the masses in process (7.3) is crucial, since there the Higgs is always produced through the Yukawa couplings $q\phi$.

We know that in the mass range 60 GeV $\lesssim M_\phi \lesssim 140$ GeV the dominant Higgs decay mode is $\phi \to b\bar{b}$. The corresponding BR in the above interval varies from ≈ 0.85 at $M_\phi = 60$ GeV to ≈ 0.38 at $M_\phi = 140$ GeV, where the off–shell $W^{\pm *} W^{\mp}$ decay channel begins to be competitive [73]. So, in order to maximise the number of signal events we look for the $\phi \to b\bar{b}$ signature. We further require flavour identification of b–jets, exploiting the possibilities offered by b–tagging techniques, to reduce the large QCD backgrounds.

In processes (7.1)–(7.3) we have additional decaying particles[10]: a $W^{\pm}$ in $q\gamma \to q'W^{\pm}\phi$, a Z^0 in $q\gamma \to qZ^0\phi$ and two t's in the $g\gamma \to t\bar{t}\phi$ contribution. So we expect the following possible final signatures[11]:

$$ep \to W^{\pm}\phi X \to (\ell \nu_\ell)(b\bar{b})X,$$

$$ep \to Z^0\phi X \to (\ell\bar{\ell})(b\bar{b})X, \qquad (7.9)$$

or

$$ep \to W^{\pm}\phi X \to (jj)(b\bar{b})X,$$

$$ep \to Z^0\phi X \to (jj)(b\bar{b})X, \qquad (7.10)$$

---

[10]In principle, we also have t–quarks in process (7.1) which could decay to bW–pairs, but in practise, contributions involving *top* quarks are here generally quite small if compared to those of the other flavours and substantially negligible when we sum up all different combinations.

[11]We know that in all processes (7.1)–(7.3) we can have additional b's from t/Z^0–decays or $b\gamma/g\gamma$–fusion, but we assume that complications coming from the fact of taking in those events a wrong combination $b\bar{b}$ can be largely avoided if we restrict to keep $b\bar{b}$–invariant masses in the window $|M_{b\bar{b}} - M_\phi| < 5$ GeV (see later on).

(where X represents the remnant jet and/or electron) depending on whether the electroweak massive vector bosons decay leptonically or hadronically, respectively[12]. As for process (7.3) we expect the signature

$$ep \rightarrow q\bar{q}\phi X \rightarrow jj(b\bar{b})X \qquad (7.11)$$

for light quark contributions, and

$$ep \rightarrow t\bar{t}\phi X \rightarrow b\bar{b}W^+W^-(b\bar{b})X \qquad (7.12)$$

for top-quarks (with BR$(t \rightarrow bW) \approx 1$).

Therefore out of the $\approx 56 - 22[6 - 0.6]$ initial femtobarns of reaction (7.1)[(7.2)] at $\sqrt{s}_{ep} = 1.36$ TeV and for $M_\phi = 60 - 140$ GeV, assuming $\mathcal{L} = 3$ fb^{-1}, we expect $\approx 99 - 18[11- < 1]$ events for hadronic decays, and $\approx 42 - 8[2- < 1]$ for leptonic modes, whereas for reaction (7.3), starting from $\approx 3.8 - 0.24$ fb, we end up with $\approx 10- < 1$ events (7 of these come from $t\bar{t}\phi$ production with $M_\phi = 60$ GeV), per year.

The irreducible backgrounds[13] to the above signatures are $ep \rightarrow W^\pm Z^0 X \rightarrow W^\pm(b\bar{b})X$ and $ep \rightarrow \bar{t}bX \rightarrow b\bar{b}W^-X$ for process (7.1), $ep \rightarrow Z^0Z^0X \rightarrow Z^0(b\bar{b})X$ for (7.2), and $ep \rightarrow q\bar{q}Z^0X \rightarrow q\bar{q}(b\bar{b})X$ for (7.3). These are always present, independently of the $W^\pm/Z^0$ decay modes in processes (7.1)–(7.2). In addition, multi-jet photoproduction, $W^\pm + jets$, $Z^0 + jets$ and $t\bar{t}X \rightarrow b\bar{b}W^+W^-X$ production and decay events must be also considered.

A few remarks concerning the $t\bar{b}X$ background are needed here. We have mentioned earlier that we take the $e \rightarrow \gamma$ conversion efficiency ϵ (into back-scattered photons) equal to 0.5. The ideal case of efficiency equal to 1 would imply that all the incoming electrons are converted into photons and hence removed from the interaction site. In practice, however, this will never be the case, as, even for very high performances of the conversion mechanism, a fraction $(1 - \epsilon)$ different from zero of the ep initiated processes will remain. Therefore, we consider here the $t\bar{b}X$ background initiated by ep scattering through the subprocess $eg \rightarrow \nu W^*g \rightarrow \nu tb$, which is expected to have very large rates [76], whereas we neglect the γp

---

[12]We do not exploit here possible missing energy decays $Z^0 \rightarrow \nu\bar{\nu}$ in process (7.2).

[13]For simplicity, and also because in general they are an order of magnitude larger if compared to bremsstrahlung photon initiated processes, we consider only background processes via back-scattered incoming γ's (apart from the $\bar{t}b$–process which proceeds through Wg–fusion).

initiated one, as it has a much smaller production cross section [65] and can be further drastically reduced by a cut in the invariant mass $M_{b\bar{b}}$ and, especially, in the M_{bW} (see later). For a generic value of ϵ the final rates for the γp initiated processes should be multiplied by a factor of ϵ whereas the ep initiated ones by $(1 - \epsilon)$. Our choice of ϵ implies that both the rates for the γp and the ep initiated processes must be at the end multiplied by 0.5, hence the significances divided by the factor $\sqrt{2}$.

While b–tagging identification should drastically reduce the backgrounds where b-quarks are not present in the final states, this requirement is not generally enough if they are. In this case, one has to look for invariant masses of the $b\bar{b}$–pair in a window around M_ϕ, since most of the signals lie within this region. In the case of top–resonant backgrounds (i.e., $\bar{t}bX$ and $t\bar{t}X$) we can also exploit the cut, e.g., $|M_{bW\to bjj} - m_t| > 5$ GeV, which should be very effective in reducing hadronic $W^\pm$–decays since top-peaks are quite narrow (in fact, $\Gamma_t \approx 1.58$ GeV for $m_t = 175$ GeV). Finally, if the Higgs mass turns out to be close to the Z^0-mass, the absolute normalizations of the processes involving $M_{b\bar{b}}$ resonances are needed.

Assuming good b–tagging performances such that it is possible to drastically eliminate the non–b multi–jet photoproduction, $W^\pm + jets$ and $Z^0 + jets$ background events [65], and that the $M_{b\bar{b}}$ cut is sufficient to suppress the above processes in the case of $\gamma/g^* \to b\bar{b}$ splittings, we end up having to deal only with the backgrounds $ep \to W^\pm Z^0 X \to W^\pm(b\bar{b})X$, $ep \to \bar{t}bX \to b\bar{b}W^- X$, $ep \to Z^0 Z^0 X \to Z^0(b\bar{b})X$, $ep \to t\bar{t}X \to b\bar{b}W^+ W^- X$ and $ep \to q\bar{q}Z^0 X \to q\bar{q}(b\bar{b})X$. Moreover, we should not forget that an additional drastic rejection factor on the multi–jet reducible backgrounds comes from requiring that $M_{jj}/M_{\ell\bar{\nu}_\ell,\ell\bar{\ell}'}$ has to reproduce $M_{W^\pm}$ or M_{Z^0} for processes (7.1)–(7.2), and that $M_{bW\to bjj} \approx m_t$ for (7.3) when $q = t$ (since this flavour is by far the largest partonic contribution at the LEP$\otimes$LHC energy).

In order to study the background rates, we have implemented their matrix elements in FORTRAN codes generated by MadGraph [74] and HELAS [75][14]. The total cross sections of these processes are displayed in Table (7.3), at $\sqrt{s_{ep}} = 1.36$

---

[14]Since processes $ep \to \bar{t}bX \to b\bar{b}W^- X$ and $ep \to t\bar{t} \to b\bar{b}W^+ W^- X$ were already studied in [76], we also checked that the helicities amplitudes we obtained reproduce the results of that study (for bremsstrahlung photons in the case of $t\bar{t}$-production and decay).

TeV, for the same γ– and $g/q(\bar{q})$–structure functions and parameters employed for the signal processes. We notice that backgrounds are in general much larger than the corresponding signals, both for the *top*–resonant cases (continuum backgrounds) and for the $Z^0 \rightarrow b\bar{b}$ ones (discrete backgrounds). While in the former case this happens because of the *top*–resonant peaks, in the latter we have that the qZ^0 coupling does not depend on the q–mass (contrary to the Higgs one), so light quarks give large contributions here. This is especially evident in the case of the reaction $ep \rightarrow q\bar{q}Z^0$. The rates for $ep \rightarrow Z^0 Z^0 X$ are of the same order of magnitude as the signal $ep \rightarrow Z^0 \phi X$, since in this case this is the contributions from Z^0–bremsstrahlung off quarks in the background (we do not have triple vector boson vertices in this case) are comparable to those of the signal in which ϕ is emitted from a Z^0–line.

However, in principle these very large rates should not be a problem since processes $ep \rightarrow W^{\pm} Z^0 X$, $ep \rightarrow Z^0 Z^0 X$ and $ep \rightarrow q\bar{q}Z^0 X$ are really important only when $M_\phi \approx M_{Z^0}$, whereas $ep \rightarrow \bar{t}bX \rightarrow b\bar{b}W^- X$ and $ep \rightarrow t\bar{t}X \rightarrow b\bar{b}W^+ W^- X$ are highly reduced when applying a cut in the $b\bar{b}$ invariant mass (i.e., $M_{b\bar{b}} \approx M_\phi$) and, eventually for $W^{\pm}$–hadronic decays, the cut $M_{bW} \approx m_t$ can be used. In fig. (7.6) we give the differential distributions in the invariant mass $M_{b\bar{b}}$ for those backgrounds in which the $b\bar{b}$–pair does not come from a Z^0–resonance: i.e., $\bar{t}bX \rightarrow b\bar{b}W^- X$ and $t\bar{t}X \rightarrow b\bar{b}W^+ W^- X$ ($W^{\pm}$–BRs are not included). For backgrounds containing a $Z^0 \rightarrow b\bar{b}$ resonance, we naively assume that all the $b\bar{b}$–invariant mass spectrum is contained in the region $|M_{b\bar{b}} - M_{Z^0}| \leq 2\Gamma_{Z^0} = 5$ GeV. Since we are concentrating on $b\bar{b}$–invariant masses in the M_ϕ–region, we require that $M_{b\bar{b}}$ of all events is in the window $|M_{b\bar{b}} - M_\phi| < 5$ GeV, assuming that 10 GeV will be the mass resolution of the detectors. The fractions of the total cross sections from $\bar{t}bX$– and $t\bar{t}X$–production which pass this cut are given by the area under the $M_{b\bar{b}}$ distributions of fig. (7.6) between $M_\phi - 5$ and $M_\phi + 5$ GeV, while we assume that those of the Z^0–resonant $b\bar{b}$–events are given by the formula [57]

$$\delta\sigma(Z^0) = \sigma(Z^0)\frac{\max(0, 10 \text{ GeV} - |M_\phi - M_{Z^0}|)}{10 \text{ GeV}}. \tag{7.13}$$

In using the above equation we tacitly assumed that the $\phi \rightarrow b\bar{b}$ peaks are also all contained in a region of 10 GeV around the ϕ–pole[15]. The number of signal (S)

---

[15]In fact, the Higgs width at $M_\phi = 140$ GeV is $\Gamma_\phi \approx 0.01$ GeV.

and background (B) events and their statistical significance ($S/\sqrt{B}$) are given in Table (7.4), for the three processes (7.1)–(7.3) and the sum of their backgrounds separately, for the usual selection of ϕ–masses, after the $M_{b\bar{b}}$ cut. Branching ratios of hadronic and leptonic $W^{\pm}/Z^0$–decays in processes (7.1)–(7.2) as well as in the backgrounds are included, giving the hadronic (leptonic) signatures of (7.9)–(7.12). We do not make any assumption about the $W^{\pm}$–decays when $q = t$ in process (7.3) and on the second $W^{\pm}$ in the background $t\bar{t}X$, treating them completely inclusively (i.e., such that $W^{\pm}$'s can decay either hadronically or leptonically).

If, as criteria for the observability of a signal, we require a rate $S \geq 6$ events with a significance $S/\sqrt{B} > 4$ for the detection of an isolated Higgs peak, while for the case of Higgs peaks overlapping with Z^0 peaks we require $S \geq 10$ with $S/\sqrt{B} > 6$ [57], then we see from Table (7.4) that the situation seems to be discouraging, both for hadronic and leptonic $W^{\pm}$– and Z^0–decays, if $M_\phi \geq 60$ GeV. It does not look much better if one tries to make an "inclusive" analysis, summing the rates for signals and backgrounds, as done in Table (7.5). This happens because the largest signal (i.e., $W^{\pm}\phi X$) has a huge background, whereas the other two signals (i.e., $Z^0\phi X$ and $q\bar{q}\phi X$), even though virtually free from backgrounds, give very few events.

Therefore, in the case of overlapping peaks there does not appear to be any possibility to disentangle the signal (see Tables (7.1) and (7.3)), even after a few years of running. If $|M_\phi - M_{Z^0}| \gtrsim 5$ GeV however, where only the continuum backgrounds are effective, one can exploit (in the case of hadronic $W^{\pm}$–decays) the restriction $|M_{bW \to bjj} - m_t| > 5$ GeV. For this, in fig. (7.7) we plot the differential distributions in $M_{b\bar{b}}$ of the $\bar{t}bX$ and $t\bar{t}X$ backgrounds, after applying the above M_{bW} cut (on just one $W^{\pm}$ in the case of $t\bar{t}$–production and decay). It is clear then how this cut turns out to be extremely useful in rejecting the continuum backgrounds, since their rates are now at least 10 times smaller than before. If we insert this reduction factor in Tables (7.4), (7.5) the scenario changes completely, since we have now to divide all B's by ≈ 10, and multiply all $S/\sqrt{B}$'s times $\approx \sqrt{10}$. This gives significancies larger that 4 over all the intermediate Higgs mass range. At the same time, the reduction factor for $W^{\pm}\phi X$ is just a few percent, since the corresponding distribution in M_{bW} is nearly flat (see fig. (7.8)).

So far we have supposed a 100% acceptance and detection efficiencies for j/ℓ's in the final states with the same for b–tagging. Assuming a 50% overall efficiency, so all $S/\sqrt{B}$'s are divided by $\sqrt{2}$, we still obtain a number of events and a significance large enough to cover almost all the intermediate mass region, even after only one year of running (only for large M_ϕ we do not have completely satisfactory rates.).

Not even the reduction of $\sqrt{2}$ of the significances, due to the $e \rightarrow \gamma$ conversion efficiency $\epsilon = 0.5$, should change the above conclusions. On the contrary, a larger value of ϵ (as it is likely, since, e.g., the performances expected at e^+e^- colliders [71]) would definitely enhance the signal versus background ratios, as the large $t\bar{b}X$ background would be further reduced.

Finally, we would like to stress here how processes like (7.1)–(7.3) could turn out to be extremely interesting if one considers their counterparts, e.g., in the Minimal Supersymmetric Standard Model (MSSM). In this model there are two $SU(2)$ Higgs doublets each with a different hypercharge Y, with $Y = -1$ couples only to down type quarks and leptons and $Y = 1$ couples only to up type quarks and leptons. The two Higgs doublets that break the symmetry have the following particular vacuum expectation values[8]

$$< 0|\Phi_1|0 > = \begin{pmatrix} v_1 \\ 0 \end{pmatrix}$$

$$< 0|\Phi_2|0 > = \begin{pmatrix} 0 \\ v_2 \end{pmatrix} \tag{7.14}$$

with

$$\tan \beta \equiv \frac{v_2}{v_1} \tag{7.15}$$

and

$$0 \leq \beta \leq \frac{\pi}{2} . \tag{7.16}$$

The spectrum from the above mechanism is five physical Higgs fields: H^0, h^0 are neutral CP–even scalars, A^0 is a neutral CP–odd pseudoscalar and there are two charged Higgses H^+, H^-. Here quark–Higgs couplings proportional to $\tan \beta$ can enhance the signals up to $\mathcal{O}(1000)$ times for very large $\tan \beta$. This drastic enhancement happens when considering the contribution of diagrams involving the bremsstrahlung of the pseudoscalar boson A^0 off massive *down*-type quarks

(i.e., b–quarks: hence masses should be included). This occurs in all the Feynman diagrams of process (7.3), while it only happens for the suppressed graphs 1–6 [and 9,10] in (7.2)[(7.1)]. These latter contribute to the total rate at the level of 1% for the SM case but are the only surviving ones for the MSSM (since the pseudoscalar boson A^0 does not couple to vector bosons at tree–level). In addition, in processes (7.1)–(7.3), once we substitute ϕ by one of the MSSM neutral Higgses H^0, h^0 and A^0 and we also include the flavour changing cases in which $\phi \leftrightarrow H^\pm$ and double Higgs productions in $q\gamma$ fusion ($W^\pm \leftrightarrow H^\pm$ and $Z^0 \leftrightarrow H^0, h^0, A^0$), we will have a very rich laboratory where all the fundamental interactions of the MSSM can be carefully studied.

For example in Table (7.6) and Table (7.7) the total production cross section for the reaction (7.3) for the production of A^0, H^0, h^0 is given for two values of $\tan \beta$ while A^0 varies over the whole of the intermediate mass range. The cross-section is two orders of magnitude bigger than the SM Higgs production for the larger value of $\tan \beta$.

7.4   Summary and Conclusions

In summary, we have studied the production cross sections of the SM Higgs ϕ with mass in the range 60 GeV $\lesssim M_\phi \lesssim$ 140 GeV at a next–generation ep collider, with 500 GeV $\lesssim \sqrt{s}_{ep} \lesssim$ 3 TeV, through the partonic processes

$$\gamma q(\bar{q}) \to q'(\bar{q}') W^\pm \phi,$$

$$\gamma q(\bar{q}) \to q(\bar{q}) Z^0 \phi$$

and

$$g\gamma \to q\bar{q}\phi \ ,$$

for all possible (massive) flavours of the quarks $q(q')$, with incoming photons generated via Compton back–scattering of laser light.

Special attention has been devoted to the case of the planned CERN LEP$\otimes$LHC ep collider (with $\sqrt{s}_{ep} \approx$ 1.36 TeV), where signatures in which the Higgs decays to $b\bar{b}$–pairs were studied, exploiting the possibilities given by b–tagging techniques.

We concluded that at this machine, apart from the case $M_\phi \approx M_{Z^0}$ which is impossible to disentangle, Higgs signals should be detectable above all the possible backgrounds over the rest of the intermediate mass range, after only one year of running if $M_\phi \lesssim 140$ GeV (searching for the hadronic decays of $W^\pm$'s and Z^0's in processes (7.1) and (7.2) respectively). Due to the fact that the leptonic decay channels of the $W^\pm$'s give small rates and that a cut in the invariant mass M_{bW} is not applicable in this case, no possibility of detections exists if $W^\pm \rightarrow \ell \bar{\nu}_\ell$. Therefore, in this respect, we disagree with the conclusions given in [65]. In the case of $Z^0 \rightarrow \ell\bar{\ell}$ decays in process (7.2), one can get significant number of events only for a value of $\mathcal{L}$ much bigger than the one assumed here.

In general, if the LHC detectors are not able to achieve the necessary performances for all the foreseen Higgs measurements then the LEP $\times$ LHC collider option would provide the prospects of detailed studies of the SM Higgs boson parameters (i.e., M_ϕ, Γ_ϕ, BRs, etc ...) in the intermediate mass range, in an environment partially free from the QCD background typical of $pp/p\bar{p}$ accelerators, especially if larger b–tagging performances and/or a higher luminosity can be achieved, in advance of a possible future NLC.

σ (fb)			
M_ϕ (GeV)	$q'W^{\pm}\phi$	$qZ^0\phi$	$q\bar{q}\phi$
60	55.61 ± 0.34	6.13 ± 0.10	3.806 ± 0.058
80	42.84 ± 0.25	3.056 ± 0.052	1.765 ± 0.029
100	34.53 ± 0.14	1.581 ± 0.028	0.872 ± 0.013
120	27.56 ± 0.11	0.798 ± 0.024	0.4513 ± 0.0068
140	22.048 ± 0.080	0.547 ± 0.018	0.2419 ± 0.0039
$\sqrt{s} = 1.36$ TeV HMRS(B)			

Table 7.1: Production cross sections for processes (7.1)–(7.3), at $\sqrt{s}_{ep} = 1.36$ TeV, with $M_\phi = 60, 80, 100, 120$ and 140 GeV. The HMRS(B) structure functions are used. The errors are the statistical errors on the numerical calculation.

Flavours	σ (fb)
$u\gamma \rightarrow dW^+\phi + \bar{u}\gamma \rightarrow \bar{d}W^-\phi$	29.58 ± 0.15
$d\gamma \rightarrow uW^-\phi + \bar{d}\gamma \rightarrow \bar{u}W^+\phi$	19.37 ± 0.30
$s\gamma \rightarrow cW^-\phi + \bar{s}\gamma \rightarrow \bar{c}W^+\phi$	4.228 ± 0.021
$c\gamma \rightarrow sW^+\phi + \bar{c}\gamma \rightarrow \bar{s}W^-\phi$	1.620 ± 0.012
$b\gamma \rightarrow tW^-\phi + \bar{b}\gamma \rightarrow \bar{t}W^+\phi$	0.7995 ± 0.0033
$\sqrt{s} = 1.36$ TeV $\qquad$ HMRS(B) $\qquad M_\phi = 60$ GeV	

Table 7.2(a) Production cross sections for process (7.1) at $\sqrt{s}_{ep} = 1.36$ TeV, with $M_\phi = 60$ GeV, for all different flavour combinations entering in the partonic subprocesses. The HMRS(B) structure functions are used. The errors are the statistical errors on the numerical calculation.

Flavours	σ (fb)
$u\gamma \to uZ^0\phi + \bar{u}\gamma \to \bar{u}Z^0\phi$	4.535 ± 0.097
$d\gamma \to dZ^0\phi + \bar{d}\gamma \to \bar{d}Z^0\phi$	0.982 ± 0.025
$s\gamma \to sZ^0\phi + \bar{s}\gamma \to \bar{s}Z^0\phi$	0.2707 ± 0.0015
$c\gamma \to cZ^0\phi + \bar{c}\gamma \to \bar{c}Z^0\phi$	0.3018 ± 0.0012
$b\gamma \to bZ^0\phi + \bar{b}\gamma \to \bar{b}Z^0\phi$	0.03839 ± 0.00017
$\sqrt{s} = 1.36$ TeV HMRS(B) $M_\phi = 60$ GeV	

Table 7.2(b) Production cross sections for process (7.2), at $\sqrt{s}_{ep} = 1.36$ TeV, with $M_\phi = 60$ GeV, for all different flavour combinations entering in the partonic subprocesses. The HMRS(B) structure functions are used. The errors are the statistical errors on the numerical calculation.

Flavours	σ (fb)
$g\gamma \to u\bar{u}\phi$	$(60.4 \pm 2.2) \times 10^{-6}$
$g\gamma \to d\bar{d}\phi$	$(51.09 \pm 0.83) \times 10^{-6}$
$g\gamma \to s\bar{s}\phi$	$(11.113 \pm 0.071) \times 10^{-3}$
$g\gamma \to c\bar{c}\phi$	0.6572 ± 0.0025
$g\gamma \to b\bar{b}\phi$	0.5188 ± 0.0019
$g\gamma \to t\bar{t}\phi$	2.6192 ± 0.0049
$\sqrt{s} = 1.36$ TeV HMRS(B) $M_\phi = 60$ GeV	

Table 7.2(c) Production cross sections for process (7.3) at $\sqrt{s}_{ep} = 1.36$ TeV, with $M_\phi = 60$ GeV, for all different flavour combinations entering in the partonic subprocesses. The HMRS(B) structure functions are used. The errors are the statistical errors on the numerical calculation.

Background	σ (fb)
$ep \rightarrow W^{\pm} Z^0 X$	224.3 ± 1.9
$ep \rightarrow \bar{t} b X \rightarrow b \bar{b} W^- X$	1236.1 ± 5.6
$ep \rightarrow t \bar{t} X \rightarrow b \bar{b} W^+ W^- X$	1114.7 ± 1.4
$ep \rightarrow Z^0 Z^0 X$	12.15 ± 0.50
$ep \rightarrow q \bar{q} Z^0 X$	4161 ± 83
$\sqrt{s} = 1.36$ TeV HMRS(B)	

Table 7.3: Production cross sections for the background processes discussed in the text. The HMRS(B) structure functions are used. The errors are the statistical errors on the numerical calculation.

Process	S	B	$S/\sqrt{B}$	M_ϕ (GeV)
$q'W^\pm\phi$	99(42)	351(150)	5.28(3.43)	60
$qZ^0\phi$	11(2)	0(0)	$-(-)$	60
$q\bar{q}\phi$	10	0	$-$	60
$q'W^\pm\phi$	75(32)	330(141)	4.13(2.69)	80
$qZ^0\phi$	5(1)	0(0)	$-(-)$	80
$q\bar{q}\phi$	4	0	$-$	80
$q'W^\pm\phi$	59(25)	292(125)	3.45(2.24)	100
$qZ^0\phi$	3(0)	1(0)	3(0)	100
$q\bar{q}\phi$	2	220	0.13	100
$q'W^\pm\phi$	41(17)	246(105)	2.61(1.66)	120
$qZ^0\phi$	1(0)	0(0)	$-(0)$	120
$q\bar{q}\phi$	1	0	$-$	120
$q'W^\pm\phi$	18(8)	198(52)	1.28(1.11)	140
$qZ^0\phi$	0(0)	0(0)	0(0)	140
$q\bar{q}\phi$	0	0	0	140

Table 7.4: Number of signal (S) and background events (B) and their statistical significance ($S/\sqrt{B}$), for the processes (7.1)–(7.3), at $\sqrt{s}_{ep}$ = 1.36 TeV, after the cut $|M_{b\bar{b}} - M_\phi| < 5$ GeV, for the usual selection of Higgs masses. Numbers correspond to hadronic(leptonic) decays of the $W^\pm/Z^0$'s. The HMRS(B) structure functions are used. The symbol "–" indicates the case in which the backgrounds do not constitute a problem in disentangling the signals.

S_{tot}	B_{tot}	$S_{\text{tot}}/\sqrt{B}_{\text{tot}}$	M_ϕ (GeV)
120(44)	351(150)	6.40(3.59)	60
84(33)	330(141)	4.62(2.78)	80
64(26)	513(345)	2.8(1.4)	100
43(18)	246(105)	2.74(1.76)	120
19(8)	198(52)	1.35(1.11)	140

Table 7.5: Total number of signal (S_{tot}) and background events (B_{tot}) and their statistical significance ($S_{\text{tot}}/\sqrt{B}_{\text{tot}}$), after summing the numbers in Table. (7.4) in "inclusive" rates.

$\gamma g \rightarrow q\bar{q}\Phi^0$					
σ (fb) for $\tan\beta = 30$					
M_{A^0} (GeV)	$M_{H^0}(GeV)$	$M_{h^0}(GeV)$	A^0	H^0	h^0
60	129.2	59.9	449.85 ± 1.64	$0.274 \pm .0006$	428.25 ± 1.70
80	129.2	79.9	$218.87 \pm .85$	$0.343 \pm .0008$	209.13 ± 0.83
100	129.4	99.7	$117.97 \pm .53$	$0.649 \pm .0020$	$115.34 \pm .55$
120	130.0	119.0	$67.66 \pm .31$	$8.649 \pm .027$	$62.86 \pm .28$
140	140.9	128.1	$40.76 \pm .19$	$36.378 \pm .167$	$4.51 \pm .02$
$\sqrt{s} = 1.36$ TeV MRS(A)					

Table 7.6: Production cross sections for process (7.3) at $\sqrt{s}_{ep} = 1.36$ TeV, with $M_{A^0} = 60 - 140$ GeV summed over all the different flavour combinations entering in the partonic subprocesses for $\tan\beta$=30. The MRS(A) structure functions [77] are used. The errors are the statistical errors on the numerical calculation

$\gamma g \to q\bar{q}\Phi^0$					
σ (fb) for $\tan\beta = 1.5$					
M_{A^0} (GeV)	$M_{H^0}(GeV)$	$M_{h^0}(GeV)$	A^0	H^0	h^0
60	144.4	56.0	$1.417 \pm .004$	$0.191 \pm .00047$	$2.10 \pm .0059$
80	150.7	63.7	$0.681 \pm .002$	$0.154 \pm .0020$	$1.66 \pm .0051$
100	159.3	70.6	$0.364 \pm .001$	$0.117 \pm .00029$	$1.39 \pm .0036$
120	170.1	76.4	$0.208 \pm .0007$	$0.084 \pm .00025$	$1.21 \pm .0030$
140	182.9	80.9	$0.125 \pm .0005$	$0.059 \pm .00014$	$1.10 \pm .0025$
$\sqrt{s} = 1.36$ TeV MRS(A)					

Table 7.7: Production cross sections for process (7.3) at $\sqrt{s}_{ep} = 1.36$ TeV, with $M_{A^0} = 60 - 140$ GeV summed over all the different flavour combinations entering in the partonic subprocesses for $\tan\beta = 1.5$. The MRS(A) structure functions [77] are used. The errors are the statistical errors on the numerical calculation

(1)

(2)
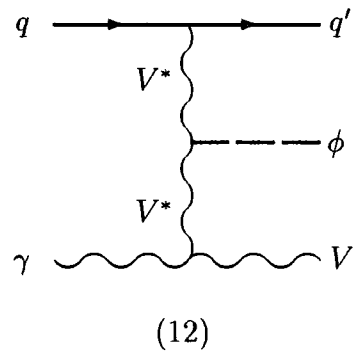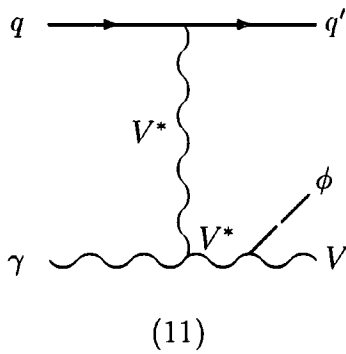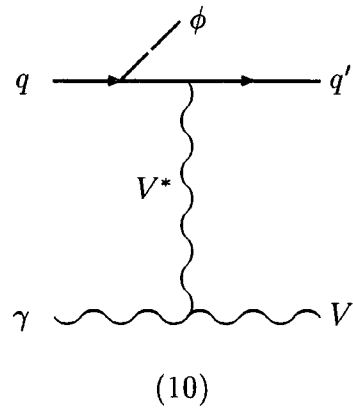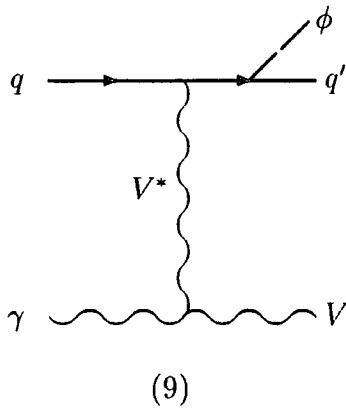
(3)

(4)

(5)

(6)

(7)

Figure 7.1

(8)

105
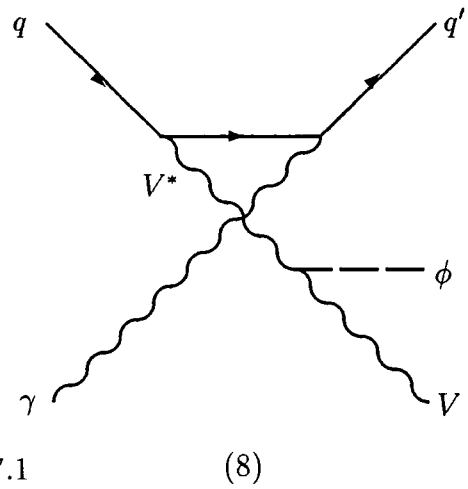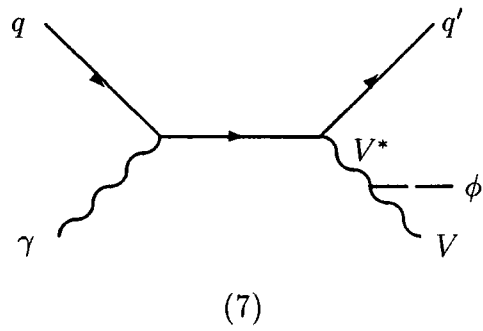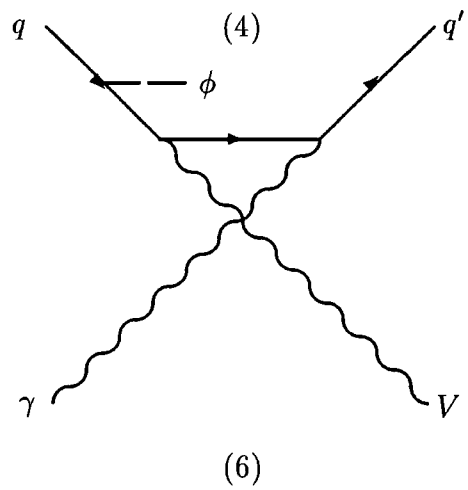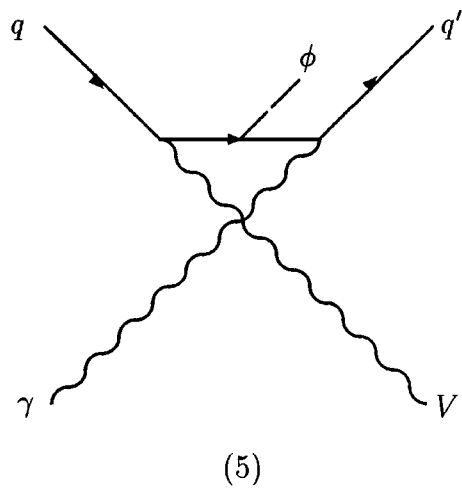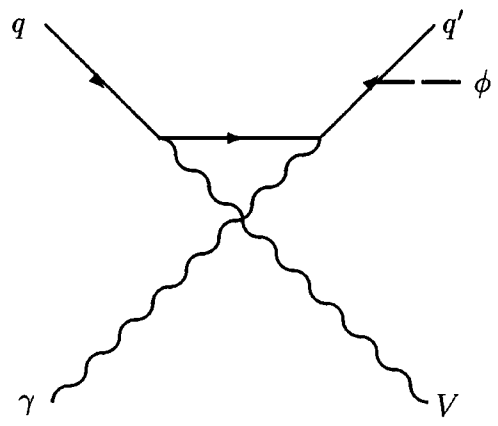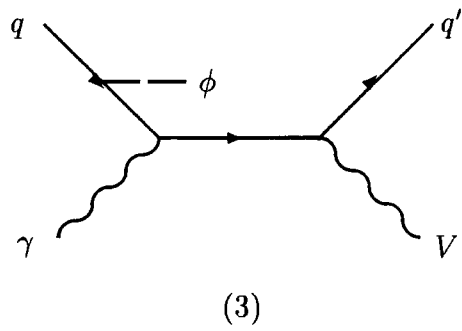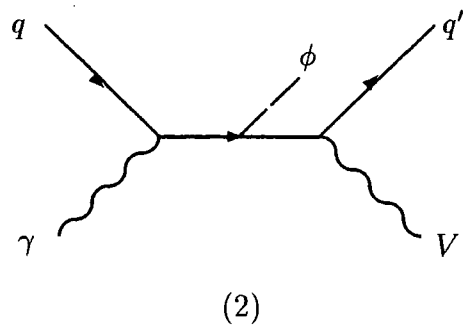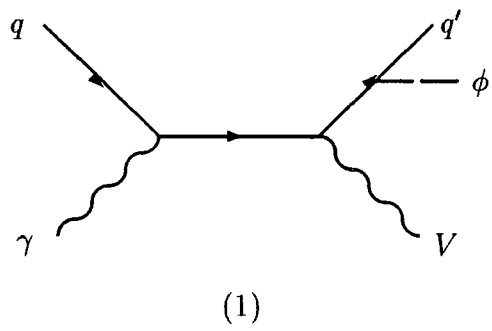
Figure 7.1(continued) Feynman diagrams contributing in lowest order to $q\gamma \rightarrow q'V\phi$, where $q(q')$ represents a quark, $V(V^*)$ an external(internal) vector boson and ϕ the SM Higgs boson, in the unitary gauge. In the case $V = Z^0$ and $q' = q$ only the first eight diagrams of fig. 1 contribute.
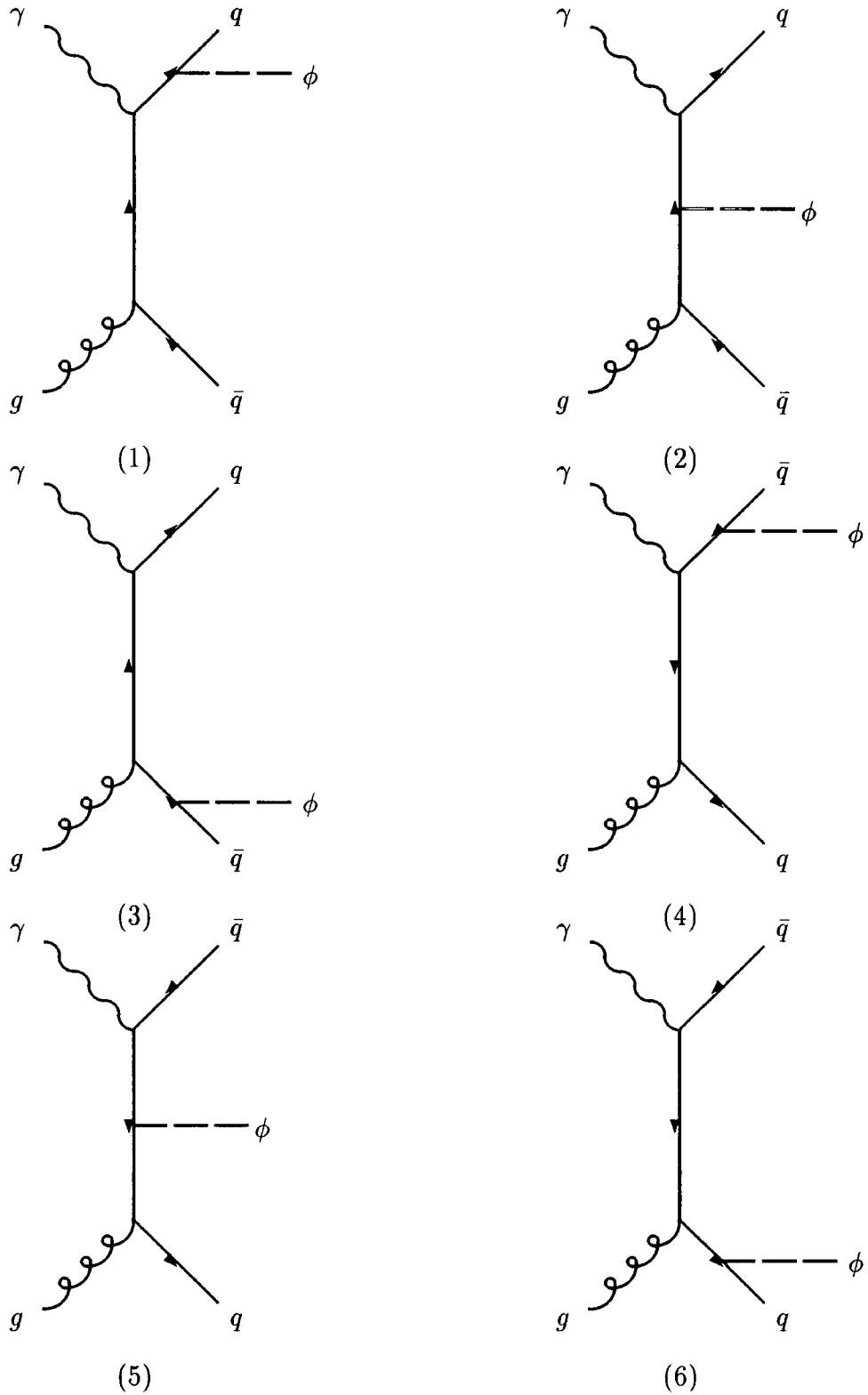
Figure 7.2: Feynman diagrams contributing in the lowest order to $g\gamma \rightarrow q\bar{q}\phi$, where q represents a quark and ϕ the SM Higgs boson, in the unitary gauge.
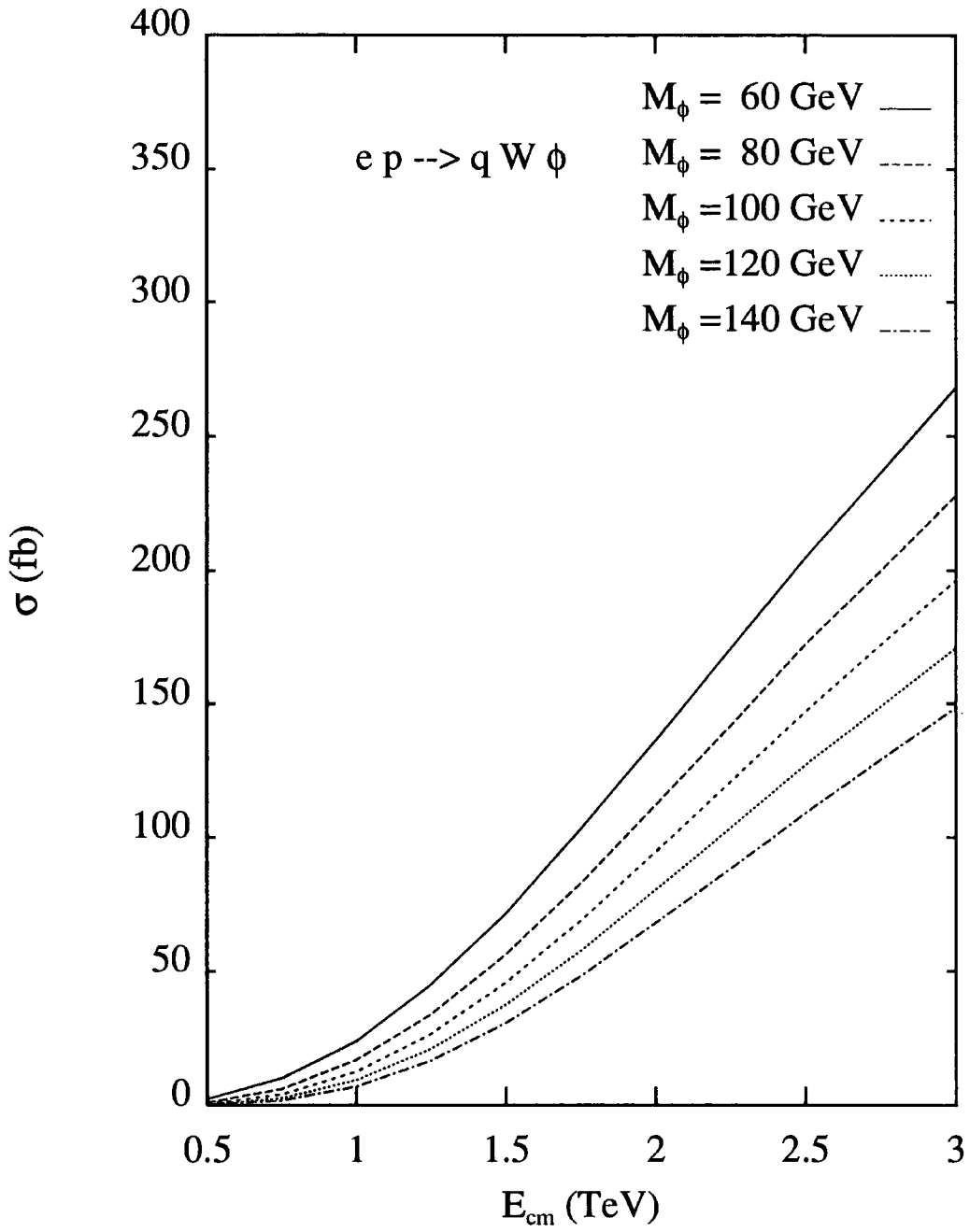
107

Figure 7.3: Cross sections of process (7.1) as a function of $\sqrt{s}_{ep}$, for a selection of Higgs masses. The HMRS(B) structure functions are used.
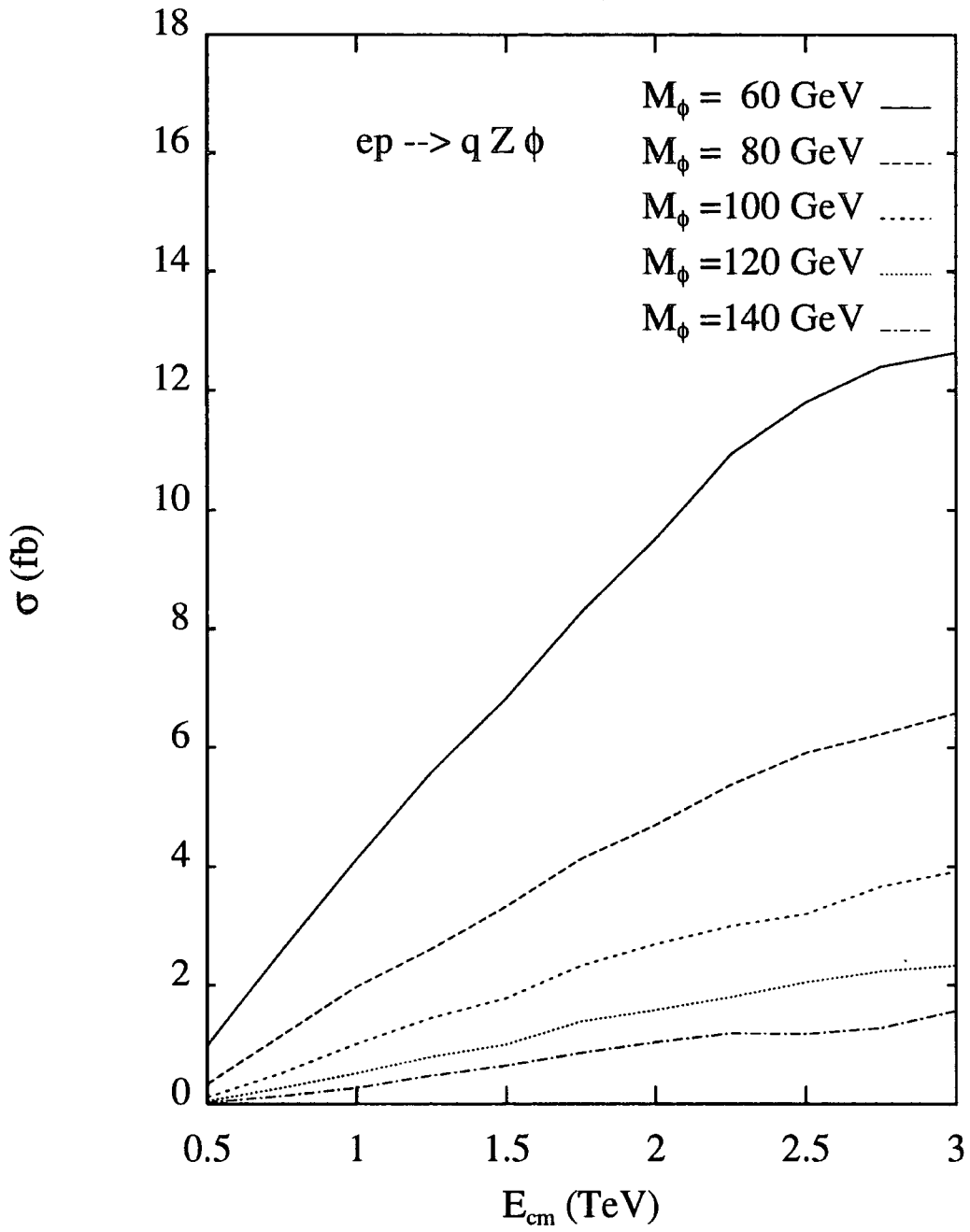
Figure 7.4: Cross sections of process (7.2) as a function of $\sqrt{s}_{ep}$, for a selection of Higgs masses. The HMRS(B) structure functions are used.
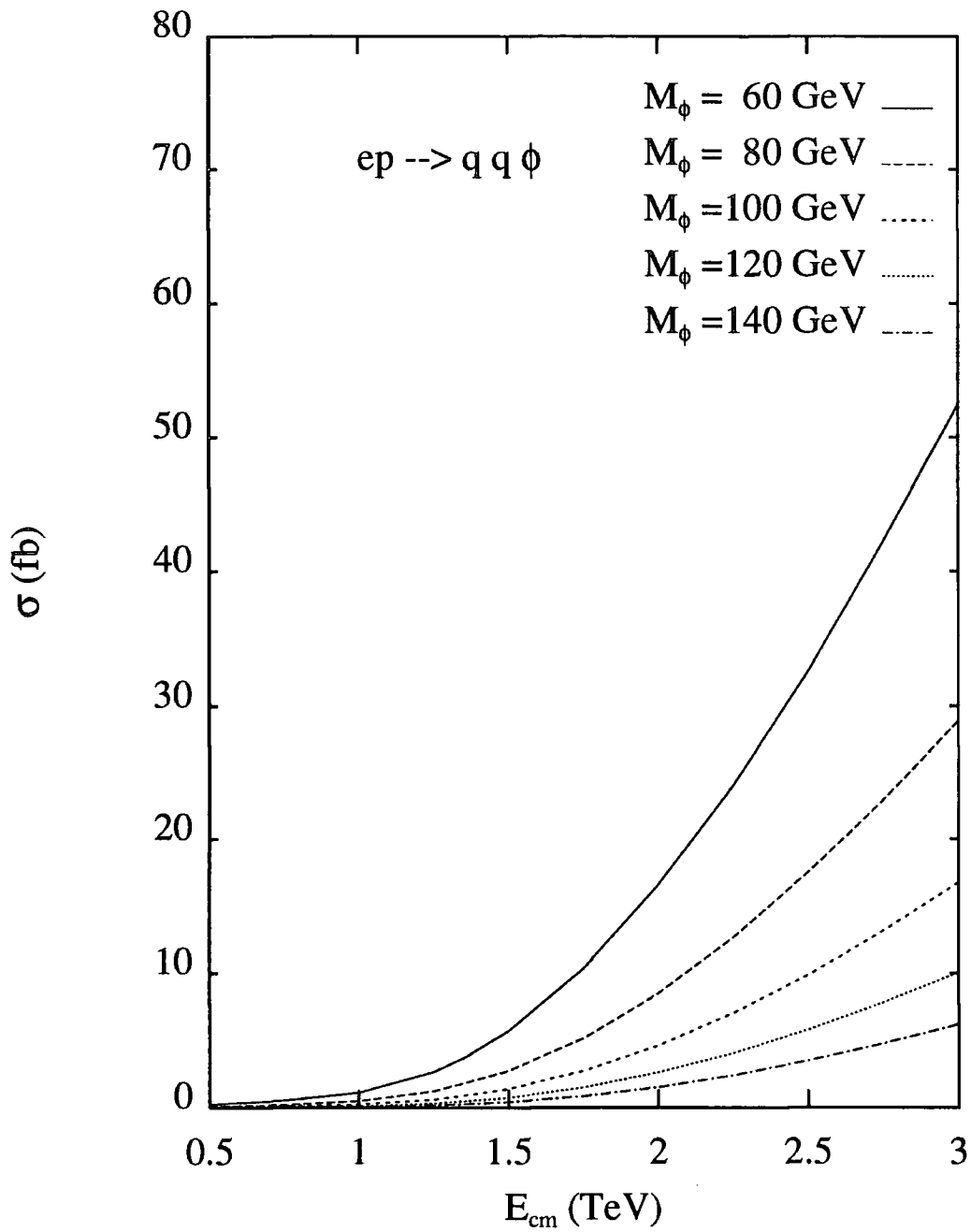
Figure 7.5: Cross sections of process (7.3) as a function of $\sqrt{s}_{ep}$, for a selection of Higgs masses. The HMRS(B) structure functions are used.

Figure 7.6: Differential distributions in the invariant mass of the $b\bar{b}$–pair $M_{b\bar{b}}$ for the $\bar{t}bX \rightarrow b\bar{b}W^-X$ and $t\bar{t}X \rightarrow b\bar{b}W^+W^-X$ backgrounds, at $\sqrt{s}_{ep} = 1.36$ TeV. The HMRS(B) structure functions are used.
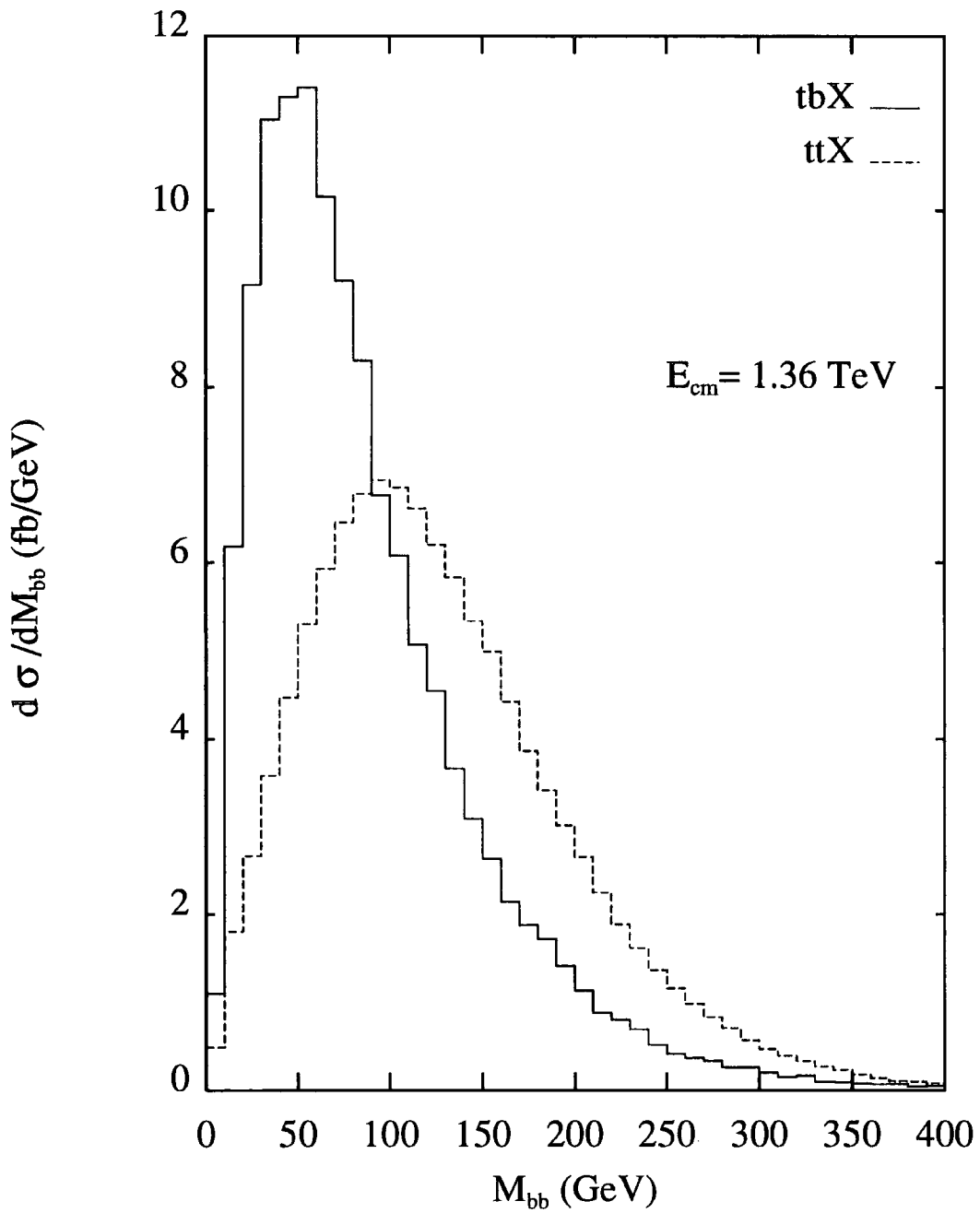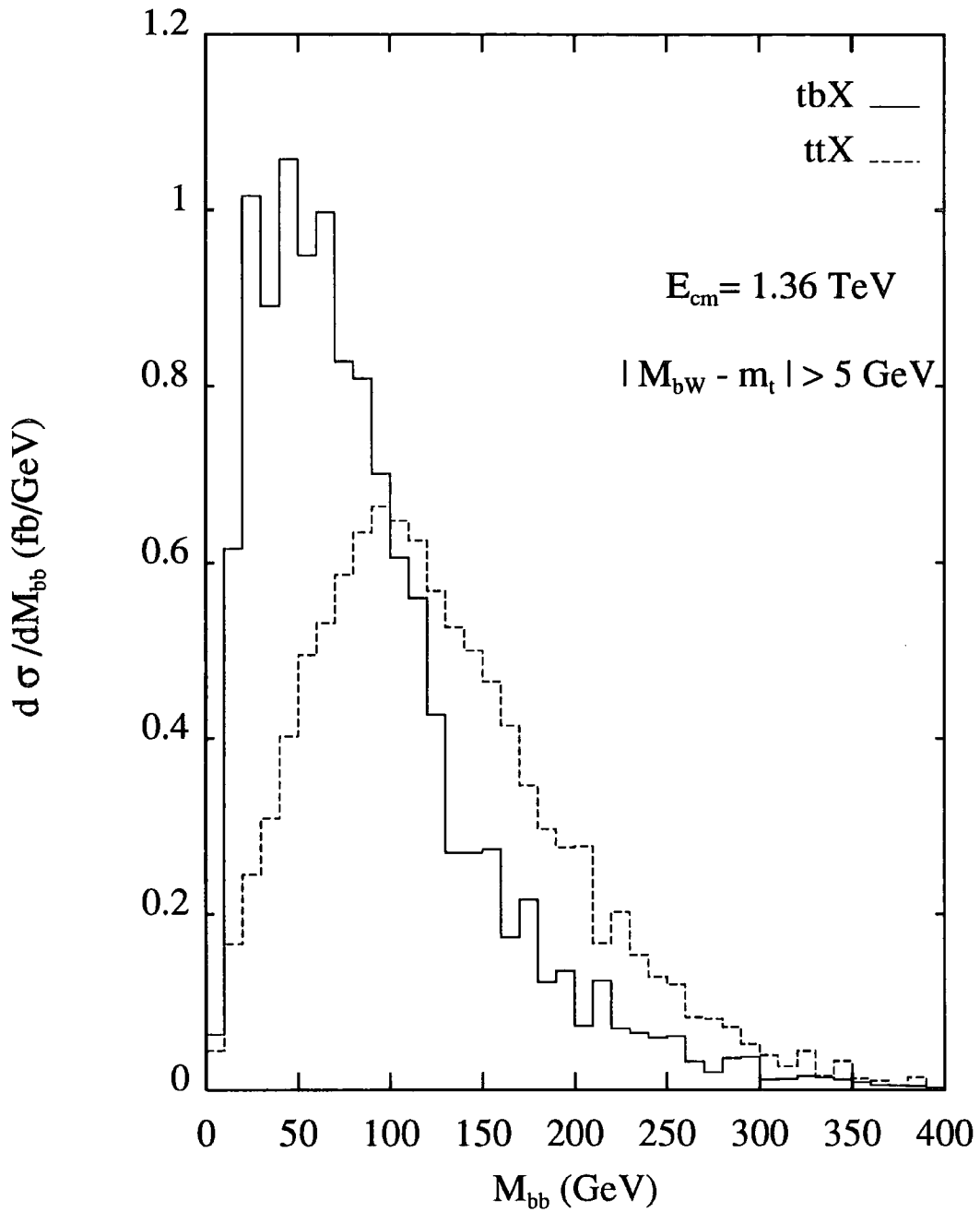
Figure 7.7: Differential distributions in the invariant mass of the $b\bar{b}$–pair $M_{b\bar{b}}$ for the $\bar{t}bX \rightarrow b\bar{b}W^-X$ and $t\bar{t}X \rightarrow b\bar{b}W^+W^-X$ backgrounds, at $\sqrt{s}_{ep} = 1.36$ TeV, after the cut $|M_{bW\rightarrow bjj} - m_t| > 5$ GeV. The HMRS(B) structure functions are used.
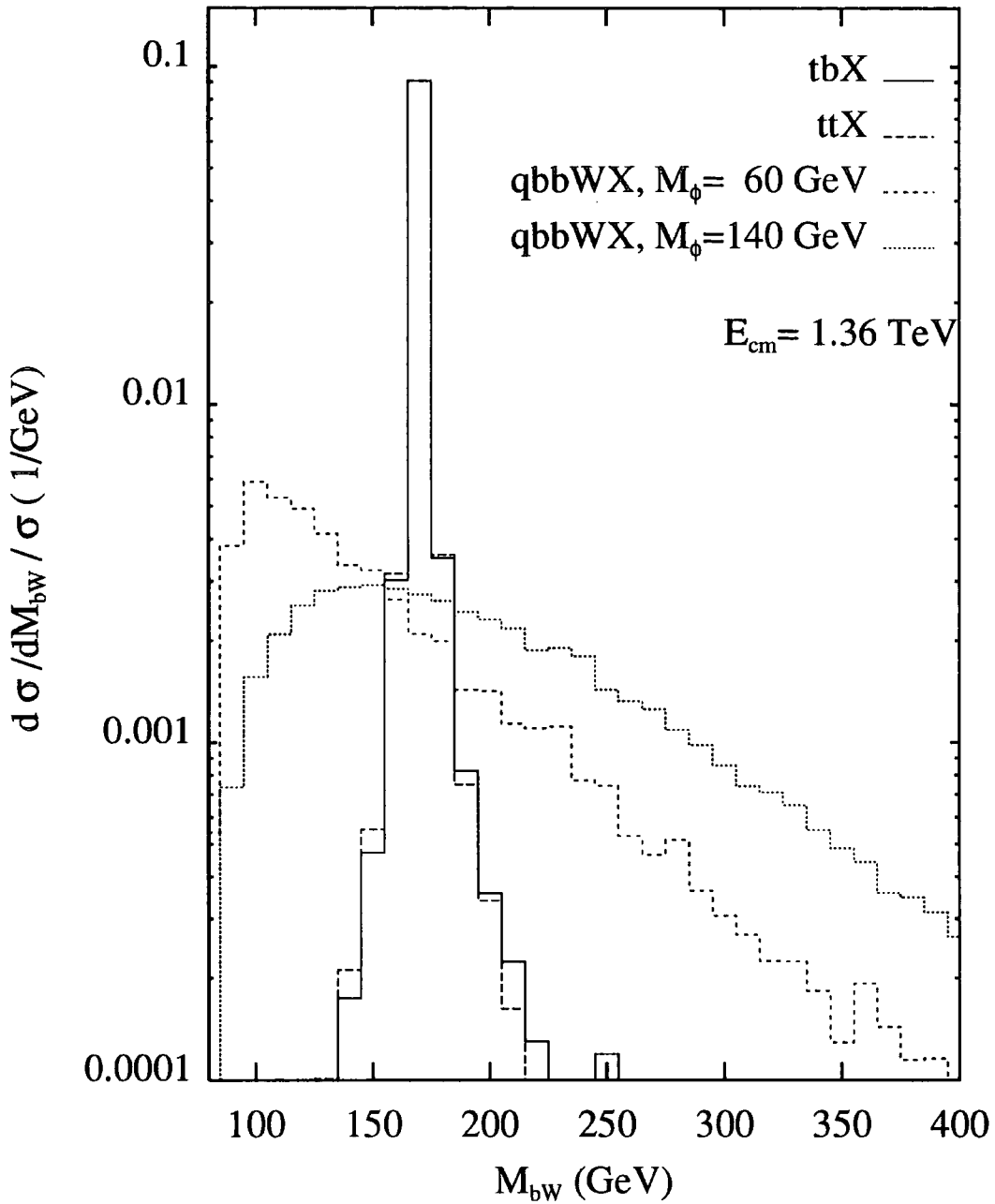
Figure 7.8: Differential distributions in the invariant mass of the bW–system M_{Wb} for the $\bar{t}bX \to b\bar{b}W^-X$ and $t\bar{t}X \to b\bar{b}W^+W^-X$ backgrounds, and the signal $W^{\pm}\phi X \to W^{\pm}(b\bar{b})X$ with $M_{\phi} = 60, 140$ GeV, at $\sqrt{s}_{ep} = 1.36$ TeV. The HMRS(B) structure functions are used.

Chapter 8

Conclusion

We first studied the reaction $e^+e^- \to W^+W^-\gamma$ and we showed that at LEP-II energies, the cross section for $W^+W^-\gamma$ production, where the photon is soft, is sensitive to the standard set of anomalous couplings used to parameterise the general form of the electroweak boson interaction Lagrangian. The dependence on these couplings is comparable in magnitude to, but qualitatively different from, the corresponding behaviour of the total W^+W^- cross section. Events with soft photons could therefore provide complementary information on the form of the electroweak boson interactions.

We have also studied the same reaction at the NLC, and have shown that quartic couplings can provide a window on new physics beyond the Standard Model. We have quantified the effect of various types of anomalous operators on the $W^+W^-\gamma$ production cross section in e^+e^- collisions. The effects are largest in the positive helicity cross section, although this represents only a small fraction of the total cross section. This type of physics is best suited to high energy colliders – there is an enormous increase in sensitivity in going from $\sqrt{s} = 300$ GeV to $\sqrt{s} = 500$ GeV – although some crude limits should be possible even from a handful of events at LEP II.

We then examined soft photon radiation in $t\bar{t}$ production and decay, the distribution of soft photon radiation in the process $e^+e^- \to t\bar{t} \to b\bar{b}W^+W^-$ is studied. We have demonstrated that the initial state radiation can easily swamp the sensitivity of the radiation pattern to the top decay width. However, for the case when the final state particles are in a plane transverse to the beam direction and when the photon itself is in this plane, then the initial state radiation effects are

114

minimized, only contributing a small constant background to the overall pattern. The dependence of the pattern on the top width, mass *etc.* is then apparent. It became clear that the minimum of the initial state radiation is valid for a much wider range of angles than just 90°. Thus, in practice, simply to keep the final state particles (including the photon) well away from the initial beam should be sufficient.

Finally, we have studied the production cross sections of the SM Higgs ϕ with mass in the range 60 GeV $\lesssim M_\phi \lesssim$ 140 GeV at a next–generation ep collider, with 500 GeV $\lesssim \sqrt{s}_{ep} \lesssim$ 3 TeV, through the partonic processes

$$\gamma q(\bar{q}) \rightarrow q'(\bar{q}')W^\pm \phi \ , \tag{8.1}$$

$$\gamma q(\bar{q}) \rightarrow q(\bar{q})Z^0 \phi \tag{8.2}$$

and

$$g\gamma \rightarrow q\bar{q}\phi, \tag{8.3}$$

for all possible (massive) flavours of the quarks $q(q')$, with incoming photons generated via Compton back–scattering of laser light.

Special attention has been devoted to the case of the planned CERN LEP$\otimes$LHC ep collider (with $\sqrt{s}_{ep} \approx$ 1.36 TeV), where signatures in which the Higgs decays to $b\bar{b}$–pairs were studied, exploiting the possibilities given by b–tagging techniques.

We concluded that at this machine, apart from the case $M_\phi \approx M_{Z^0}$ which is impossible to disentangle, Higgs signals should be detectable above all the possible backgrounds over the rest of the intermediate mass range, after only one year of running if $M_\phi \lesssim$ 140 GeV (searching for the hadronic decays of $W^\pm$'s and Z^0's in processes (8.1) and (8.2) respectively). Due to the fact that the leptonic decay channels of the $W^\pm$'s give small rates and that a cut in the invariant mass M_{bW} is not applicable in this case, no possibility of detections exists if $W^\pm \rightarrow \ell\bar{\nu}_\ell$. Therefore, in this respect, we disagree with the conclusions given in ref. [65]. In the case of $Z^0 \rightarrow \ell\bar{\ell}$ decays in process (8.2), one can get significant number of events only for a value of $\mathcal{L}$ much bigger than the one assumed here.

In general, if the LHC detectors are not able to achieve the necessary performances for all the foreseen Higgs measurements then the LEP × LHC collider

option would provide the prospects of detailed studies of the SM Higgs boson parameters (i.e., M_ϕ, Γ_ϕ, BRs, etc ...) in the intermediate mass range, in an environment partially free from the QCD background typical of $pp/p\bar{p}$ accelerators, especially if larger b–tagging performances and/or a higher luminosity can be achieved, in advance of a possible future NLC. It is also true that such an option will provide a rich laboratory for studying the MSSM Higgs interactions.

Bibliography

[1] F. Halzen and A.D. Martin, Quarks & Leptons, John Wiley and Sons, (1984).

[2] W.E. Burcham, Elements of Nuclear Physics, second edition, Longman, (1981).

[3] I.J.R. Aitchison and A.J.G. Hey, Gauge Theories in Particle Physics, second edition, Adam Hilger Bristol and Philadelphia, (1988).

[4] CDF collaboration, F. Abe *et al.*, *preprint* FERMILAB-PUB-94/022-E, CDF/PUB/TOP/PUBLIC/3040, March 1995;
D0 Collaboration, S. Abachi *et al.*, *preprint* FERMILAB-PUB-95-028-E, March 1995.

[5] F. Mandl and G. Shaw, Quantum Field Theory, John Wiley and Sons, (1984).

[6] I.J.R. Aitchison, Standard Model Foundations, High Energy Phenomenology, Proceedings of the Forty Second Scottish Universities Summer School in Physics, eds. K. J. Peach, L. L. J. Vick, P. Osborne. SUSSP and IOP Publishings Bristol and Philadelphia, (1993).

[7] S.L. Glashow, *Nucl. Phys.* **22** (1961) 579;
S. Weinberg, *Phys. Rev. Lett.* **19** (1967) 1264;
A. Salam, Proceedings of the *"Nobel Symposium"*, ed. N. Svartholm, Almqvist and Wiksells, Stockholm, 1968, 367.

[8] J.F. Gunion, H.E. Haber, G.L. Kane and S. Dawson, *"The Higgs Hunter's Guide"* (Addison-Wesley, Reading MA, 1990).

[9] P.W. Higgs, *Phys. Rev. Lett.* **12** (1964) 132.

[10] W.J. Stirling, Topics in Modern Phenomenology, Lecture Notes– HEP Summer School, RAL (1987).

[11] Review of Particle Properties, *Phys. Rev. D.* **50** (1994) 1173.

[12] A. Blondel *et al.*, *The study of the reaction* $e^+e^- \to W^+W^-$, in Proc. ECFA Workshop on LEP 200 (Aachen, Germany, 1986), Vol. 1, eds. A. Bohm and W. Hoogland, p.120.

[13] R.W. Brown and K.O. Mikaelian, *Phys. Rev. D.* **3** (1979) 922.

[14] K.Hagiwara et al.,Nucl. Phys. **B282** (1987) 253.

[15] E.N. Argyres *et al.*, Phys. Lett. **B280** (1991) 324.

[16] E.N. Argyres *et al.*, Phys. Lett. **B259** (1991) 195.

[17] CDF collaboration, F. Abe *et al.*, CDF-ANAL-ELECTROWEAK-CDFR-2951, FERMILAB-PUB-95-036-E, March (1995).

[18] G. Couture and J.N. Ng, Z. Phys. **C35** (1987) 65.

[19] G.F. Abu Leil, Mod. Phys. Lett. **A8** (1993) 1191.

[20] Yu.L. Dokshitzer *et al.*, Nucl. Phys. **B403** (1993) 65.

[21] G. Bélanger and F. Boudjema, in Proc. Workshop on "e^+e^- Collisions at 500 GeV: the Physics Potential", Munich, Annecy, Hamburg (1991), ed. P.M. Zerwas, report DESY 92-123B (1992) p.763.

[22] G. Bélanger and F. Boudjema, Phys. Lett. **B288** (1992) 201.

[23] O.J.P. Eboli, M.C. Gonzalez-Garcia and S.F. Novaes, Nucl. Phys. **B411** (1994) 381.

[24] F. Boudjema, presented at the 2nd International Workshop on Physics and Experiments with Linear e^+e^- Colliders, Waikoloa, HI, 26-30 April 1993, LAPP preprint ENSLAPP-A-431/93 (1993).

[25] V.A.Khoze, L.H.Orr and W.J.Stirling, Nucl. Phys. B378 (1992) 413.

[26] G.Jikia, Phys. Lett. 275B (1991) 196.

[27] Yu.L.Dokshitzer, V.A.Zhoze and S.I.Troyan, J.Phys. G.Nucl. Part. Phys. 17 (1991) 1602.

[28] P. Janet, Talk delivered at First General Meeting of the LEP2 Workshop, CERN, Geneva, Switzerland, 2-3 February 1995.

[29] M. Veltman, *Phys. Lett.* **B70** (1977) 253.

[30] B.W. Lee, C. Quigg and G.B. Thacker, *Phys. Rev. Lett.* **38** (1977) 883; *Phys. Rev.* **D16** (1977) 1519.

[31] Proceedings of the *"ECFA Workshop on LEP 200"*, A. Bohm and W. Hoogland eds., Aachen FRG, 29 Sept.–1 Oct. 1986, CERN 87-08.

[32] Proceedings of the *"Large Hadron Collider Workshop"*, Aachen, 4–9 October 1990, eds. G. Jarlskog and D. Rein, Report CERN 90–10, ECFA 90–133, Geneva, 1990.

[33] J.D. Bjorken, Proceedings of the *"Summer Institute on Particle Physics"*, *SLAC Report* 198 (1976);
B.W. Lee, C. Quigg and H.B. Thacker, *Phys. Rev.* **D16** (1977) 1519;
J. Ellis, M.K. Gaillard and D.V. Nanopoulos, *Nucl. Phys.* **B106** (1976) 292;
B.L. Ioffe and V.A. Khoze, *Sov. J. Part. Nucl.* **9** (1978) 50.

[34] H. Georgi, S.L. Glashow, M.E. Macahek and D.V. Nanopoulos, *Phys. Rev. Lett.* **40** (1978) 692.

[35] R.N. Cahn and S. Dawson, *Phys. Lett.* **B136** (1984) 196.

[36] S.L. Glashow, D.V. Nanopoulos and A. Yildiz, *Phys. Rev.* **D18** (1978) 1724.

[37] R. Kleiss, Z. Kunszt and W.J. Stirling, *Phys. Lett.* **B253** (1991) 269;
M.L. Mangano, SDC Collaboration note SSC–SDC–90–00113.

[38] R. Raitio and W.W. Wada, *Phys. Rev.* **D19** (1979) 941;
J.N. Ng and P. Zakarauskas, *Phys. Rev.* **D29** (1984) 876.

[39] J.F. Gunion, *Phys. Lett.* **B261** (1991) 510;
W.J. Marciano and F.E. Paige, *Phys. Rev. Lett.* **66** (1991) 2433;
A. Ballestrero and E. Maina, *Phys. Lett.* **B268** (1992) 437;
Z. Kunzst, Z. Trócsányi and W.J. Stirling, *Phys. Lett.* **B271** (1991) 247;
D.J. Summers, *Phys. Lett.* **B277** (1992) 366.

[40] C. Seez et al., in ref.[32].

[41] J. Dai, J.F. Gunion and R. Vega, *Phys. Rev. Lett.* **71** (1993) 2699.

[42] *Solenoidal Detector Collaboration Technical Design Report*, E.L. Berger *et al.*, *Report* SDC–92–201, SSCL–SR–1215, 1992.

[43] D. Froidevaux and E. Richter-Was, *preprint* CERN-TH.7459/94.

[44] Proceedings of the Workshop *"Physics and Experiments with Linear Colliders"*, Saariselkä, Finland, 9–14 September 1991, eds. R. Orawa, P. Eerola and M. Nordberg, World Scientific Publishing, Singapore, 1992.

[45] Proceedings of the Workshop *"e^+e^- Collisions at 500 GeV. The Physics Potential"*, Munich, Annecy, Hamburg, 3–4 February 1991, ed. P.M. Zerwas, DESY pub. 92–123A/B/C, August 1992.

[46] Proceedings of the ECFA workshop on *"e^+e^- Linear Colliders LC92"*, R. Settles ed., Garmisch Partenkirchen, 25 July–2 Aug. 1992, MPI-PhE/93–14, ECFA 93–154.

[47] Proceedings of the *"I Workshop on Japan Linear Collider (JLC)"*, KEK 1989, KEK-Report 90–2;
Proceedings of the *"II Workshop on Japan Linear Collider (JLC)"*, KEK 1990, KEK-Report 91–10.

[48] V. Barger, K. Cheung, A. Djouadi, B.A. Kniehl and P.M. Zerwas, *Phys. Rev.* **D49** (1994) 79.

[49] D.R.T. Jones and S.T. Petkov, *Phys. Lett.* **B84** (1979) 440;
R.N. Chan and S. Dawson, *Phys. Lett.* **B136** (1984) 196;
K. Hikasa, *Phys. Lett.* **B164** (1985) 341;

G. Altarelli, B. Mele and F. Pitolli, *Nucl. Phys.* **B287** (1987) 205;

B. Kniehl, *preprint* DESY 91–128, 1991.

[50] V. Barger, K. Cheung, B.A. Kniehl and R.J. Phillips, *Phys. Rev.* **D46** (1992) 3725.

[51] K. Hagiwara, J. Kanzaki and H. Murayama, *Durham Univ. Report* No. DTP–91–18, 1991.

[52] J.F. Gunion and H.E. Haber, *preprint* UCD–90–25, September 1990, Presented at "*1990 DPF Summer Study on High Energy Physics*, Snowmass, Colorado, June 25–July 13, 1990;

J.F. Gunion and H.E. Haber, in Proceedings of the "*1990 Summer Study on High Energy Physics: Research Directions for the Decade*", ed. E.L. Berger, Snowmass, Colorado, 1990;

J.F. Gunion and H.E. Haber, *Phys. Rev.* **D48** (1993) 5109.

[53] D. Borden, D. Bauer and D. Caldwell, *SLAC Report No.* SLAC–PUB–5715, 1992;

F. Richard, in ref. [45];

D. Bowser-Chao and K. Cheung, *Phys. Rev.* **D48** (1993) 89.

[54] K. Cheung, *Phys. Rev.* **D47** (1993) 3750;

E. Boos, I. Ginzburg, K. Melnikov, T. Sack and S. Shichanin, *Z. Phys.* **C56** (1992) 487.

[55] E. Boos, M. Dubinin, V. Ilyin, A. Pukhov, G. Jikia and S. Sultanov, *Phys. Lett.* **B273** (1991) 173.

[56] K. Hagiwara, I. Watanabe and P.M. Zerwas, *Phys. Lett.* **B278** (1992) 187.

[57] K. Cheung, *Phys. Rev.* **D48** (1993) 1035.

[58] O.J.P. Eboli and M.C. Gonzales-Garcia, *Phys. Rev.* **D49** (1994) 91.

[59] Proceedings of the "*HERA Workshop*", ed. R.D. Peccei, Desy, Hamburg, October 1987;

Proceedings of the "*HERA Workshop*", eds. W. Buchmüller and G. Ingelman, Desy, Hamburg, October 1991.

[60] K.J.F. Gaemers, R.M. Godbole and M. van der Horst, in ref. [59] (1987).

[61] K. Hikasa, Particle Data Book, *Phys. Rev.* **D45** 11-II (1992).

[62] G. Grindhammer, D. Haidt, J. Ohnemus, J. Vermaseren and D. Zeppenfeld, in ref. [32].

[63] T. Han and C. Liu, *Z. Phys.* **C28** (1985) 295;
D.A. Dicus and S. Willenbrock, *Phys. Rev.* **D32** (1985) 1642.

[64] J. Blumlein, G.J. van Oldenborgh and R. Ruckl, *Nucl. Phys.* **B395** (1993) 35.

[65] K. Cheung, *Phys. Lett.* **B319** (1993) 244.

[66] B. Grzadkowski, S. Pokorski and J. Rosiek, *Phys. Lett.* **B272** (1991) 143.

[67] R. Kleiss and W.J. Stirling, *Nucl. Phys.* **B262** (1985) 235.

[68] C. Mana and M. Martinez, *Nucl. Phys.* **B287** (1987) 601.

[69] G. Abu Leil and S. Moretti, work in progress.

[70] P.N. Harriman, A.D. Martin, R.G. Roberts and W.J. Stirling, *Phys. Rev.* **D42** (1990) 798.

[71] V. Telnov, *Nucl. Instrum. Methods* **A294** (1990) 72;
I. Ginzburg, G. Kotkin, V. Serbo V. Telnov, *Nucl. Instrum. Methods* **A205** (1983) 47, **A219** (1984) 5.

[72] G.P. Lepage, *Jour. Comp. Phys.* **27** (1978) 192.

[73] Z. Kunszt and W.J. Stirling, in ref. [32];
P.M. Zerwas, in ref. [46].

[74] T. Stelzer and W.F. Long, *Comp. Phys. Comm.* **81** (1994) 357.

[75] E. Murayama, I. Watanabe and K. Hagiwara, HELAS: HELicity Amplitude Subroutines for Feynman Diagram Evaluations, *KEK Report* 91-11, January 1992.

[76] U. Baur and J.J. Van der Bij, *Nucl. Phys.* **B304** (1988) 451.

[77] A.D. Martin, R.G. Roberts and W.J. Stirling, *Phys. Rev.* **D50** ((1994)) 6734